

Fault Tolerant Operation of Series Connected H-Bridge Multilevel Inverters

Vom Fachbereich Elektrotechnik und Informatik
der Universität Siegen
zur Erlangung des akademischen Grades

**Doktor der Ingenieurwissenschaften
(Dr.-Ing.)**

genehmigte Dissertation

von

Ingeniero Civil Pablo Ignacio Correa Vasquez
aus Santiago, Chile

1. Gutachter: Prof. Dr.-Ing. Mario Pacas
2. Gutachter: Prof. Dr.-Ing. Joachim Holtz
3. Gutachter: Prof. Dr.-Ing. José Rodríguez

Tag der mündlichen Prüfung: 31. August 2006

urn:nbn:de:hbz:467-2764

PREFACE

This thesis was written in the institute of power electronics and electrical drives of the University of Siegen, during my stay of three years in Germany as exchange student. First of all, I wish to thank the head of the institute, Prof. Dr.-Ing. Mario Pacas, for supervising my thesis and for his helpfully advise in numerous technical discussions.

I want to thank Prof. Dr.-Ing. Joachim Holtz for his valuable comments which improved this work. I wish to express my gratitude with Prof. Dr.-Ing. Rainer Patsch for assuming the guidance of the graduation process and with Prof. Dr.-Ing. Jose Rodriguez for his inspirational guidance.

Further, I want to thank the whole personnel of the institute for providing a pleasant working atmosphere. Especially, I want to thank Mr. Schmick for his cooperation to build the experimental set-up and Dipl.-Ing. W. Bruch and Dipl.-Ing. E. Oerter for supplying technical assistance. Thanks to the colleagues of the institute Eva, Roberto, Piotr, Joanna, and Dr. Ing. Martin Schulz for being truly friends and for being with me also on rainy days, which were the most ones.

I want to thank to my family their unconditional support and encouragement in all the moments of my life, in particular, to my two grandfathers Gustavo and Rene for teaching me to appreciate the value of knowledge and education.

This work has been carried out thanks to the financial support of the German Academic Exchange Service (DAAD).

Pablo Correa Vasquez

Index of Contents

- Nomenclature 5
 - Symbols 5
 - Superscript indexes 6
 - Subscript indexes 6
 - Acronyms 7
- 0. Introduction 9
- 1. Fundamentals 12
 - 1.1 Space Phasors 12
 - 1.2 Induction Machine Model 13
 - 1.3 Multilevel Inverter topologies 16
 - 1.3.1 Neutral Point Clamped Voltage Source Inverter (NPC-VSI) 16
 - 1.3.2 Flying Capacitor Voltage Source Inverter (FLC-VSI) 18
 - 1.3.3 Multilevel Serial Connected H-Bridge Voltage Source Inverter (SCHB) 19
 - 1.4 Summary of chapter 1 21
- 2. Torque and flux control of the induction machine 22
 - 2.1 Indirect Stator quantities Control (ISC) 22
 - 2.2 Operation in Field Weakening Region 26
 - 2.2.1 Steady State Flux Weakening Magnitude 27
 - 2.2.2 Dynamic Field Weakening Factor 27
 - 2.3 Summary of chapter 2 30
- 3. Modulation methods for SCHB multilevel inverters 31
 - 3.1 Phase-Shift PWM (PS-PWM) 31
 - 3.2 Space Phasor Modulation (SPM) 33
 - 3.2.1 Nearest space phasors selection and on-duration calculation 34
 - 3.2.2 Determination of the sequence of states 36
 - 3.2.3 Generation of the firing pulses 42
 - 3.2.4 Implementation of the SPM 43
 - 3.3 Summary of chapter 3 48
- 4. Fault tolerant operation of the schb-vsi 49
 - 4.1 Reliability in the SCHB-VSI 49
 - 4.2 Faults in SCHB multilevel inverter 50

4.3	Operation with bypassed cells.....	51
4.3.1	Fault Tolerant PS-PWM.....	51
4.3.2	Modified Fault Tolerant PS-PWM.....	56
4.3.3	Fault tolerant Space Phasor Modulator	60
4.3.4	Control strategy with faulty cells	68
4.4	Summary of chapter 4	74
5.	Experimental results.....	76
5.1	Multilevel Inverter.....	76
5.2	Laboratory set-up	78
5.3	Measurements of the steady state operation with bypassed cells.....	79
5.4	Switching frequency with bypassed cells.....	81
5.5	Dynamic response of the torque controller with bypassed cells	82
5.6	Transition between two inverter configurations.....	85
5.7	Summary of chapter 5	88
6.	Conclusions.....	89
7.	Abstract.....	91
8.	Zusammenfassung.....	92
9.	Bibliography	93
10.	Appendix : Parameters of the machine	95

NOMENCLATURE

Symbols

a	modulation index
a_r	reliability index
C	capacitor, carrier
d	differential operator, on-time normalized duration of a space phasor
D	diode (general)
f	frequency
i, I	current
Im	imaginary part
J	inertia
j	imaginary unit
K, k	cartesian coordinates, gain of a controller
L	inductance
p	pair of poles
P	polar coordinates
M	torque
N_{cell}	number of cells per phase
R	resistance
Re	real part
S	switch (general)
\mathbf{s}	switching state matrix
\mathbf{Seq}	sequence hyper-vector
Sch	switch of the chopper
t	time
T_s	modulation period
u, U	voltage
U_1	first cell in phase U
U_2	second cell in phase U
U_{ce}	collector-emitter voltage
V_1	first cell in phase V
V_2	second cell in phase V
W_1	first cell in phase W

W2	second cell in phase W
α	phase angle in phase U
β	phase angle in phase V
χ	space phasor angle
Δ	difference operator
δ_1	voltage space phasor angle referred to the imaginary axis of a rotating frame
ϕ	carrier phase angle
γ	phase angle phase W, angle of a reference frame
σ	leakage factor
ϑ	angle between stator and rotor fluxes
Ψ	flux linkage
ω	angular frequency
\propto	proportional to
\approx	approximately equal to
\underline{x}	lower limit of x
\overline{x}	upper limit of x

Superscript indexes

*	reference, conjugate complex space phasor
'	transformed space phasor, transformed coordinate system
^	maximum value, maximum magnitude of a phasor
~	mean value
T	transposed matrix
.	derivative

Subscript indexes

0	zero sequence component
1	stator-
2	rotor-
b	break-down value
d	DC link (voltage) / real part of a space phasor in an arbitrary reference frame
dyn	dynamic component

g	fundamental component
h	magnetizing
k	discrete time point
L	load
mech	mechanical (rotor speed/ rotor position)
p	projection
q	imaginary part of a space phasor in an arbitrary reference frame
steady	steady state component
N	neutral point of the inverter, nominal value
U	phase U of the inverter
V	phase V of the inverter
W	phase W of the inverter
α	real part of a space phasor in a coordinate frame fixed to the stator
β	imaginary part of a space phasor in a coordinate frame fixed to the stator
–	space phasor

Acronyms

ANPC	Active Neutral Point Clamped
EEPROM	Electrically Erasable Programmable Read-Only Memory
ESR	Equivalent Series Resistance
DSC	Direct Self Control
DSP	Digital Signal Processor
DTC	Direct Torque Control
FLC	FLying Capacitor
FPGA	Field Programmable Gate Array
IGBT	Insulated Gate Bipolar Transistor
IGCT	Integrated Gate Commutated Thyristor
ISC	Indirect Stator Control
NPC	Neutral Point Clamped
PI	Proportional-Integral (controller)
PWM	Pulse Width Modulation

PS-PWM	Phase-Shift Pulse Width Modulation
PD-PWM	Phase-Disposition Pulse Width Modulation
SCHB	Series Connected H-Bridge
SPM	Space Phasor Modulation
VSI	Voltage Source Inverter

0. INTRODUCTION

Medium voltage inverter technology has experienced a fast growth in areas of power generation, power transmission and distribution and in a wide variety of applications such as traction, rolling mills, and in the marine, chemical and mining industry. Thanks to the development of high voltage IGBTs and IGCTs and the introduction of multilevel voltage source inverter topologies, higher nominal voltages and power ratings were possible. The use of these technologies enabled also system improvements such as an increased reliability, a higher dynamic performance of the drive, extended operation range and reduced harmonic contents in the line-to-line voltages and in the phase motor currents. For these reasons, voltage source inverters constitute a better alternative in many applications in the range of 300kVA-30MVA, instead of other older technologies such as the current source inverter.

Besides the conventional two level inverters, the majority of manufacturers offer multilevel inverters with different topologies for medium voltage applications. The most common topology used in industrial drives is the three-level Neutral Point Clamped (NPC) inverter, whereas for higher voltage applications the four level Flying Capacitor (FLC) and the multilevel Series Connected H-Bridge (SCHB) inverter with five, seven and nine levels also find a niche in the market [1]. More recently, multilevel inverters are also offered for high performance low voltage applications, in particular those where the torque ripple detracts the quality of the process or a very high speed is required.

The state of the art control techniques of induction machines are implemented in industrial multilevel inverters, that is, the field oriented control and the Direct Torque Control (DTC). Both control schemes attain an excellent torque dynamics, being the main difference the performance of the control strategy in field weakening region. The classical field oriented control considers the inverter as an ideal voltage amplifier and it uses the rotor flux to define the reference frame for the control of the currents. In contrast, the DTC takes into account the discrete nature of the inverter to control the trajectory of the stator flux by using bang-bang controllers. The stator flux can be modified quickly by the voltage, which is advantageous for the operation in field weakening as the torque dynamic response can be increased by using techniques such as the Dynamic Field Weakening [2]. For this reason, stator flux oriented control schemes are preferable in applications where the machine operates in this condition.

A relevant topic of study in multilevel inverters is the fault tolerant operation. In comparison with other topologies, multilevel inverters offer multiple freedom degrees which can be used to permit the operation of the drive with faulty elements. Specially suited for fault tolerant

operation are the topologies with a high number of levels, such as the FLC and the SCHB. Since one cell of the inverter contributes only to a small part of the inverter phase potential generation, the bypass of one cell does not affect significantly the voltages delivered to the machine. As a result, the reliability of the drive can be increased, despite of the higher number of power switches and components in comparison to the three-level NPC topology.

The industrial SCHB inverter offers the possibility of bypassing the faulty cells and replacing them with redundant ones [3]. The bypass of a faulty cell is carried out by a switch, which isolates it from the load and at the same time preserves the current path in the corresponding phase, as is described in [4]. In this way, the operation of the inverter with a reduced number of cells is possible at reduced output voltage, which is still advantageous so as to maintain the production in a minimum level and avoid higher costs associated to a standstill condition.

Because the topology of the inverter changes after the occurrence of a fault, a voltage unbalance can be produced if no other actions in the control are carried out. The easiest solution to this problem consists in bypassing the same number of cells in each phase, in order to obtain a balanced inverter configuration. The disadvantage of this approach is however, that healthy cells are being bypassed to force the condition of balanced load. A better utilization of the available healthy cells could be obtained by means of the phase shift reference method described in [5]. This method assumes that there is no physical connection between the neutral point of the inverter and the neutral point of the machine; in this way by using the maximum phase potential and an appropriate phase shift of the references, balanced line-to-line voltages can be obtained with an unsymmetrical inverter topology and by bypassing only the faulty cells. The main disadvantage of the reference shift approach is that the addition of third harmonic is not considered; therefore the inverter capacity for voltage generation is not fully utilized.

An alternative method for the fault tolerant operation considers the use of the so called Space Phasor Modulation (SPM) for multilevel inverters. This modulation scheme extends the principles used for the classical SPM of two-level inverters to multilevel inverters, generating output voltages with a very low harmonic distortion. It was recently demonstrated that some PWM methods with an adequate third harmonic injection achieve a similar performance to the SPM schemes [6], however the increase of the computational capacity in microprocessors in conjunction with the development of FPGAs make nowadays the real time implementation of this algorithm an affordable alternative. Additionally, the use of voltage space phasors provides an alternative approach to study different inverter fault configurations and apply the optimal remedial action. Although the idea of using a space phasor modulator for fault

tolerant operation is not new [7], the main contributions of this work are the study of different fault cases and the development of a strategy which enhances the performance of the multilevel inverter with the remaining healthy cells.

This work is structured as follows: in chapter 1 and 2 the fundamentals about the induction machine model, the most common multilevel inverters topologies and a description of the stator flux oriented control are summarized. In chapter 3, the algorithm of an optimized space phase modulator for a SCHB multilevel topology is presented. In chapter 4, different strategies for fault tolerant operation will be analyzed, including a new approach based on voltage space phasors. The modulator is also optimized to obtain the maximum output voltage of the inverter and to keep the commutation frequency of the power switches at nominal levels. The restrictions of the control strategy caused by the operation at lower voltages are also analyzed. In chapter 5, experimental results are obtained with a 5-level H-bridge inverter prototype, in order to validate the technical feasibility of the proposed methods for the fault-tolerant operation.

1. FUNDAMENTALS

This chapter presents some fundamental concepts that will be used in this work. A brief description of the induction machine equations and of the most common multilevel inverter topologies shall be given.

1.1 Space Phasors

The space phasor theory presented by Kovacs [8] provides a powerful tool for the description of the dynamic behaviour of three phase machines. This theory is based on the idea that the revolving field generated by currents in symmetrically spatially distributed windings can be represented by a space phasor pointing to the maximum magnetic flux wave density. Due to the relationship existing between fluxes, currents and voltages, this concept can be extended to other quantities in the machine. In general, the instantaneous values of a three-phase quantity Z can be summarized in the complex space phasor form as follows:

$$\underline{Z}(t) = Z_\alpha(t) + jZ_\beta(t) = \frac{2}{3} (\underline{a}^0 Z_u(t) + \underline{a}^1 Z_v(t) + \underline{a}^2 Z_w(t)), \quad (1.1)$$

where $\underline{a} = e^{j2\pi/3}$ is the spatial operator. The space phasor is usually expressed in the real and imaginary components as:

$$\left. \begin{aligned} Z_\alpha(t) &= \frac{1}{3} (2Z_u(t) - Z_v(t) - Z_w(t)) \\ Z_\beta(t) &= \frac{1}{\sqrt{3}} (Z_v(t) - Z_w(t)) \end{aligned} \right\}, \quad (1.2)$$

which can be interpreted as the quantities generated by a simplified machine model with two orthogonal phase-windings. Under the assumption of a three-phase system without zero sequence components, i.e.

$$Z_0(t) = \frac{1}{3} (Z_u(t) + Z_v(t) + Z_w(t)) = 0, \quad (1.3)$$

the space phasor defined in (1.1) contains the complete information for the description of the three-phase system. This allows the calculation of the original three-phase quantities out of the projections on the respective phase windings axis as follows:

$$\left. \begin{aligned} Z_u(t) &= Z_\alpha(t) \\ Z_v(t) &= -\frac{1}{2}Z_\alpha(t) + \frac{\sqrt{3}}{2}Z_\beta(t) \\ Z_w(t) &= -\frac{1}{2}Z_\alpha(t) - \frac{\sqrt{3}}{2}Z_\beta(t) \end{aligned} \right\} \quad (1.4)$$

On the contrary, the zero sequence component $Z_0(t)$ has to be added to fully describe the three-phase system:

$$\left. \begin{aligned} Z_u(t) &= Z_\alpha(t) + Z_0(t) \\ Z_v(t) &= -\frac{1}{2}Z_\alpha(t) + \frac{\sqrt{3}}{2}Z_\beta(t) + Z_0(t) \\ Z_w(t) &= -\frac{1}{2}Z_\alpha(t) - \frac{\sqrt{3}}{2}Z_\beta(t) + Z_0(t) \end{aligned} \right\} \quad (1.5)$$

1.2 Induction Machine Model

The standard model of the induction machine, which includes differential equations for each phase, will be simplified by using the previously described space phasor representation. The following assumptions will be used for this model:

- a) Only the fundamental wave of the air gap field will be considered in the calculation of the inductances.
- b) The neutral point of the motor is not connected, i.e. there are no zero sequence components.
- c) The machine has symmetrical three-phase windings, i.e. no phase misalignments.
- d) There are no eddy currents or core losses in the stator and in the rotor of the motor.
- e) Temperature dependence and the iron saturation will not be considered. Resistances and inductances will be assumed constant.

The model of the induction machine is usually referred to a coordinate system, which usually depends on the working principle of the control scheme. For stator flux oriented control, two coordinate systems are usually employed; the first one coupled to the stator, also known as $\alpha\beta$ -system, and the second one coupled to a rotating frame attached to the stator flux space phasor, which it is known as dq-system. Considering the relationships between the angles of the stator axis, the rotor axis and the reference system depicted for the simplified two poles machine model in Fig.1.1, the following set of equations in the $\alpha\beta$ -system are obtained:

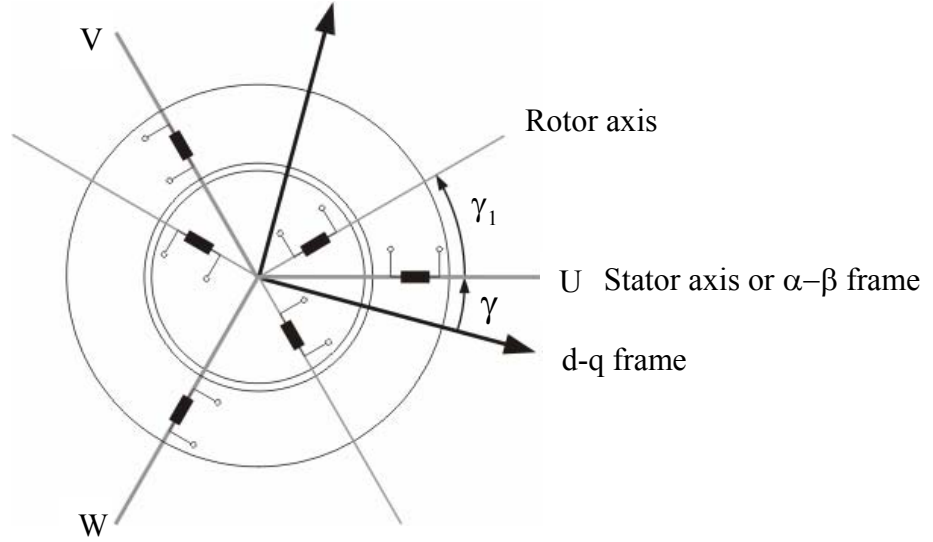


Fig. 1.1 Simplified two-poles induction machine model and angular relation between the stator or α - β frame, the rotor frame and the d-q frame.

$$\underline{u}_1 = R_1 \dot{\underline{i}}_1 + \frac{d\underline{\Psi}_1}{dt} \quad (1.6)$$

$$0 = R_2 \dot{\underline{i}}'_2 - j\dot{\gamma} \underline{\Psi}'_2 + \frac{d\underline{\Psi}'_2}{dt} \quad (1.7)$$

$$\dot{\underline{i}}_1 = \frac{1}{\sigma L_1} \underline{\Psi}_1 - \frac{L_h}{\sigma L_1 L'_2} \underline{\Psi}'_2 \quad (1.8)$$

$$\dot{\underline{i}}'_2 = \frac{1}{\sigma L'_2} \underline{\Psi}'_2 - \frac{L_h}{\sigma L_1 L'_2} \underline{\Psi}_1 \quad (1.9)$$

The same equations for a frame of coordinates rotating with frequency $\omega_1 = -\dot{\gamma}_1$ with respect to the stator, is given by:

$$\underline{u}_1 = R_1 \dot{\underline{i}}_1 + j\omega_1 \underline{\Psi}_1 + \frac{d\underline{\Psi}_1}{dt} \quad (1.10)$$

$$0 = R_2 \dot{\underline{i}}'_2 + j(\omega_1 - \dot{\gamma}) \underline{\Psi}'_2 + \frac{d\underline{\Psi}'_2}{dt} \quad (1.11)$$

$$\dot{\underline{i}}_1 = \frac{1}{\sigma L_1} \underline{\Psi}_1 - \frac{L_h}{\sigma L_1 L'_2} \underline{\Psi}'_2 \quad (1.12)$$

$$\dot{\underline{i}}'_2 = \frac{1}{\sigma L'_2} \underline{\Psi}'_2 - \frac{L_h}{\sigma L_1 L'_2} \underline{\Psi}_1 \quad (1.13)$$

The electrical and the mechanical quantities of the induction machine are connected through the electrical torque equation, which can be expressed in different ways, depending on the available quantities:

$$M = \frac{3}{2} p \cdot \text{Im} \{ \underline{\Psi}_1^* \cdot \underline{i}_1 \} \quad (1.14)$$

$$M = \frac{3}{2} p \cdot \text{Im} \{ \underline{\Psi}'_2^* \cdot \underline{i}_2 \} \quad (1.15)$$

$$M = \frac{3}{2} p \cdot \frac{L_h}{\sigma L'_2 L_1} \{ \underline{\Psi}_1 \cdot \underline{\Psi}'_2^* \} = \frac{3}{2} p \cdot \frac{L_h}{\sigma L'_2 L_1} |\underline{\Psi}_1| |\underline{\Psi}'_2| \sin(\vartheta) \quad (1.16)$$

The mechanical angular velocity $\omega_{\text{mech}} = \dot{\gamma}_{\text{mech}}$ is defined as a function of the electrical angular velocity $\dot{\gamma}$ and the number of pairs of poles p :

$$\dot{\gamma}_{\text{mech}} = \frac{\dot{\gamma}}{p} \quad (1.17)$$

Finally, the mechanical equation completes the description of the system:

$$M - M_L = J \cdot \frac{d\omega_{\text{mech}}}{dt}, \quad (1.18)$$

where M_L is the load torque and J the moment of inertia of the machine.

1.3 Multilevel Inverter topologies

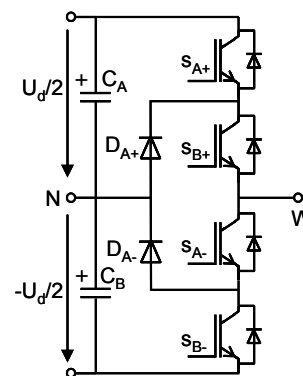
The synthesis of an output voltage waveform with several levels is a rather old concept, being possible to find references in the sixties [9]. In contrast with the two-level inverter, multilevel topologies have the ability to synthesise a stepped output waveform with three or more levels, reducing in this way the distortion in the currents. Furthermore, it was found that the resulting output voltage could be increased beyond the voltage rating of the individual power switches, making the topology particularly useful in medium voltage applications. The most attractive features of multilevel converters can be summarized as follows:

- They produce stepped output voltages with low distortion.
- They can generate phase potentials with low zero sequence components, reducing in this way motor bearings stresses [10].
- Using the same power switches, they can achieve output voltages with a higher carrier frequency than a two level inverter. This is especially important in medium voltage applications, where the power switches are commutated relatively slow in order to keep the switching losses within allowable ranges (275 Hz - 1475 Hz).

Three different topologies have been proposed for multilevel inverters: the neutral point clamped topology, the capacitor clamped inverter or flying capacitor inverter, and the series connected H-bridge multilevel inverter. The main features of each topology will be presented in the following sections.

1.3.1 Neutral Point Clamped Voltage Source Inverter (NPC-VSI)

The three-level NPC topology is broadly extended in commercial applications and it is supplied by the most important converter manufacturers [1]. The simplest version of this inverter splits the DC-link voltage into three-levels using two series connected capacitors C_A and C_B as it is shown in Fig. 1.2 for one phase of this inverter. Considering the middle point N of the two capacitors as the neutral point, each phase can generate three different states: $U_d/2$ when the switches S_{A+} and S_{B+} are turned on, 0



Output u_{WN}	Switch State: [S_{A+} S_{B+}]
$U_d/2$	[1 1]
0	[0 1]
$-U_d/2$	[0 0]

Fig. 1.2. One phase of a three-level NPC inverter and the corresponding switching table

when the switches S_{A-} and S_{A+} are turned on and $-U_d/2$ when the switches S_{A-} and S_{B-} are turned on. The notation S^- and S^+ is introduced to point out that the operation of the switches is complementary.

Key components in this inverter are the diodes D_A and D_B which clamp the phase potential to half the level of the DC-link when the switches S_{A-} and S_{B+} are turned on. The clamp diodes make the implementation of this topology complicated for inverters with more than three levels. As it is shown in Fig. 1.3-a, the voltage ratings of the diodes must be increased to accomplish the reverse blocking in a five level NPC. This can be illustrated for the diode D_{A-} from Fig. 1.3-a. When the devices S_{A-} , S_{B-} , S_{C-} and S_{D-} are turned on for the generation of a voltage $-U_d/2$, the diode needs to block the voltage of the three capacitors C_B , C_C , C_D . Another disadvantage is the unequal switching rating, as it can be seen in the switching table of figure 1.3-a. S_{A+} conducts only when the output is $U_d/2$, whereas the switch S_{D+} conducts over the entire cycle except when the output is $-U_d/2$. Moreover, the NPC inverter requires a coordinated turn-off sequence and a voltage balancing strategy.

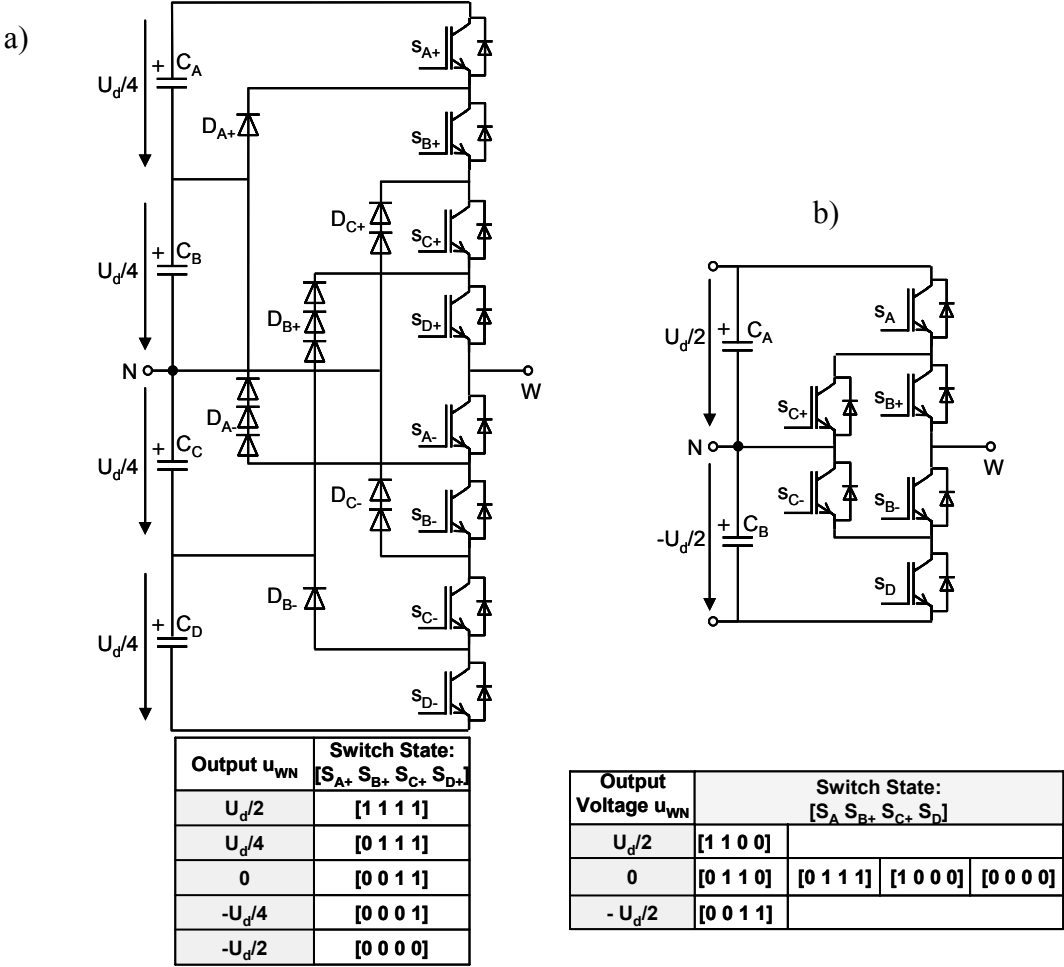


Fig.1.3. One phase of a NPC inverter and the respective switching table: a) five-level inverter, b) three-level ANPC.

The unequal loss distribution of the power switches can be substantially improved, if the diodes are combined with active switches in both NPC branches (Fig. 1.3-b). The corresponding circuit configuration is called three-level Active Neutral Point Clamped inverter (3L-ANPC) [11]. This configuration allows the flow of a positive or negative phase current through the upper and the lower NPC path respectively, if the switches S_{B+} and S_{C+} or S_{B-} and S_{C-} are turned on. In contrast to a conventional three-level NPC, the three-level ANPC topology has several switching states which can be used to distribute the switching losses among the power semiconductors.

1.3.2 Flying Capacitor Voltage Source Inverter (FLC-VSI)

The flying capacitor topology is a recent development with patents dating from the nineties [12]. This inverter consists of several independent floating capacitors charged at a predefined voltage. The operation of this inverter can be explained using the simplified three-level leg

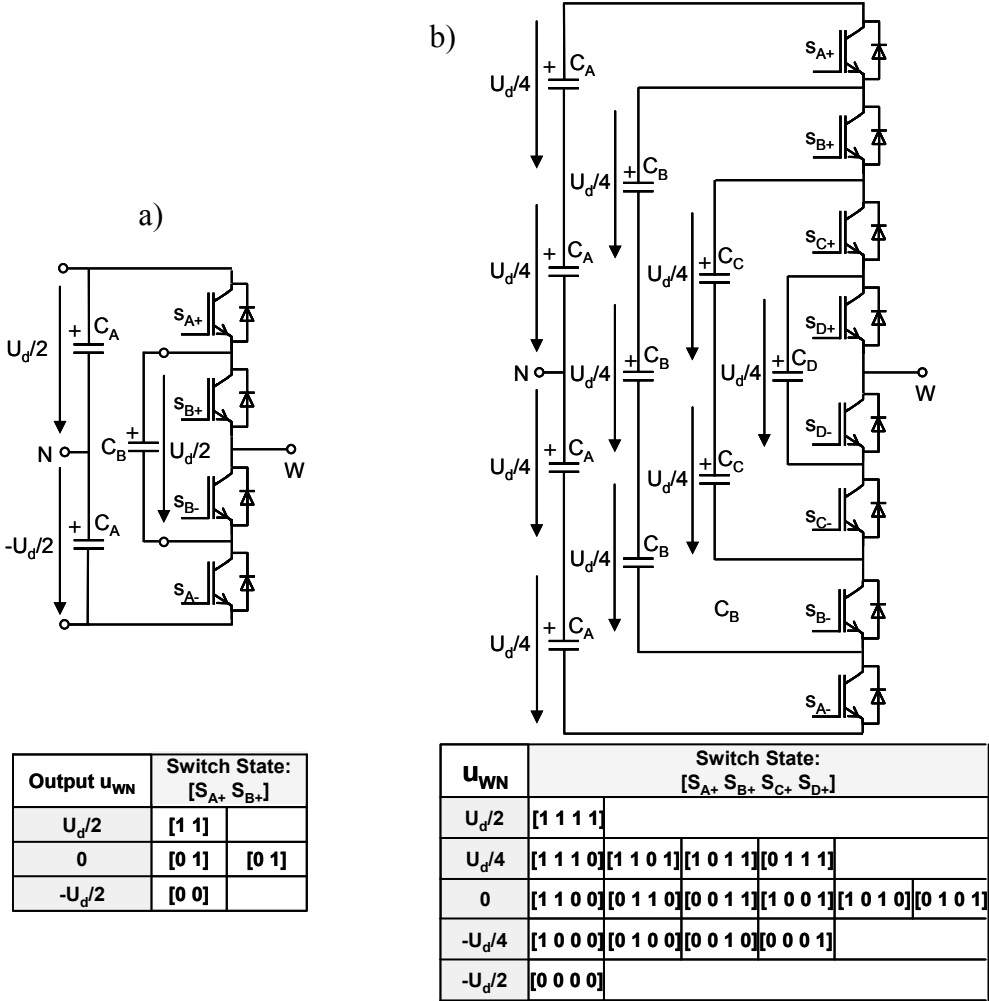


Fig.1.4. FLC-VCI topology with their respective switching tables; a) three-level inverter, b) five-level inverter.

depicted in the Fig. 1.4-a: for a voltage $U_d/2$, the switches S_{A+} and S_{B+} are turned on, whereas for the negative output $-U_d/2$ the complementary switches S_{A-} and S_{B-} are turned on. A voltage zero in the output is produced by two different switching states, either the pair S_{A+} , S_{B-} turned on, or the pair S_{B+} , S_{A-} turned on. The five-level leg operates in the same way as the three-level version: the turn-on of all upper switches produces the maximum output voltage, whereas the minimum voltage is obtained by turning on the complementary transistors. More than one switching state is available for the intermediate voltage levels. For example, a voltage $+3U_d/4$ can be achieved by four different switching states: $S_{A+}, S_{B+}, S_{C+}, S_{D-}$ / $S_{A+}, S_{B+}, S_{C-}, S_{D+}$ / $S_{A+}, S_{B-}, S_{C+}, S_{D+}$ / $S_{A-}, S_{B+}, S_{C+}, S_{D+}$. Other available switching states and their respective output voltage are summarized in the table shown in Fig. 1.4-b.

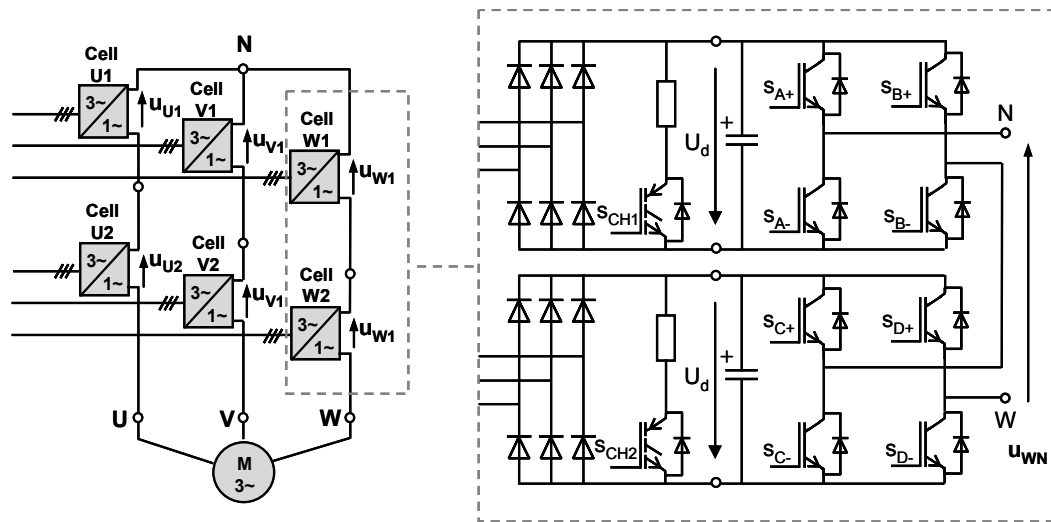
The high number of freedom degrees is an advantage of this topology in comparison with the NPC, given that the firing pulses can be distributed in higher number of switches. Depending on the way that each capacitor is connected to the output, it can be charged or discharged; obtaining in this way a method to balance the voltage in the DC-links.

1.3.3 Multilevel Serial Connected H-Bridge Voltage Source Inverter (SCHB)

References about the series connection of separated half-bridge inverters can be traced back to 1975 [13]. Although the idea was conceived earlier than the other topologies, the applications of the multicell topology did not prevail until middle of the nineties. Fig. 1.5 shows the circuit for one phase of the inverter and the different switching states. Each single cell of the inverter generates three different voltages in the output $+U_d$, 0 , $-U_d$. Additional cells can be connected in series in order to add more levels. Commercial versions of this inverter are available starting from three cells per phase and use Low Voltage IGBTs (LV-IGBT) as switching devices ($U_{ce} < 1700$ V). The multicell topology has as many degrees of freedom as the capacitor clamped inverter, but they do not require a voltage DC-link balance method since each cell includes an independent power supply.

Each cell of the SCHB inverter is powered by an independent rectifier connected to the secondary side of an isolation transformer. The secondary windings of these transformers are phase-shifted in order to cancel the harmonics of high frequency in the mains currents [14].

A 5-level SCHB converter will be considered in this work. Since the diode rectifier in the input of each cell does not permit regeneration, a chopper will be included in each cell to enable the braking. The power switches devices will be considered ideal and other phenomena such as the voltage drop and the dead time will be neglected.



u_{WN}	Switch State: [S_{A+} S_{B+} S_{C+} S_{D+}]					
	$-2U_d$	[1 0 1 0]				
$-U_d$	[1 0 0 0]	[0 0 1 0]	[1 0 1 1]	[1 1 1 0]		
0	[0 0 0 0]	[0 0 1 1]	[1 1 1 1]	[1 1 0 0]	[1 0 1 0]	[0 1 0 1]
U_d	[0 0 0 1]	[0 1 1 1]	[1 1 0 1]	[0 1 0 0]		
$2U_d$	[0 1 0 1]					

Fig.1.5. Circuit diagram of the 5-level multicell inverter topology and its corresponding switching table.

1.4 Summary of chapter 1

Multilevel inverters are found today in a wide range of applications, mainly related to high power and high frequency drives. Mainly, two characteristics make multilevel inverters ideal for those applications: first, they can generate output voltages with higher rating than the power switches being utilized, and second they offer redundancy degrees which can be used to reduce the switching frequency, and hence, the switching losses. Three common industrial multilevel topologies have been described in this chapter: the Neutral Point Clamped Voltage Source Inverter, the Flying Capacitor Voltage Source Inverter and the Multilevel Serial Connected H-Bridge Voltage Source Inverter. The first topology has been adopted as the standard commercial solution in three-level applications. Because the complexity of this topology increases with the number of levels, the NPC topology is impractical for more than five levels. In applications with a high number of levels the Flying Capacitor and the H-Bridge multilevel inverter offer a better compromise. Comparing both topologies, the H-Bridge inverter has the advantage that does not need a strategy for the voltage balancing, as each cell is independently fed by means of an isolation transformer. This transformer also enables the reduction of the currents distortion in the mains. In contrast with the NPC converters, which use high voltage power switches in high voltage applications, the high number of levels in the H-Bridge topology permits the use of low voltage IGBTs.

The fundamental equations about the induction machine and the space phasor theory have been also summarized in this chapter. They will be the basis for the description of the field oriented control strategy and for the multilevel space phasor modulation.

2. TORQUE AND FLUX CONTROL OF THE INDUCTION MACHINE

The control scheme used in this work is based on the Indirect Stator Control (ISC), which is a predictive control scheme based on the same principles as the Direct Self Control (DSC), i.e. the stator flux is guided through a defined trajectory, while the torque is governed by means of the angular position of the stator flux space phasor. Similar to the DSC and Direct Torque Control (DTC) schemes, the ISC has no underlaid current controllers. Using the concepts previously developed in [2],[15], a brief description of this control scheme will be given in the following sections.

2.1 Indirect Stator quantities Control (ISC)

Different from the conventional rotor flux field oriented control, where main quantities are the stator currents, the main goal of the ISC scheme is the control of the stator flux phasor. The choice of this variable lies in the fact that the stator flux can be directly influenced by the stator voltages to accomplish the basic aims of torque control. In order to explain this statement, a d-q reference frame coupled to the stator flux will be first considered. By neglecting the stator resistance, as this quantity is small compared to the rated phase winding impedance in high power machines, eq. (1.10) can be expressed in the following simplified form:

$$\underline{u}_1 \approx j\omega_1 \underline{\Psi}_1 + \frac{d\underline{\Psi}_1}{dt}, \quad R_1 \approx 0 \quad (2.1)$$

Given that in a stator flux oriented frame $\underline{\Psi}_1 = \Psi_{1d}$, the previous equation can be separated into the d and q components, as follows:

$$u_{1d} = \frac{d\Psi_{1d}}{dt} \quad (2.2)$$

$$u_{1q} = \omega_1 \Psi_{1d} \quad (2.3)$$

Both equations show that for an infinitely high switching frequency, there is a radial component of the stator voltage u_{1d} which determines the variation of the flux amplitude and a tangential component u_{1q} which affects the rotational frequency of this space phasor, as it is depicted in Fig. 2.1.

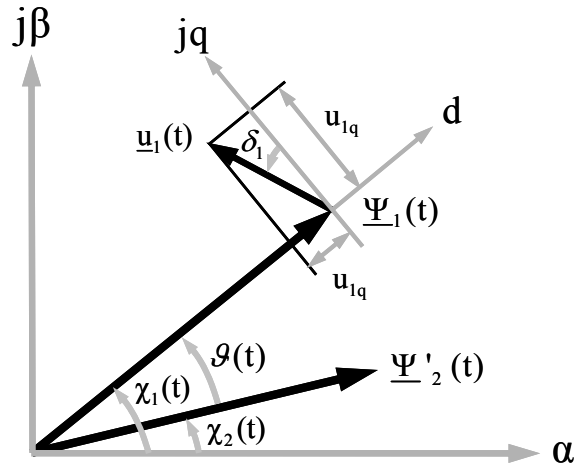


Fig. 2.1. Stator flux trajectory changes due to the d-q components of the voltage space phasor.

From eq. (1.16), it follows that the torque mainly depends on the angle $\vartheta = \chi_1 - \chi_2$ between both space phasor fluxes. Since the rotor flux angle χ_2 is mainly affected by the rotor speed $\dot{\lambda}$, which changes slowly at the mechanical time constant, a fast variation of the angle ϑ and, hence of the torque, can be obtained by modifying the rotational frequency $\dot{\chi}_1$ of the stator flux.

In the digital implementation, the values of the variables are considered at discrete time intervals and the modulator has a defined non-infinite switching frequency. In this case, the application of a predictive control structure using the same previously presented principles may be advantageous. By discretizing the continuous time eq. (1.6), and neglecting the stator resistance, it follows that the stator flux changes its amplitude and its angle at the next sampling time according to the mean values of the voltage space phasor over one modulation period Δt (Fig. 2.2):

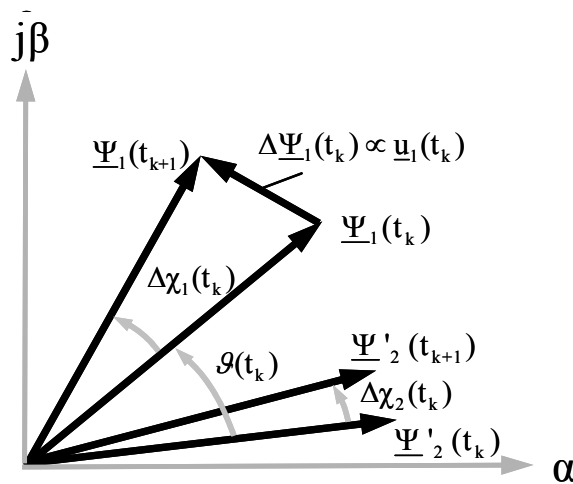


Fig. 2.2. Stator and rotor flux space phasor changes over one calculation period.

$$\tilde{u}_1(t_k) \approx \frac{\Delta \Psi_1(t_k)}{\Delta t} = \frac{\Psi_1(t_{k+1}) - \Psi_1(t_k)}{\Delta t} \quad (2.4)$$

By using this idea, the rather simple control scheme depicted in Fig. 2.3 can be developed. A controller with the torque error as input delivers the necessary torque-determining stator flux angle increment $\Delta\chi_1$, whereas a flux controller determines the variation of the stator flux magnitude by means of the stretching or shortening term $\Delta\Psi_1$. Since additional factors influence the torque, such as the rotor flux angle increment, a PI controller is more suitable to compensate the neglected dynamics of the model. From the information proportioned by the aforementioned controllers, a predicted value of the stator flux at the time instant t_{k+1} can be calculated as:

$$\Psi_1(t_{k+1}) = (1 + \Delta\Psi_1(t_k)) |\Psi_1(t_k)| e^{j(\Delta\chi_1(t_k) + \chi_1(t_k))}, \quad (2.5)$$

which is finally used to calculate the output voltage delivered to the modulator:

$$u_1(t_k) = i_1(t_k) \cdot R_1 + \frac{\Psi_1(t_{k+1}) - \Psi_1(t_k)}{\Delta t}. \quad (2.6)$$

The control scheme can be enhanced by including the neglected terms in the torque control loop. A first improvement is achieved by adding the rotor flux angle variation $\Delta\chi_2$ to the output of the torque controller as a feed forward, relieving in this way the controller's integral part. Since the angle variation $\Delta\chi_2$ is equal to the stator flux space phasor angle increment in steady state conditions, the PI-controller deals after the addition of the feed forward only with changes in the angle variation $\Delta\chi_1$, i.e. changes in the torque. The rotor flux angle increment $\Delta\chi_2$ is derived from the rotor flux space phasor in α - β coordinates, eq. (1.7) and eq. (1.15):

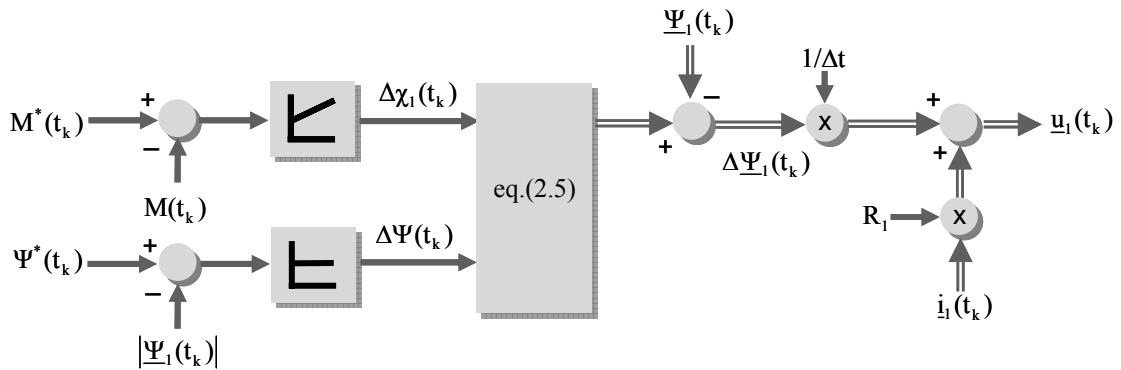


Fig. 2.3. Basic torque and flux controllers of the ISC.

$$\frac{d\chi_2(t)}{dt} = \frac{d}{dt} \left(\arctan \left(\frac{\Psi'_{2\beta}(t)}{\Psi'_{2\alpha}(t)} \right) \right) = \frac{1}{\Psi'^2_{2\alpha}(t) + \Psi'^2_{2\beta}(t)} \left(-\Psi'_{2\beta}(t) \frac{d\Psi'_{2\alpha}(t)}{dt} + \Psi'_{2\alpha}(t) \frac{d\Psi'_{2\beta}(t)}{dt} \right) \quad (2.7)$$

$$\frac{d\chi_2(t)}{dt} = \dot{\gamma}(t) + \frac{R'_2}{\Psi'^2_{2\alpha}(t) + \Psi'^2_{2\beta}(t)} \left(\Psi'_{2\beta}(t) i'_{2\alpha}(t) - \Psi'_{2\alpha}(t) i'_{2\beta}(t) \right) = \dot{\gamma}(t) + \underbrace{\frac{R'_2}{|\underline{\Psi}'_2(t)|^2} \frac{2}{3p} M(t)}_{\omega_2} \quad (2.8)$$

The term containing the torque $M(t)$ corresponds to the so called rotor frequency $\omega_2(t)$. Thus, for an interval of time Δt , the increment of rotor flux angle is given as a function of the electrical speed of the shaft $\dot{\gamma}(t)$ and the rotor frequency $\omega_2(t)$:

$$\Delta\chi_2 = (\dot{\gamma}(t) + \omega_2(t)) \cdot \Delta t \quad (2.9)$$

The resulting term $\Delta\chi_2$ is equal to the stator flux angle variation $\Delta\chi_{1_steady}$ in steady state. This expression can be approximated using the reference value of ω_2^* instead, which depends on the reference torque:

$$\Delta\chi_{1_steady} = \left(\dot{\gamma}(t) + \frac{R'_2}{|\underline{\Psi}'_2(t)|^2} \frac{2}{3p} M^* \right) \cdot \Delta t = (\dot{\gamma}(t) + \omega_2^*(t)) \cdot \Delta t. \quad (2.10)$$

Attending to the fact that the rotor frequency in steady state is directly related to the “torque generating” angle ϑ , an alternative control scheme is achieved by using the former to control the latter. The slip controller uses the difference between the reference and the calculated rotor frequency values to determine the dynamic angle increment $\Delta\chi_{1_steady}$ which will be added to the steady state angle variation previously calculated. The control scheme with these improvements is depicted in Fig. 2.4. A torque limitation is still necessary in order to not exceed the break-down value. The break-down torque can be calculated using the relationship between rotor flux magnitude and stator flux magnitude in steady state:

$$|\underline{\Psi}'_2| = |\underline{\Psi}_1| \cos(\vartheta), \quad (2.11)$$

in the torque equation:

$$M = \frac{3pL_h}{2\sigma L'_2 L_1} |\underline{\Psi}_1|^2 \cos(\vartheta) \sin(\vartheta) = \frac{3pL_h}{4\sigma L'_2 L_1} |\underline{\Psi}_1|^2 \sin(2\vartheta). \quad (2.12)$$

This expression reaches its maximum at $\vartheta = \pi/4$, and it depends on the magnitude of the stator flux space phasor:

$$M_b = \frac{3pL_h}{4\sigma L'_2 L_1} |\underline{\Psi}_1|^2 \Rightarrow \hat{\omega}_{2b}(|\underline{\Psi}_1|) \quad (2.13)$$

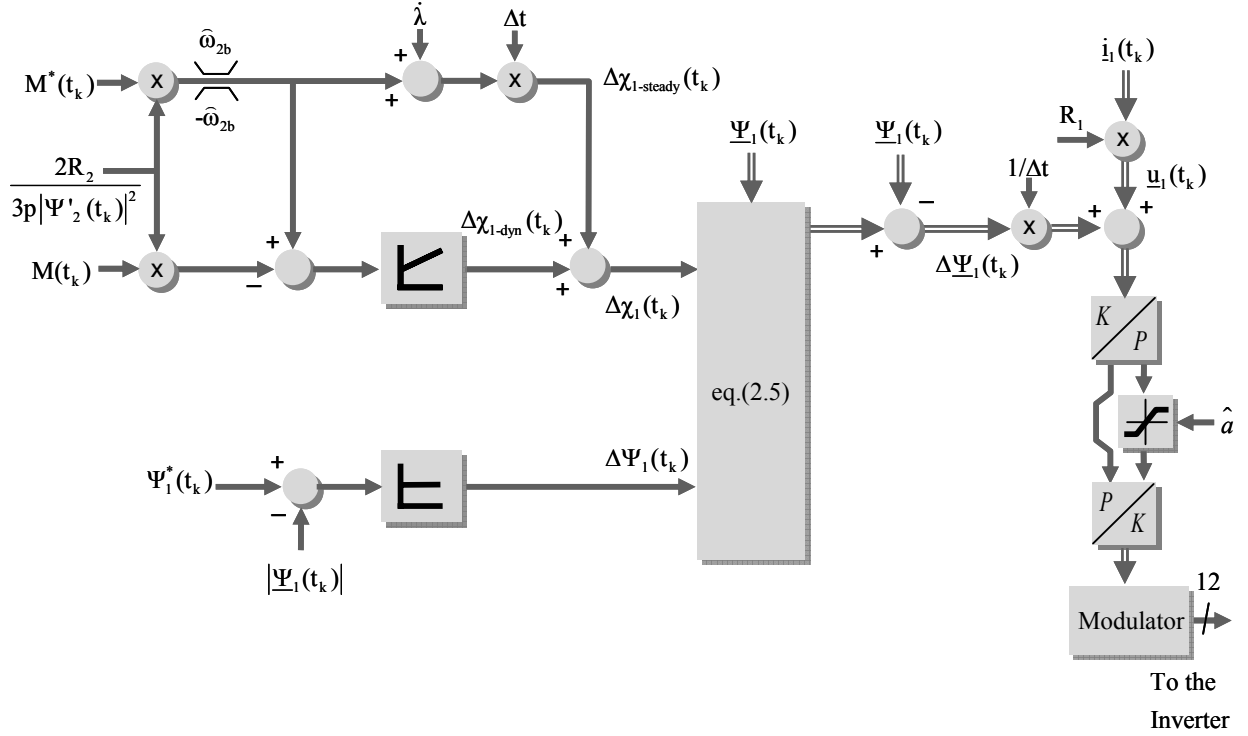


Fig. 2.4. ISC torque and flux controller including feed forward.

2.2 Operation in Field Weakening Region

In the usual design of drives, the starting point for field weakening operation is defined when the inverter reaches its maximum output voltage at rated speed operation. As the output voltage has reached the limit, the necessary angle increment $\Delta\chi_1$ for a torque change can not be gained if the stator flux is maintained at its rated value. Therefore, a reduction beyond the magnitude of the flux in this point is necessary, the so called field weakening range, in order to obtain higher stator flux frequencies. The available freedom degree of the space phasor voltage depicted in Fig. 2.1, the angle δ_1 , can be used to drive the stator flux space phasor to a trajectory with a lower magnitude than the nominal point. Because a change in the angle δ_1 affects both torque and flux simultaneously, the control of these variables in this operating point is not decoupled anymore.

The flux controller accomplishes two functions in the field weakening region: first, it defines a steady-state magnitude of the stator flux according to the steady-state value of the flux frequency $\Delta\chi_{steady}$ and, second, it can be used to generate the torque changes with higher dynamics. In the following, each of these functions will be explained.

2.2.1 Steady State Flux Weakening Magnitude

The flux magnitude in the field weakening region in steady state can be derived from eq. (1.10), under the assumptions of $R_1=0$ and constant stator flux magnitude, as:

$$\Psi_{\text{steady}}^*(t_k) = \frac{\hat{u}_1}{\dot{\lambda}_{1_steady}(t_k)} = \frac{\hat{u}_1}{\dot{\lambda}(t_k) + \omega_2(t_k)} \quad (2.14)$$

where \hat{u}_1 is the maximum amplitude of the stator fundamental voltage. For the sake of clarity, the calculated value will be normalized with respect to the nominal flux Ψ_{1N} as follows:

$$K_{\text{steady}} = \frac{\Psi_{\text{steady}}^*(t_k)}{\Psi_{1N}} = \frac{\hat{u}_1 / \dot{\lambda}_{1_steady}(t_k)}{\hat{u}_1 / \omega_{1N}} = \frac{\omega_{1N}}{\dot{\lambda}_{1_steady}(t_k)} = \frac{\omega_{1N}}{\dot{\lambda}(t_k) + \omega_2(t_k)}, \quad K_{\text{steady}} \leq 1 \quad (2.15)$$

By using the iterative algorithm described in [2], the stator resistance R_1 and the stator currents can be taken into account for the calculation of the flux with more precision. In this work only this simple approach will be implemented.

2.2.2 Dynamic Field Weakening Factor

As it was previously explained, a stator flux frequency increment, i.e. a torque increment, can be gained through a change in the angle δ_1 of the voltage space phasor. This basic torque generating mechanism shall be explained using Fig. 2.5. At the starting point with nominal speed $\dot{\lambda}$, both space flux phasors $\underline{\Psi}_1(t_k)$ and $\underline{\Psi}_2(t_k)$ have the same rotational speed. During a motoring torque transition, the stator flux must be weakened to the steady state trajectory with amplitude Ψ_{steady}^* . The fastest way to reach this track and at the same time to gain the angle difference $\Delta\theta$, is the use of a straight trajectory. Due to the fact that the flux is weakened by a factor K smaller than the steady state factor K_{steady} , the name “dynamic flux weakening” is

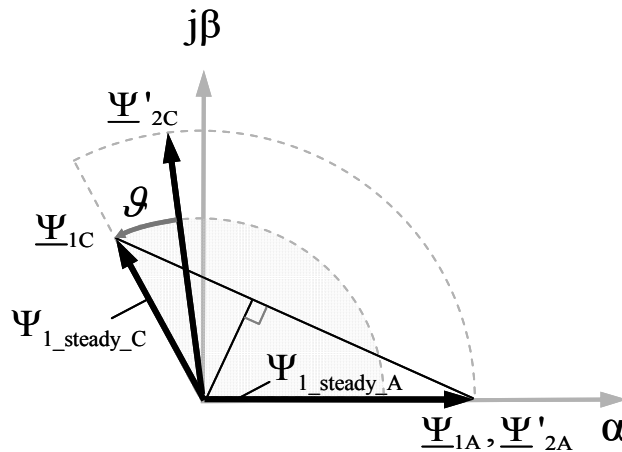


Fig. 2.5. Ideal stator flux trajectory for dynamic field weakening.

used. A direct application of this strategy is not possible, since the equations needed to determine the optimal trajectory are difficult to calculate in real time. Instead, a proportional controller presented in [15], can be used to obtain a similar short-cut effect. In this way, the dynamic flux weakening factor is obtained out of the output of the torque and a gain factor k_v :

$$K_{\text{dyn}} = 1 - k_v \Delta \chi_{l_{\text{dyn}}}, \quad K_{\text{dyn}} \leq 1. \quad (2.16)$$

By means of this factor, the trajectory of the stator flux is not modified as a straight line, but the short-cut effect is obtained through the extra reduction of the stator flux magnitude. This can be observed in the Fig. 2.6 for a torque transition at nominal output voltage. The magnitude of the flux is reduced in an extra degree during the torque transition, until the steady state value is reached.

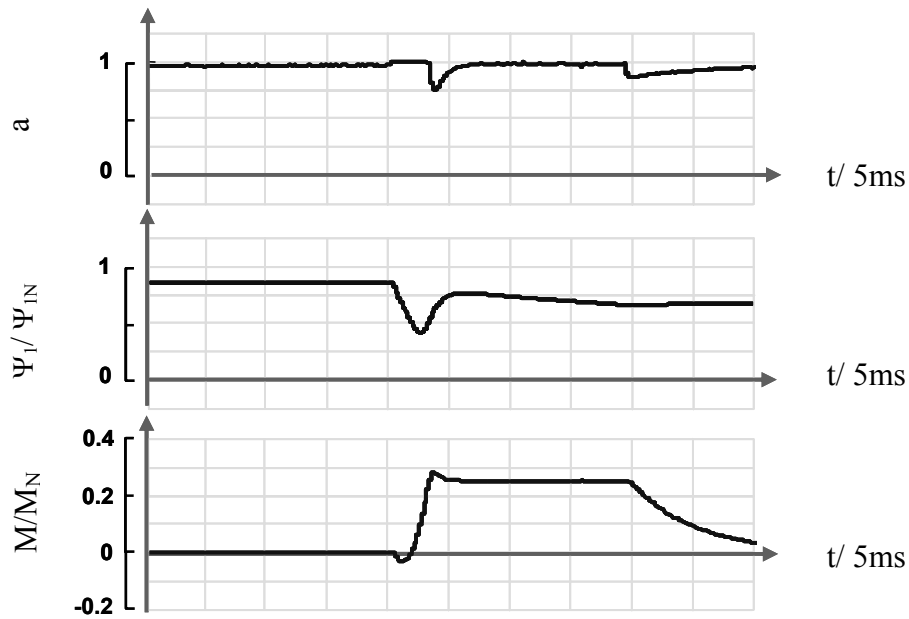


Fig. 2.6. Modulation index a and stator flux magnitude for a torque step with ω_{mech} equal to 115% of the nominal value (no load torque).

An important aspect to be considered is that without saturation, the output of the flux weakening controller could decrease the stator flux magnitude near to zero, causing stator currents near to the short circuit values. This condition can be avoided by limiting the maximum possible angle δ in the output of the flux controller. The operation of the dynamic

flux controller must be disabled during regenerative break operation, as the torque can be produced by reducing the output voltage. This constraint can be expressed as follows:

$$K_{\text{dyn}} = 1 - \text{sign}(\omega_{\text{mech}}) \cdot k_v \Delta\chi_{1_dyn} \quad K_{\text{dyn}} \leq 1 \tag{2.17}$$

Finally, the ideas presented for the stator flux controller with field weakening capability are summarized in the diagram shown in fig. 2.7.

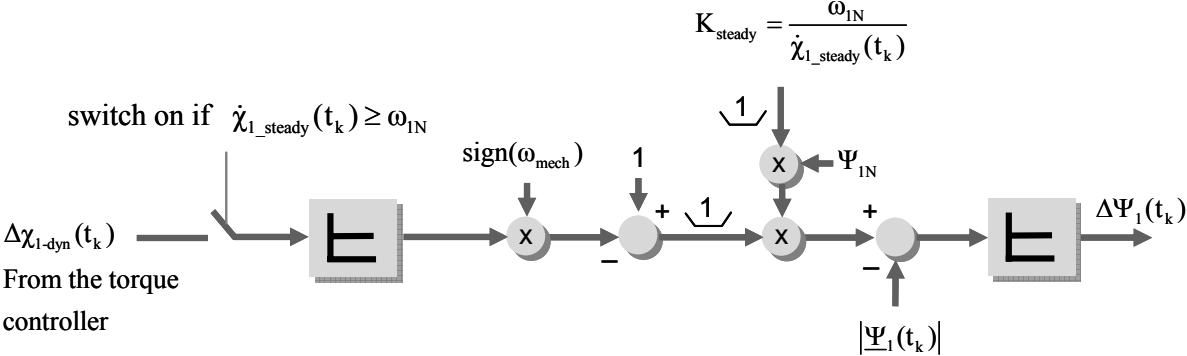


Fig. 2.7. Extended flux controller for operation in the field weakening region.

2.3 Summary of chapter 2

A stator flux field oriented control scheme has been presented in this chapter. This control is based on the prediction of the stator flux space phasor according to the requirements of the torque and flux references. The electromagnetic torque is generated increasing or decreasing the rotational speed of the stator flux space phasor, changing in this way the torque-producing angle between rotor and stator flux. The rotational speed of the stator flux phasor is obtained out of the torque error by means of a PI controller with a feed-forward. With a precise model of the machine, the torque dynamic is given by the PI controller, whereas the steady state value is delivered by the feed-forward.

Compared with the standard rotor flux field oriented control, the main advantage of this control scheme is the capability to increase the dynamics of the torque in field weakening operation. In this operating mode the output voltage has reached the limit and there is only a small reserve which can be used to increase the torque. An improvement can be achieved by using a “short-cut” in the stator flux trajectory which drives the stator flux space phasor faster to the new steady state operation point. This is obtained in the practical implementation by subtracting the output of the torque controller to the reference of the flux controller. In this way, the magnitude of the stator flux is reduced to a lower value than the steady state reference, and the short-cut effect is achieved. This is especially important for applications which operate in the field weakening range. This is the case in a fault tolerant inverter.

3. MODULATION METHODS FOR SCHB MULTILEVEL INVERTERS

The standard modulation method in commercial versions of the SCHB multilevel inverter is the Phase-Shift PWM (PS-PWM) [14]. A simple implementation and the operation of the power switches at constant commutation frequency are the most relevant features of this modulation method; however, it exhibits an inferior harmonic distortion in comparison to other strategies such as the Phase-Disposition PWM (PD-PWM) and the Space Phasor Modulation (SPM) [6]. Other interesting modulation methods are based on the selective harmonic elimination to generate a stepped output waveform with power switches commutating only at fundamental frequency [16]. In the following, the Phase-Shift PWM and the SPM methods will be analyzed, as well as enhancements dealing with the sequence selection and the firing pulses generation for the 5-level SCHB multilevel inverter.

3.1 Phase-Shift PWM (PS-PWM).

The Phase-Shift PWM is based on the unipolar PWM for single phase H-bridge inverters. As it is illustrated in Fig. 3.1 for the case of one cell, the firing pulses for the two legs in the H-bridge inverter are obtained comparing the triangular carrier signal u_c with the voltage references u_{U1}^* and $-u_{U1}^*$. The resulting output voltage waveform u_{U1} presents three-levels, as it is shown in Fig. 3.1.b.

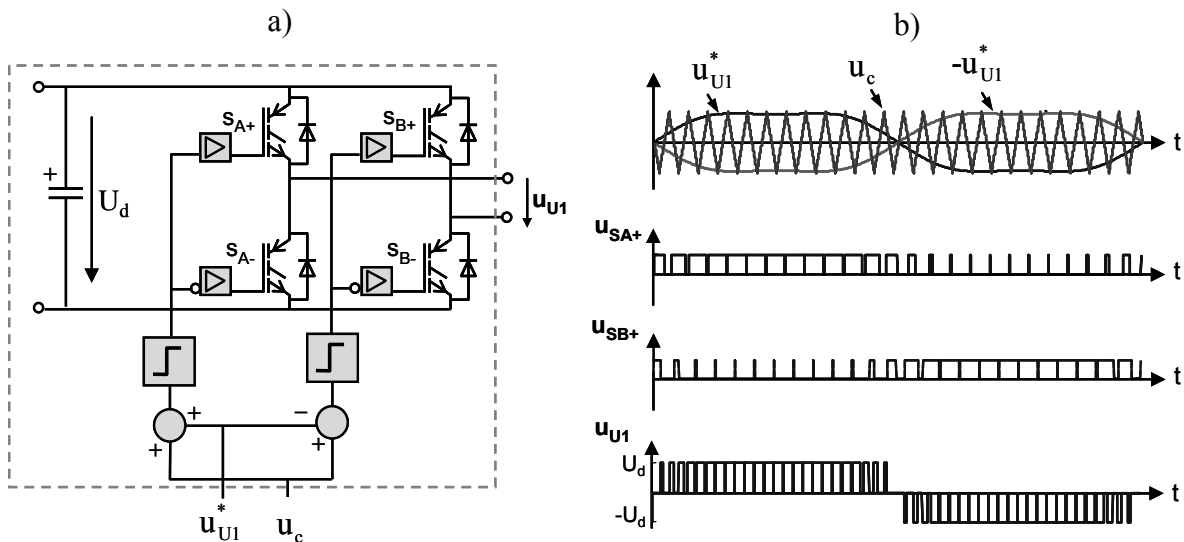


Fig. 3.1. Unipolar PWM for H-bridge inverter; a) block diagram including the PWM modulator; b) carrier waveform u_c and voltage references u_{U1}^* , $-u_{U1}^*$, firing pulses u_{SA} and u_{SB} and output voltage u_{U1} .

The series-connection of several cells allows the generation of an output voltage with additional voltage levels, provided that the carrier of each cell includes a proper phase shift. It has been determined that a phase shift equal to:

$$\Delta\phi_y = 180^\circ / N_{\text{cell}} \quad (3.1)$$

where N_{cell} is the number of cells in each phase, generates the output voltage waveform with the lowest possible distortion. In addition, the simultaneous switching of cells pertaining to different phases can be reduced by adding a phase-shift between the phase carriers equal to:

$$\Delta\phi_x = \Delta\phi_y / N_{\text{cell}} \quad (3.2)$$

In this way, the number of double steps in the line-to-line voltage waveform is reduced improving the quality of the output voltage waveform.

In particular, for the case of the 5-level inverter the resulting phase shift for each cell is indicated in Fig. 3.2.a. The output voltage waveforms u_{W1} and u_{W2} with the resulting 5-level phase potential u_{WN} , and the line to line voltage u_{WU} are illustrated in Fig. 3.2.b. It can be observed from this figure, that the double steps in the line-to-line voltage u_{WU} are not completely eliminated. This problem does not exist with the SPM method, as it will be explained in the next section.

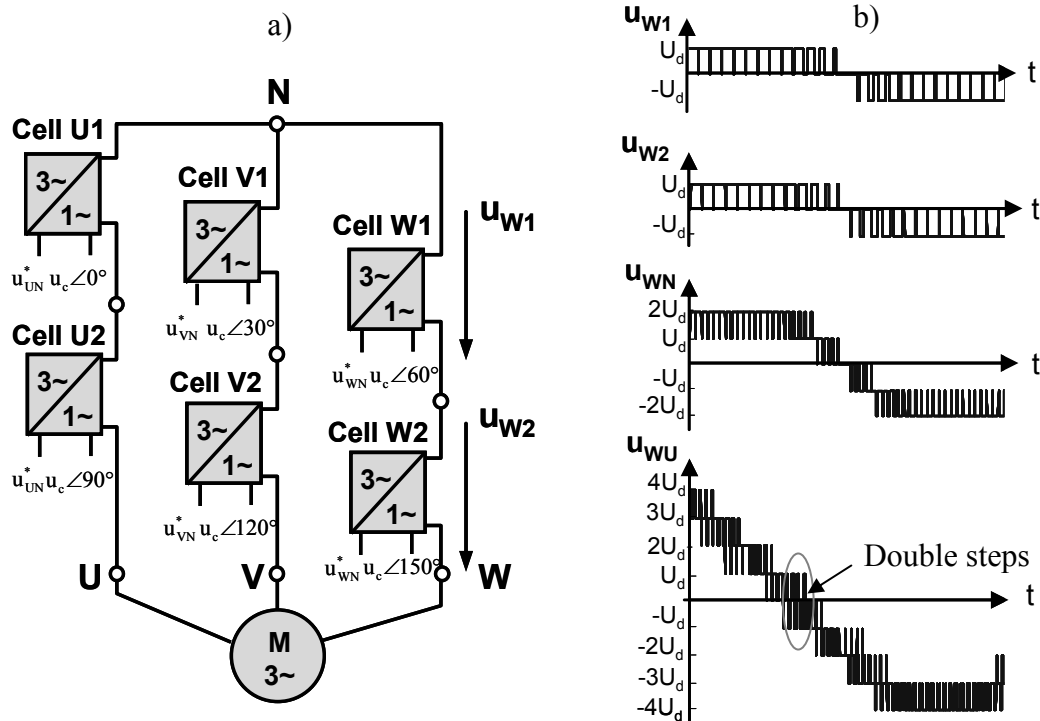


Fig. 3.2. Five level SCHB multilevel inverter including the references voltages and carrier signals for a PS-PWM; a) Block diagram of a 5-level inverter with the corresponding phase shift for the carriers; b) Output waveforms of two cells for the phase W and the equivalent phase voltage.

3.2 Space Phasor Modulation (SPM)

The high number of freedom degrees in multi-level inverters with more than three levels makes the implementation of a space phasor modulation algorithm difficult. Taking as an example the five-level multicell inverter presented in Fig. 1.4, there are 125 output states available, which generate the 61 different inverter voltage space phasors depicted in Fig. 3.3. One of the first solutions to this problem was given in [17], where a coordinate transformation based on linear functions was used to simplify the search algorithm for the detection of the nearest three space phasors to the reference in order to obtain a reduced harmonic distortion in the output voltage waveforms. In that work, however, details about how to select the sequences of the space phasors are not provided. In a later work [6], despite giving a good insight of the possible sequences for a 5-level multilevel inverter, the analysis lacks of an algorithm to generate them, as well as of a method to generate the corresponding firing pulses. Furthermore, the reduction of the common mode voltage is also an aspect that should be taken into consideration, as it can affect the reliability of the drive and the machine [10],[18].

In this work, a space phasor modulator taking into account those aspects, including a new algorithm to reduce the common mode voltage generation, is considered. Due to the complexity of the modulator, it will be described in three steps:

- 1) Selection of the three space phasors nearest to the reference and calculation of the on-durations.

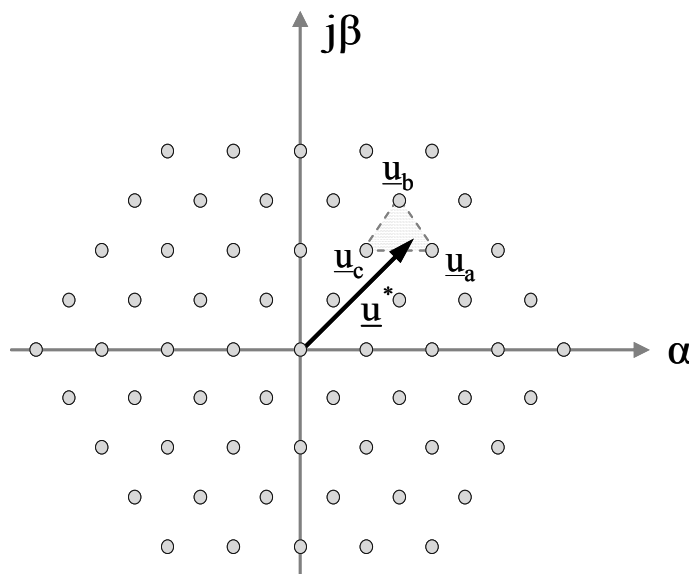


Fig. 3.3. Space phasor diagram of a 5-level inverter.

2) Generation of the states corresponding to the selected space phasors and determination of the sequence.

3) Generation of the firing pulses.

In the following sections, each step is described in detail.

3.2.1 Nearest space phasors selection and on-duration calculation

The first step in the SPM algorithm is the selection of the nearest three inverter space phasors to the reference. This is a complicated task in inverters with a high number of levels, since they present a higher number of sectors than the conventional two-level inverter. The method presented in [17] can be used to simplify the search algorithm, which is based on the following linear transformation:

$$\begin{bmatrix} u'_\alpha \\ u'_\beta \end{bmatrix} = \frac{1}{U_d} \begin{bmatrix} 3/2 & -\sqrt{3}/2 \\ 0 & \sqrt{3} \end{bmatrix} \begin{bmatrix} u_\alpha \\ u_\beta \end{bmatrix} \quad (3.1)$$

In the normalized complex coordinate system α' - β' , the location of each inverter space phasor is always defined by integer numbers without unit, as it is shown in Fig. 3.4.

Thanks to this property, the nearest set of inverter space phasors $\underline{u}'_a, \underline{u}'_b, \underline{u}'_c$ can be directly obtained out of the transformed reference space phasor $\underline{u}'^* = u'_\alpha + j \cdot u'_\beta$ by using the elementary

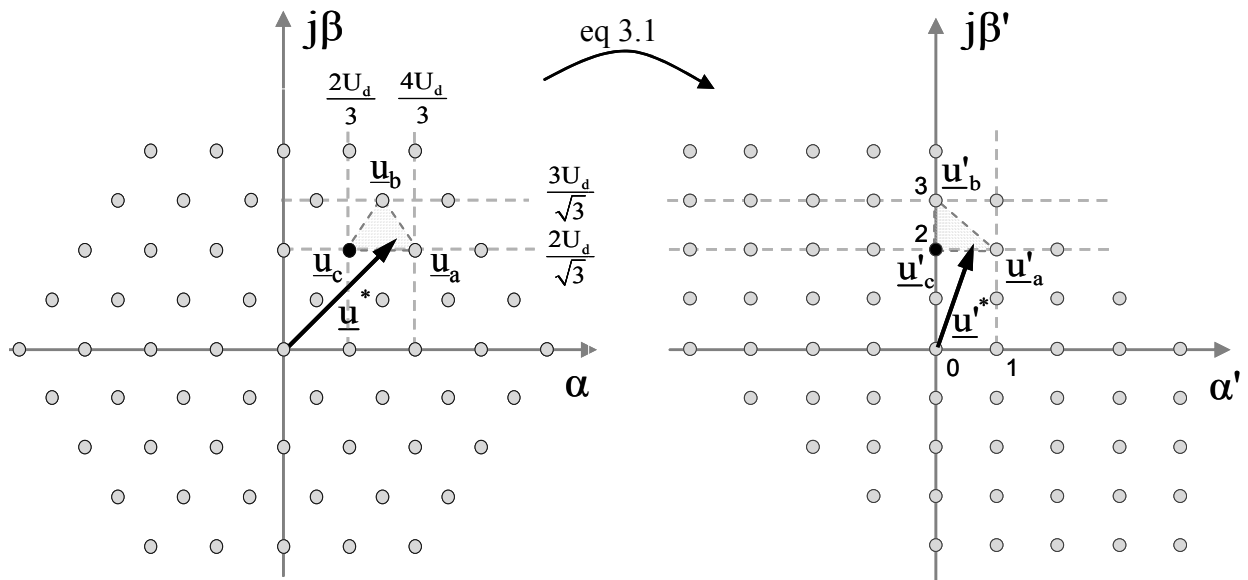


Fig 3.4. Space phasors before and after the transformation defined in eq. 3.1.

operations *nearest integer greater than* ($\lceil \cdot \rceil$) and *nearest integer less than or equal to* ($\lfloor \cdot \rfloor$):

$$\left. \begin{array}{l}
 \text{if } \left\{ u'_a + u'_b - (\lceil u'_a \rceil + \lfloor u'_b \rfloor) \right\} > 0 \\
 \underline{u}'_c = \lceil u'_a \rceil + j \lfloor u'_b \rfloor \\
 \underline{u}'_a = \underline{u}'_c - j \\
 \underline{u}'_b = \underline{u}'_c - 1 \\
 \text{else} \\
 \underline{u}'_c = \lfloor u'_a \rfloor + j \lceil u'_b \rceil \\
 \underline{u}'_a = \underline{u}'_c + 1 \\
 \underline{u}'_b = \underline{u}'_c + j
 \end{array} \right\} \quad (3.2)$$

The same principle of the classical two-level SPM applies for the calculation of the on-duration of each selected space phasor. As it is shown in Fig. 3.5, one of the space phasors, in this case \underline{u}'_c , plays the role of the zero phasor, and the projections of the reference phasor on the sides of the corresponding sector, \underline{u}_{pb} and \underline{u}_{pa} , are proportional to the time of application. This task is simplified by using the transformation given in eq. 3.1, since in this case the projections are directly equal to the fractional parts of the reference phasor \underline{u}^* . The normalized time of application “d” for each space phasor, where d=1 corresponds to an on-duration equivalent to the complete modulation period, is given by the following equation:

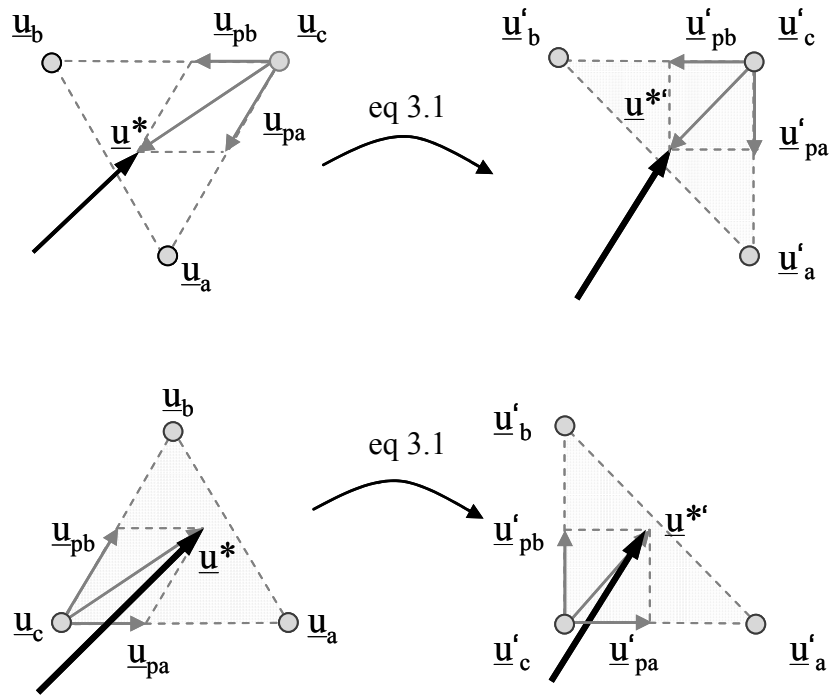


Fig. 3.5. Projections of the reference space phasor on the respective sector side before and after the transformation.

$$\left. \begin{array}{l}
\text{if } \left\{ \mathbf{u}'_{\alpha} + \mathbf{u}'_{\beta} - \left(\lceil \mathbf{u}'_{\alpha} \rceil + \lfloor \mathbf{u}'_{\beta} \rfloor \right) \right\} > 0 \\
\text{then} \\
d_a = |\text{Im}(\underline{\mathbf{u}}'_c - \underline{\mathbf{u}}'^*)| \\
d_b = |\text{Re}(\underline{\mathbf{u}}'_c - \underline{\mathbf{u}}'^*)| \\
d_c = 1 - d_a - d_b \\
\text{else} \\
d_a = |\text{Re}(\underline{\mathbf{u}}'_c - \underline{\mathbf{u}}'^*)| \\
d_b = |\text{Im}(\underline{\mathbf{u}}'_c - \underline{\mathbf{u}}'^*)| \\
d_c = 1 - d_a - d_b
\end{array} \right\} \quad (3.3)$$

3.2.2 Determination of the sequence of states

The multilevel inverter can be seen as a discrete three-phase voltage generator with a defined number of available voltage states. The set of space phasors selected by the algorithm must be expressed as phase voltage states that can be applied by the inverter. As it is shown in Fig. 3.6 for a sextant of the space phasor diagram, many of these states are redundant, i.e. they are associated to the same space phasor. In order to select the appropriate set of states, several criteria must be taken into account, such as the common mode voltage and the generation of a minimum number of switching actions. In the following points, an algorithm to generate the optimum sequence of states based on the previously stated criteria is presented.

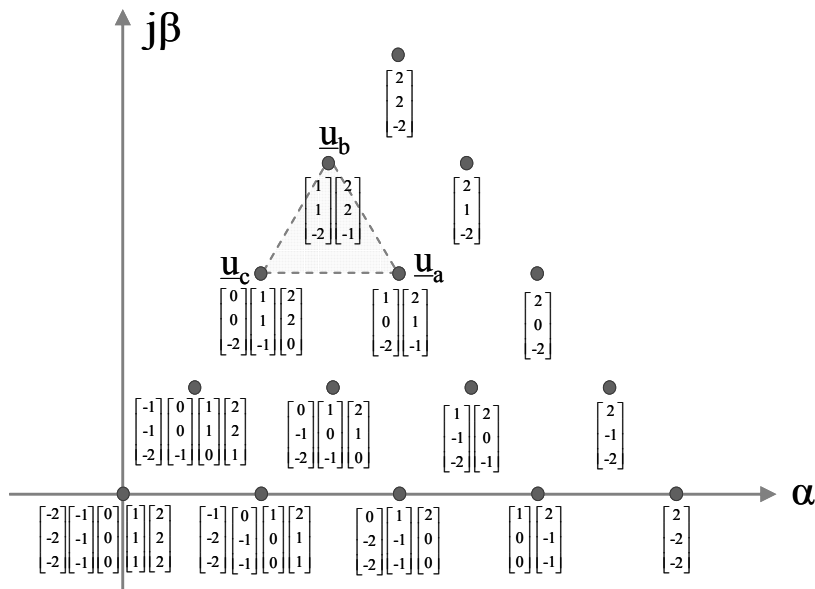


Fig. 3.6. A sextant of the space phasor diagram of a five-level inverter including all possible normalized states for each space phasor.

3.2.2.1 Phase potentials with minimum common mode voltage

In applications where a high common mode voltage generation could affect the reliability of the drive, the selection of space phasors can be restricted to those produced by a voltage state with common mode voltage equal to zero. Since many space phasors lack of a voltage state fulfilling this condition, there is a reduction in the number of available space phasors, as it is shown in Fig. 3.7. As a consequence, the modulator must choose the three space phasors from a grid with a higher number of voltage space phasors, resulting in voltage waveforms with a lower modulation index and higher harmonic distortion [18].

A better compromise is reached when the output voltage state corresponding to each space phasor has the minimum possible common mode voltage.

A straightforward calculation of the voltage state with minimum common mode voltage can be made by using the transformation defined between the α' - β' - $0'$ and UVW quantities, which is derived from eq. 1.4 and eq. 3.1. By using the normalized components α' - β' of a given space phasor, the voltage state can be calculated as:

$$\left. \begin{aligned} u_{UN} &= K \\ u_{VN} &= -u'_{\alpha} + K \\ u_{WN} &= -u'_{\beta} - u'_{\alpha} + K \end{aligned} \right\} \quad (3.4)$$

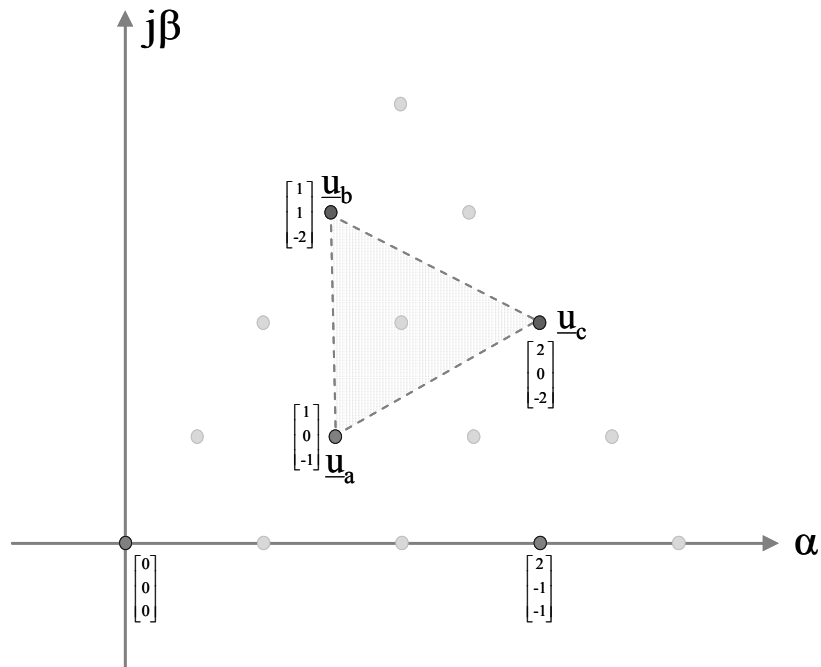


Fig. 3.7. The same sextant of Fig. 3.6 considering only the space phasors with zero common mode voltage.

where K is an integer value which can be adjusted to generate redundant states. By defining the common mode voltage as in eq.1.3,

$$u_0 = \frac{u_{UN} + u_{VN} + u_{WN}}{3} = -\frac{1}{3}(2u'_\alpha + u'_\beta) + K, \quad (3.5)$$

the parameter K can be determined in such a way that the common mode voltage is minimized:

$$K = \text{round}\left(\frac{1}{3}(2u'_\alpha + u'_\beta)\right). \quad (3.6)$$

The eq. 3.6 and 3.4. can be used to determine a valid voltage state with minimum common mode voltage for most space phasors except for those ones located in the boundaries. For the latter, a valid voltage state can be determined by adjusting the value of K to the next integer value.

3.2.2.2 Optimal sequences

The sequence of the states now plays an important role in the generation of switching actions. Ideally, a transition between two states should not consider more than one switching action; otherwise the unnecessary commutations may increase the losses of the power switches. In conventional two level-inverters, the sequences are defined a priori for each sector and stored in tables. This approach makes sense when dealing with a reduced number of voltages states and therefore of sequences; which is not the case of multilevel inverters with five or more levels.

Generally, two types of sequences are normally used differing in the number of states used in each modulation cycle: the so called *discontinuous PWM* and the *continuous PWM*. In the *discontinuous PWM* two of the phases exhibit a switching action per modulation cycle, while the remaining phase exhibits no switching actions and therefore its output voltage is kept constant. This is achieved by using three voltage states, each one corresponding to one selected space phasor. Considering for example the triangle depicted in Fig. 3.8-a, the sequence $[1 \ 0 \ -2]^T$, $[1 \ 1 \ -2]^T$, $[1 \ 1 \ -1]^T$ exhibits only one switching action per state transition whereas the voltage in the first phase is kept constant during the modulation cycle, as it is shown in Fig. 3.8-b. The alternative sequence $[0 \ 0 \ -2]^T$, $[1 \ 0 \ -2]^T$, $[1 \ 1 \ -2]^T$ also fulfils this condition, but the amount of common mode voltage generated is higher, therefore it is non-optimal. It should be pointed out that a sequence with minimum number of switching actions also generates common mode voltage with increasing or decreasing discrete values.

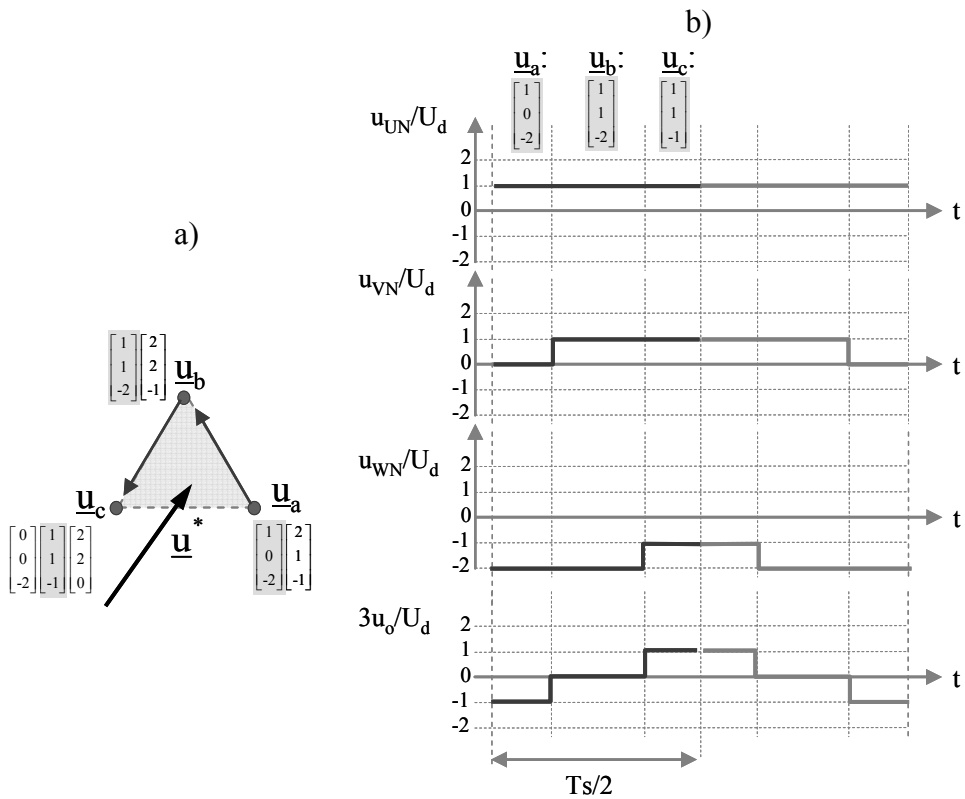


Fig. 3.8. Sequences for *discontinuous PWM*: a) Space phasor representation; b) Output voltages waveforms of the sequence with minimum common mode voltage states.

According to this fact, the common mode voltage can be used to determine the order of each state in the sequence.

In the *continuous PWM*, each phase exhibits a switching action per modulation cycle. This can be achieved by using a fourth voltage state which must be redundant to the first one of the sequence. In the conventional SPM for two-level inverters, this fourth voltage state corresponds to a redundant state of the zero space phasor, as the sequences always start with this space phasor. For the case of multilevel inverters this is not straightforward, since sequences do not start with a predetermined space phasor. For example, by considering the sector in Fig. 3.9, there are two possible sequences with minimum common mode voltage generation: $[1\ 0\ -2]^T, [1\ 1\ -2]^T, [1\ 1\ -1]^T, [2\ 1\ -1]^T$ and $[0\ 0\ -2]^T, [1\ 0\ -2]^T, [1\ 1\ -2]^T, [1\ 1\ -1]^T$. Now, the modulator has to be able to generate the optimum sequences out of the coordinates of the space phasors. For this task, the relationship between the common mode voltage of the states and the condition of minimum number of switches transitions will be applied.

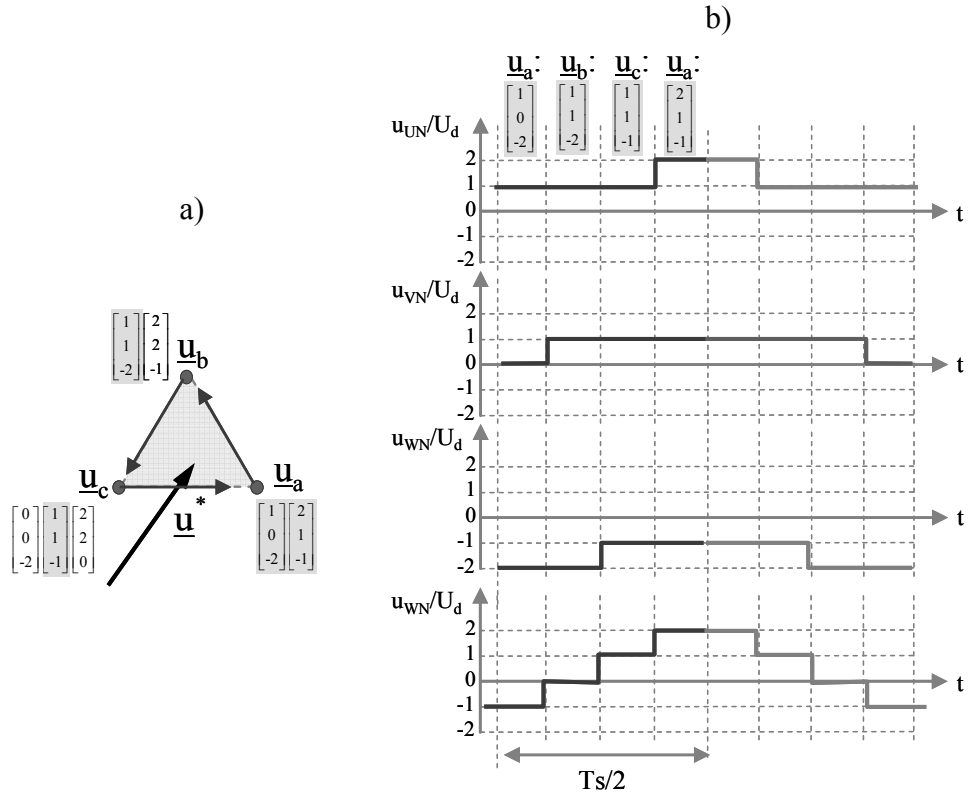


Fig. 3.9. Sequences for *continuous PWM*: a) Space phasor representation; b) output voltages in each phase.

Let \mathbf{S} be the hyper vector whose elements $\mathbf{s}_k, \mathbf{s}_{k+1}, \mathbf{s}_{k+2} \dots \mathbf{s}_{k+n}$ are states arranged according the normalized common mode voltage. For the sake of clarity, the indexes are equal to the normalized common mode voltage $3u_0/U_d$ of each voltage state. Using this notation, the sequence of Fig. 3.9 can be expressed as:

$$\mathbf{Seq} = [\mathbf{s}_{-1} \ \mathbf{s}_0 \ \mathbf{s}_1 \ \mathbf{s}_2] = \left[\begin{bmatrix} 1 \\ 0 \\ -2 \end{bmatrix} \ \begin{bmatrix} 1 \\ 1 \\ -2 \end{bmatrix} \ \begin{bmatrix} 1 \\ 1 \\ -1 \end{bmatrix} \ \begin{bmatrix} 2 \\ 1 \\ -1 \end{bmatrix} \right]. \quad (3.7)$$

In a more general way, the vector \mathbf{S} can be defined to contain all possible states of a given sector:

$$\mathbf{Seq} = [\dots \ \mathbf{s}_{-3} \ \mathbf{s}_{-2} \ \mathbf{s}_{-1} \ \mathbf{s}_0 \ \mathbf{s}_1 \ \mathbf{s}_2 \ \mathbf{s}_3 \ \dots]. \quad (3.8)$$

A subset of three or four states is finally selected and applied by the modulator. It must be remarked that only three states are necessary to determine the whole matrix, as the other states are redundancies of these states. In this way, the same matrix can be defined as follows:

$$\text{Seq} = \left[\dots \begin{matrix} s_0 - 1 \\ 1 \\ 1 \end{matrix} \quad \begin{matrix} s_1 - 1 \\ 1 \\ 1 \end{matrix} \quad s_{-1} \quad s_0 \quad s_1 \quad s_{-1} + 1 \quad s_0 + 1 \quad \dots \right]. \quad (3.9)$$

The three states with minimum common mode voltage can be determined by using equations (3.4) and (3.6).

3.2.2.3 Constraints

Sectors located in the boundaries contain space phasors without any redundancy degree; therefore the number of possible sequences in those cases is reduced. E.g., only one sequence is possible for the sector A in Fig. 3.10: $[1 \ 1 \ -2]^T, [2 \ 1 \ -2]^T, [2 \ 2 \ -2]^T, [2 \ 2 \ -1]^T$. The sequences start always with a space phasor with redundant voltage states; otherwise the fourth voltage state can not be generated. To detect this exception, the modulator algorithm first checks the sequence with minimum common mode voltage. If one of the states is invalid, i.e. a state with phase potentials that can not be produced by the inverter, a sequence with higher common mode voltage is used. For the example in consideration, the original calculated sequence with minimum common mode voltage criteria is:

$$\text{Seq} = [s_{-1} \ s_0 \ s_1 \ s_2] = \left[[1 \ 1 \ -3]^T \ [1 \ 1 \ -2]^T \ [2 \ 1 \ -2]^T \ [2 \ 2 \ -2]^T \right]. \quad (3.10)$$

Because the first state is not valid in a five-level inverter topology, a sequence with higher common mode voltage is selected:

$$\text{Seq} = [s_0 \ s_1 \ s_2 \ s_3] = \left[[1 \ 1 \ -2]^T \ [2 \ 1 \ -2]^T \ [2 \ 2 \ -2]^T \ [2 \ 2 \ -1]^T \right]. \quad (3.11)$$

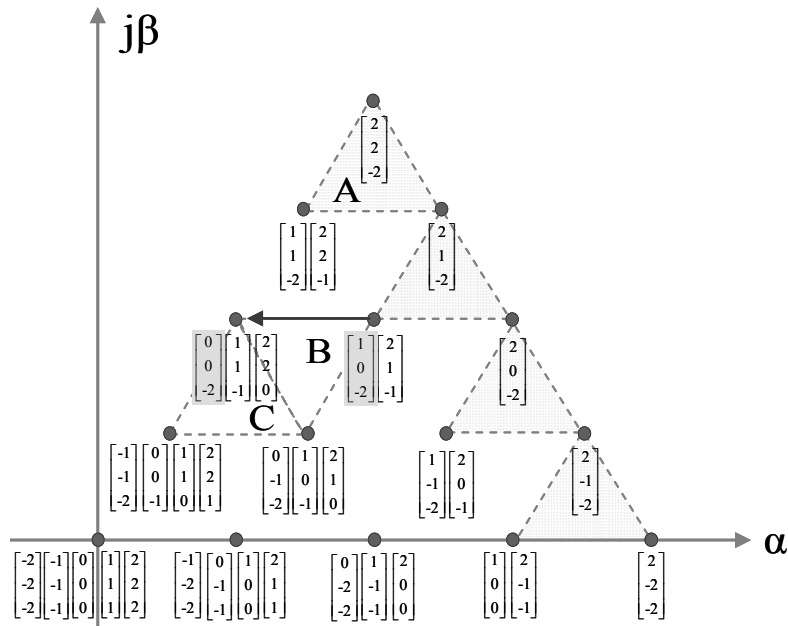


Fig. 3.10. A sextant of the space phasor diagram with the respective voltage states. Sectors with only one possible sequence are indicated by shaded triangles.

3.2.2.4 Switching minimization for transitions between sectors

Now, it will be considered the case in which the reference space phasor changes its position to a new sector and a new set of space phasors and their corresponding states are calculated by the modulator. Because the first voltage state probably differs from the first voltage state of the last sequence, additional switching actions will be generated by the modulator. A convenient change of the sequences could mitigate this problem as follows: If the first voltage state using the old sequence is the same as in the last sector, no change in the sequence is necessary and no extra switching takes place. If the first voltage state is different, an adjacent valid sequence shall be used.

For example, considering the same example as in Fig. 3.10, a reference space phasor located in sector B defines the following optimal sequence: $[1\ 0\ -2]$, $[1\ 0\ -1]$, $[1\ 1\ -1]$, $[2\ 1\ -1]$. A transition of the reference phasor to the sector C defines a new first voltage state, which is given by $[0\ 0\ -1]$ if the last sequence is used, i.e. a space phasor with the same common mode voltage is used to start the sequence. The transition to this new state needs three switching actions, which is clearly non-optimal. The next adjacent sequence with minimum common mode voltage is given by $[0\ 0\ -2]$, $[0\ 0\ -1]$, $[1\ 0\ -1]$, $[1\ 1\ -1]$; in this case only one switching action is needed for the sector transition.

3.2.3 Generation of the firing pulses

The last step is to determine the switching state of each cell according to the selected phase potentials. In order to distribute the switching actions evenly between the power semiconductors, the state machine described in [19] will be applied in this work. In this approach each state defines a configuration of the phase switches $S_{A+}, S_{B+}, S_{C+}, S_{D+}$ which can be changed depending on the desired voltage and the last state. The states are defined in such a way that each voltage transition is obtained by only one switching action, as is depicted in the Fig 3.11. If the

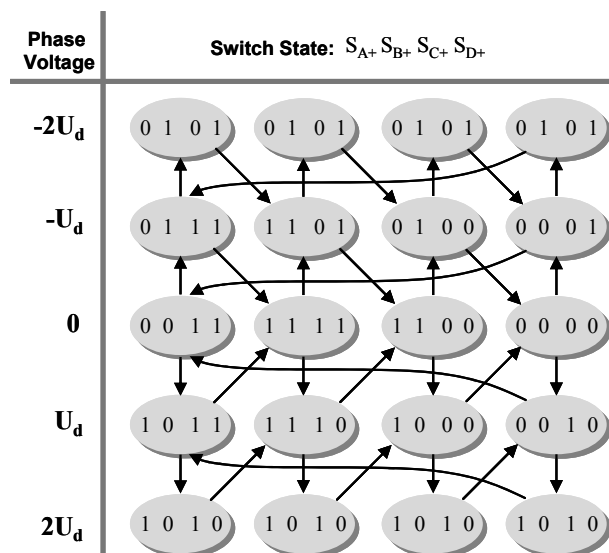


Fig. 3.11 State Machine for one phase of the SCHB multilevel inverter.

phase potential changes between U_d and 0, the switching actions are cyclically allocated as is depicted in Fig. 3.12. The commutation frequency of each switch is equivalent to 1/4 of the frequency of the phase waveform.

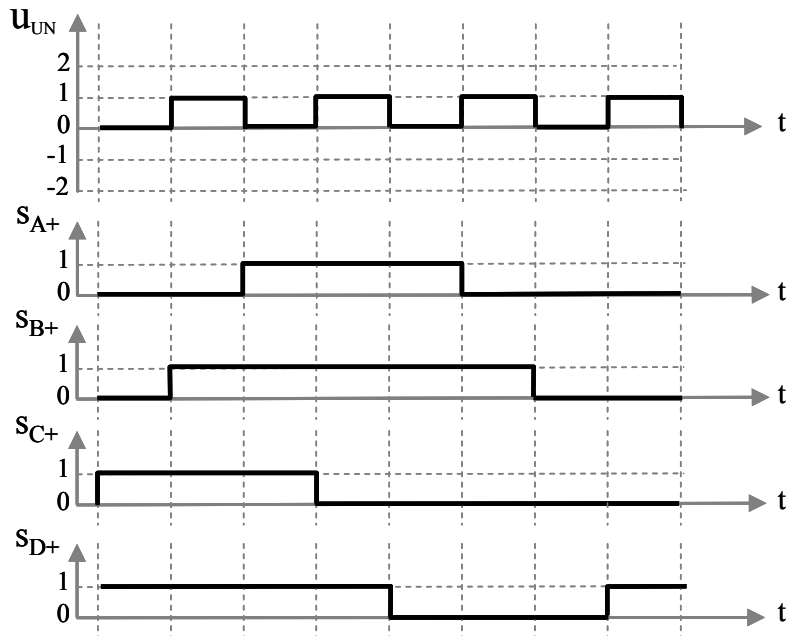


Fig. 3.12. Cyclical allocation of the firing pulses for a phase voltage variation between 0 and U_{dc} .

3.2.4 Implementation of the SPM

The implementation of this algorithm in software would unnecessary overload the processor; for this reason the use of an external logic unit was considered to support the modulation task. The first part of the algorithm, i.e. the selection of the three nearest space-phasors and the calculation of the on-durations, was implemented in software, whereas a FPGA deals with the sequence optimization and the state machines for the firing pulses generation. The modulator operates in the following manner: in the middle of the modulation period, the FPGA generates an interrupt which is used to trigger the measurement of the currents and to determine the reference voltage phasor according to the control algorithm. The processor delivers to the FPGA a set of three voltage states with minimum common mode voltage and the on-durations of each space phasor. At the beginning of the modulation cycle, the FPGA calculates the other redundant states of the same sector, discarding those which are not possible to be generated with the inverter. Depending on the selected type of sequence, *continuous* or *discontinuous* PWM, three or four valid states are selected, which are arranged according to their respective common mode voltage. If the reference space phasor changes to

another sector with multiple possible sequences, the sequences are then changed according to the method explained in section 3.2.2. After this step, the set of four or three inverter states are delivered to the modulator block with their respective on-duration. The output of the modulator provides the instantaneous voltage state of the inverter, which is decoded in each phase by the state machine described in section 3.2.3. In this way, the firing pulses for each cell of the inverter are obtained. The block diagram of fig 3.13 summarizes the FPGA program of the proposed modulation strategy.

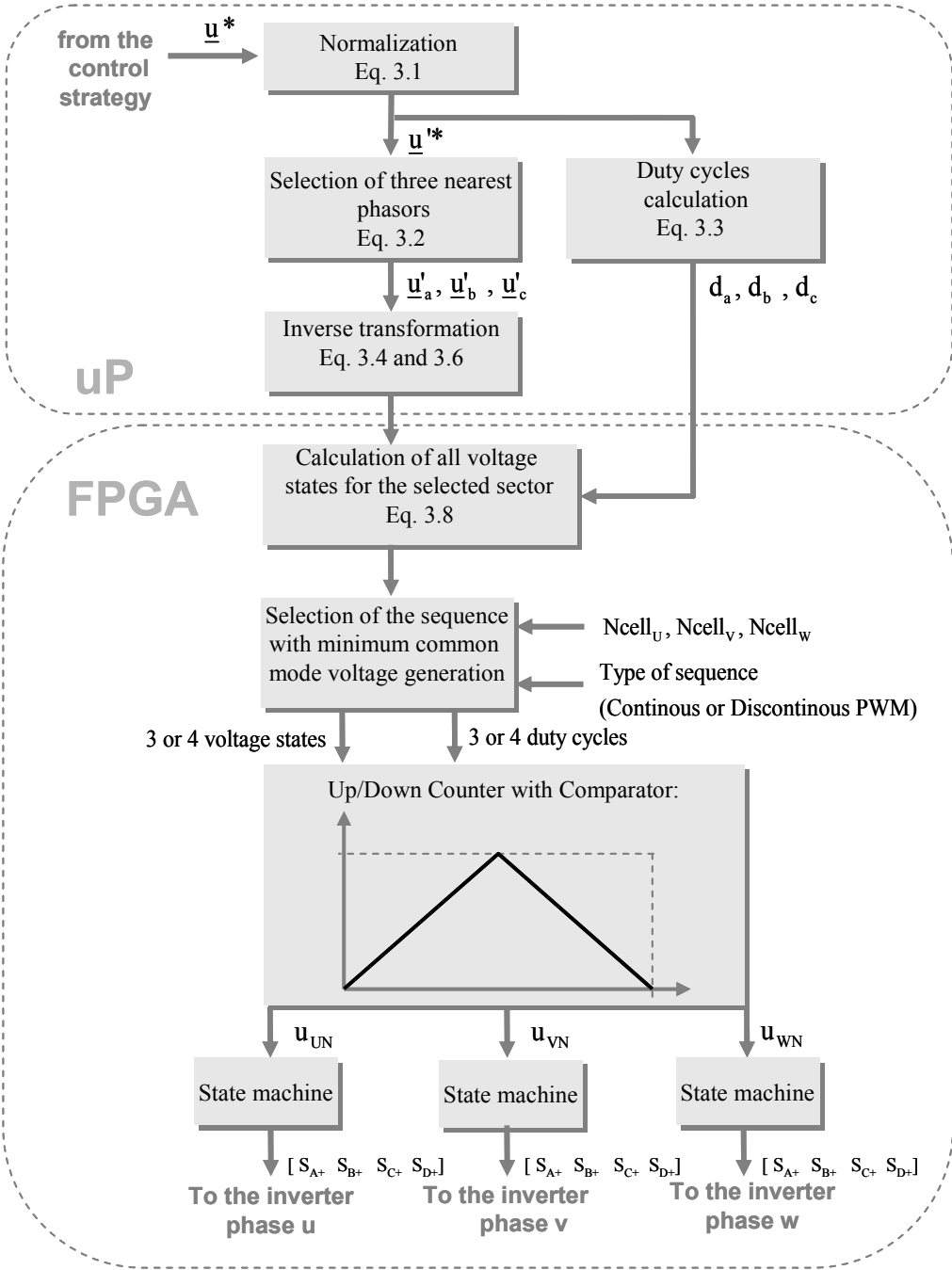


Fig. 3.13. Block diagram of the multilevel modulation algorithm.

Fig 3.14-a and Fig. 3.14-b show the output voltage waveforms of one phase of the inverter and the voltages generated by each cell at different modulation depths. Although for low modulation index the output voltage is synthesized with less than 5 levels, each cell is involved in the output voltage generation and they operate at a lower switching frequency in a

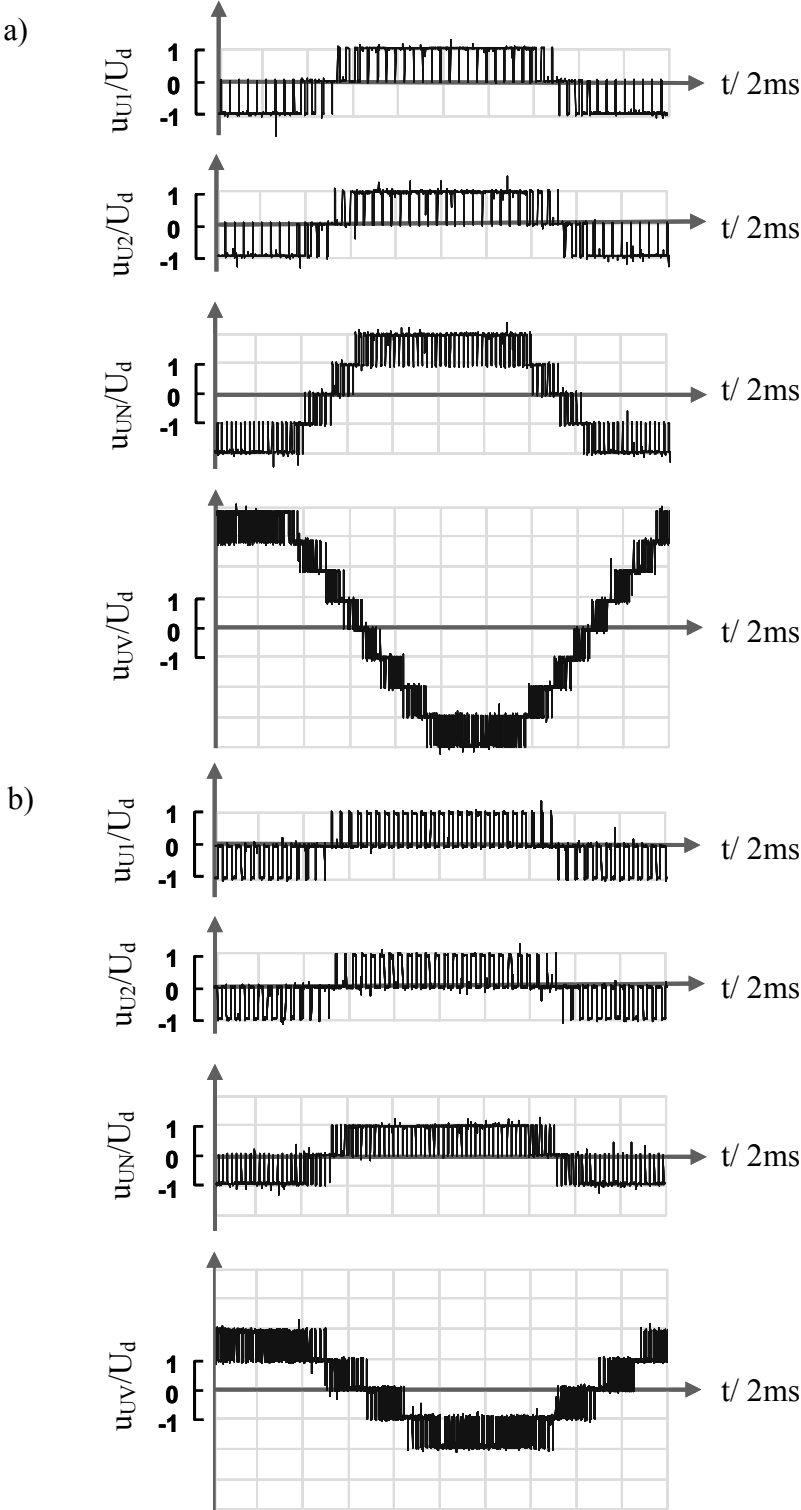


Fig 3.14. Cell voltages u_{U1} , u_{U2} , phase potential u_{UN} and line-to line voltage u_{UV} : a) modulation index $a=0.98$, b) modulation index $a=0.48$.

similar way as the PS-PWM method. The SPM method does not generate double steps in the line-to-line voltage, as it can be seen in the same figures.

A very important point deals with the switching frequency of each power semiconductor. As it was explained in section 3.2.3 the modulator generates one switching event per modulation cycle in each phase, which results for 5-level multilevel inverter in a switching frequency of a quarter of the modulation frequency. The voltage waveforms of the firing pulses are similar to the waveforms obtained with PS-PWM as is shown in Fig. 3.15-a and 3.15-b. Since extra switching actions are necessary when the reference phasor changes between sectors, a fixed switching frequency for each power device can not be expected. The switching frequency with the SPM is slightly higher than with PS-PWM approach. This can be confirmed by counting the number of switching transitions per fundamental period, and expressing this result as a frequency, as it is depicted in the Fig. 3.16. This figure also shows that the number of commutations does not seem to be affected by the modulation index.

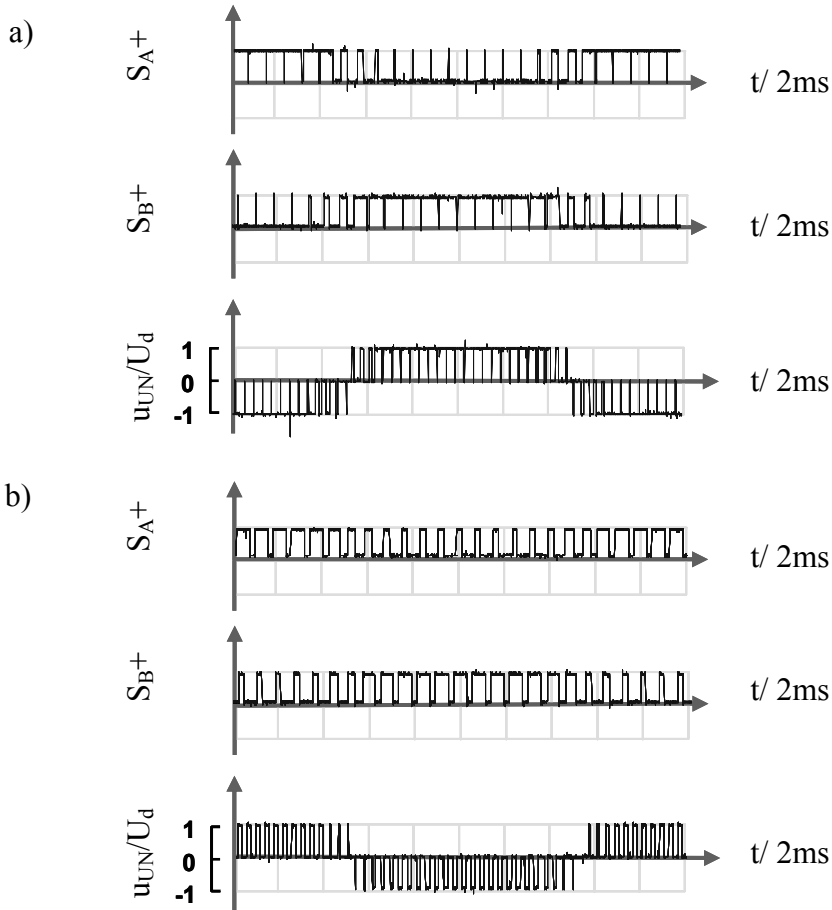


Fig 3.15. Cell voltage u_{UI} with the corresponding firing pulses S_{A+} and S_{B+} ; a) modulation index $a=0.98$, b) modulation index $a=0.48$.

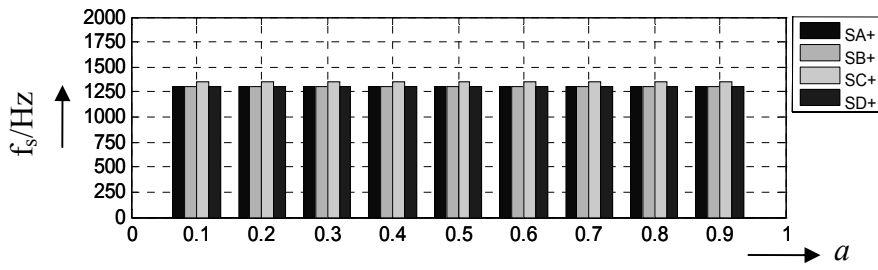


Fig 3.16. Switching frequency of the firing pulses S_{A+} , S_{B+} , S_{C+} , S_{D+} of phase U for different modulation indexes and a modulation frequency of 5 kHz.

3.3 Summary of chapter 3

Several modulation approaches have been developed for multilevel inverters. These can be divided in two categories: PWM carrier based modulation and space phasor modulation. The industrial version of the SCHB multilevel inverter uses the so called PSPWM, which is based on the phase-shift of the carriers to obtain an output voltage with multiple levels. The main advantage of this modulation is its simplicity, but it generates line-to-line voltage with a higher harmonic distortion compared with other modulation strategies. The reason of this higher distortion can be found in the double steps of the line-to-line voltages. On the other hand, the SPM approach eliminates this problem by always choosing adjacent space phasors. In this chapter the working principles of a new SPM algorithm for SCHB multilevel inverters were discussed. The SPM for multilevel inverters works in a similar way to the two-level modulation approach: for a given reference space phasor, the three nearest space phasors with their respective on-durations are calculated. With the information of the selected space phasor, an optimal set of four states is generated, taking into account that the sequence must produce the minimum number of switching transitions and the minimum common mode voltage. Afterwards, a state machine decodes each phase potential into the corresponding firing pulses. The commutation frequency of the power semiconductors is not constant, but it is close to a quarter of the modulation frequency for a 5-level inverter. In this aspect, the SPM obtains a similar performance compared to the PS-PWM.

4. FAULT TOLERANT OPERATION OF THE SCHB-VSI

Electrical drives are part of many critical industrial processes with high associated standstill costs; therefore, a high degree of availability is usually an important requirement. This problem has motivated a big interest in the study of diagnosis methods and remedies to increase the reliability of the drive, mainly for applications with the conventional two-level inverter topology [20],[21],[22]. The problem is especially relevant for multilevel inverters, as the complexity degree of the topology is higher than the conventional two-level inverters. A survey of the scarce up-to-date works in the literature reveals that the problem has been analyzed for the FLC inverter [23],[24], the SCHB inverter [4],[5].

To increase the reliability of the drive, the commercial SCHB multilevel inverters may optionally include redundant cells which can replace the faulty ones. A further alternative consists of the use of cells that the inverter still has available to permit the operation at reduced output power. Two original methods to obtain higher power ratings out of a SCHB multilevel inverter with bypassed cells will be presented, one based on the PS-PWM approach and the other one based on the space phasor modulation. Considerations about the controller adjust to the new operating conditions and the firing pulse generation will be also discussed in this chapter.

4.1 Reliability in the SCHB-VSI

Reliability is the ability of a system to perform its required function under stated conditions for a specified period of time. In this regard, the high complexity of an SCHB multilevel inverter constitutes a disadvantage if compared to other multilevel inverter topologies, since it has a higher number of components that could fail. For example, if one cell has a reliability a_r for a determined period of time, the reliability of an inverter with n cells without fault tolerant operation is a_r^n . Nevertheless, the reliability is increased to $a_r^n + n a_r^{n-1} (1 - a_r)$ if the operation of inverter with a faulty cell is possible [5]. Considering a reliability index of $a_r=99\%$ for one cell, the reliability of a seven level multicell inverter with three cells per phase is 91.3% if no fault is tolerated, but 99.6% if one fault is tolerated. Furthermore, the reliability is improved if the inverter tolerates more than one faulty cell. Even though the cost of repairing a cell has to be considered, the cells in this topology are based on common off-the-self low voltage components. Moreover, depending on the cost of the stand-still, and how critical is the process driven by the inverter, the repairing cost may be not an important factor.

4.2 Faults in SCHB multilevel inverter

Possible failure causes in conventional voltage source IGBT-based inverters are:

- AC line fault:

- single line to ground
- line to line short circuit

- DC bus fault:

- capacitor short circuit
- line of the dc bus to ground
- capacitor break down

- Power semiconductor fault:

- open/short-circuited transistor
- open/short-circuited diode

- Sensor failures:

- ac current sensor fault
- dc-link voltage sensor fault
- encoder fault.

- Control fault

- loss of gate signals

The analysis of faults can be focused on the SCHB inverter cell, as this unit has the most failure sensitive components. Figure 4.1 illustrates different failures in an H-Bridge cell. Most of these can be detected by the standard protection system which is included in each cell.

Rectifier diode short circuit fault, such as F1 in the picture below. Short circuits in one rectifier diode that can produce an excessive current stress on the line fuses. If a fuse corresponding to the faulty rectifier leg blows first, the rectifier continues its operation in single phase mode. If one fuse in the healthy leg of the rectifier blows first, the fault continues until the fuse in the faulty phase blows and the power of the cell is interrupted [21]. In both cases, monitoring the DC-link voltage can be utilized to detect the problem.

Capacitor short circuit or capacitor break-down as hinted by F2 result for damaged capacitors due to former over-current. The cell is shut down due to insufficient smoothing factor in the DC-link. Capacitors have a shorter life span than power semiconductors.

Therefore, fault diagnosis in this component is an important subject to be considered. Methods have been developed to calculate the aging process using the internal series resistance (ESR), in order to provide preventive maintenance [22].

The Transistor short circuit, represented by F3, can be detected by standard IGBT drivers including over-current protection via desaturation detection. As soon as this fault signal is detected, the cell is shut down to avoid further damage.

Transistor open as in F4 is rather a matter of control signal failure. Several diagnosis methods have been reported to detect open transistor faults in conventional two level inverters, mainly based on the current behaviour after the fault [22],[25]. This problem has not been studied in multilevel topologies.

If a fault is detected, the cell is bypassed using a contactor as shown Fig. 4.1.

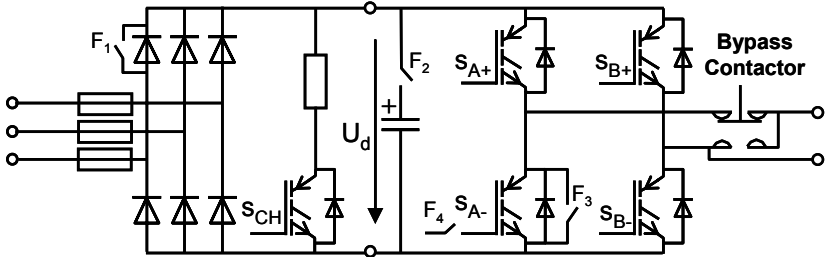


Fig. 4.1. Different failure types in the H-Bridge cell.

4.3 Operation with bypassed cells

After the detection of a fault, the controller must optimize the operation with the remaining healthy cells. The most important aspects to be considered deal with the loss of voltage due to the operation with less number of cells and the resulting voltage originated. Both problems can be solved by modifying the modulation strategy. In the following, two new alternatives will be presented, the first one based in the PS-PWM and the second one using the SPM approach.

4.3.1 Fault Tolerant PS-PWM

For the following analysis, each cell will be considered as an ideal sinusoidal voltage generator, so only the fundamental component of the output voltage of each cell will be taken

into consideration. Under this assumption, the voltages generated by the cells of the inverter can be represented as phasors which can be used to derive the line-to-line voltages.

By using this standard notation, the bypass of one cell can be represented by the unbalanced three-phase phasor diagram depicted in Fig.4.2a. The simplest solution to balance the three-phase system consists of bypassing two additional cells in the other phases, as it is shown in Fig. 4.2.b.

For the five-level inverter considered in this work, this action results in an equivalent three-level topology which can deliver only half of the maximum voltage of the healthy inverter. This is clearly a non optimum solution, as some healthy cells are bypassed to regain balanced voltages.

A PWM modulation approach which generates balanced voltages in the machine without bypassing healthy cells has been proposed in [4,5]. This method takes advantage of the fact

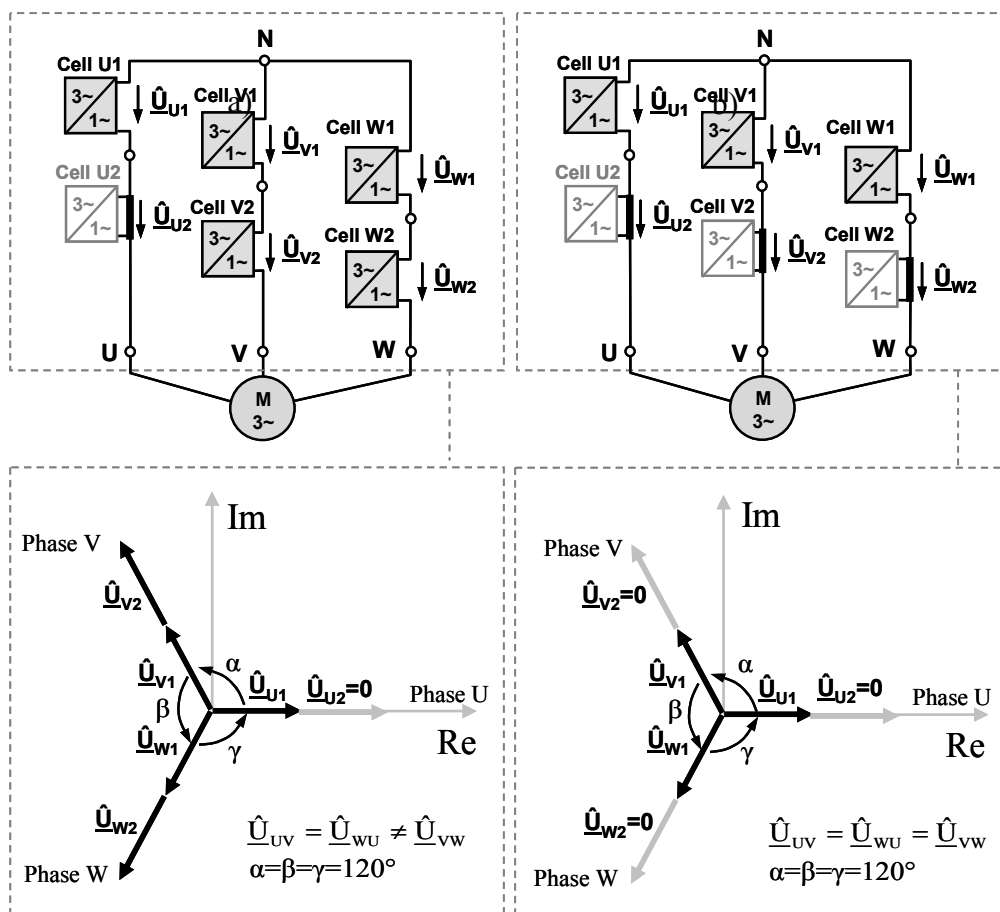


Fig 4.2. Phasor representation of the phase output voltages with bypassed cells:

- a) Unbalanced operation through the bypass of one cell; b) Balanced operation through the bypass of healthy cells in other phases.

that the neutral point N of the inverter is floating and it is not connected to the neutral point of the machine. In this way, the inverter neutral point can be shifted away from the neutral point of the machine by adjusting the phase angles of the voltage reference, so that balanced machine voltages are obtained even though the inverter phase potentials are not balanced.

Thus, the phase angles of the voltages references \hat{U}_{UN} , \hat{U}_{VN} , \hat{U}_{WN} can be calculated by fulfilling the following condition for the line-to-line voltage phasors:

$$|\hat{U}_{VU}| = |\hat{U}_{WU}|, \quad (4.1)$$

$$|\hat{U}_{VU}| = |\hat{U}_{VW}|, \quad (4.2)$$

By considering a phasor \hat{U}_{UN} located in the real axis, the last equations can be expressed in terms of the real and the imaginary part as follows:

$$\left. \begin{aligned} (\text{Re}\{\hat{U}_{VN}\} - \text{Re}\{\hat{U}_{UN}\})^2 + \text{Im}\{\hat{U}_{VN}\}^2 &= (\text{Re}\{\hat{U}_{WN}\} - \text{Re}\{\hat{U}_{UN}\})^2 + \text{Im}\{\hat{U}_{WN}\}^2 \\ (\text{Re}\{\hat{U}_{VN}\} - \text{Re}\{\hat{U}_{UN}\})^2 + \text{Im}\{\hat{U}_{VN}\}^2 &= (\text{Re}\{\hat{U}_{VN}\} - \text{Re}\{\hat{U}_{WN}\})^2 + (\text{Im}\{\hat{U}_{VN}\} - \text{Im}\{\hat{U}_{WN}\})^2 \end{aligned} \right\} (4.3)$$

Additionally, the maximum magnitude of the voltage phasors are known, as they depend on the number of available cells N_{cell_u} , N_{cell_v} , N_{cell_w} in phases U,V,W respectively and the maximum voltage delivered by each cell \hat{U}_{cell} . This leads to

$$\left. \begin{aligned} \text{Re}\{\hat{U}_{VN}\}^2 + \text{Im}\{\hat{U}_{VN}\}^2 &= (\hat{U}_{\text{cell}} N_{\text{cell}_v})^2 \\ \text{Re}\{\hat{U}_{WN}\}^2 + \text{Im}\{\hat{U}_{WN}\}^2 &= (\hat{U}_{\text{cell}} N_{\text{cell}_w})^2 \\ \text{Re}\{\hat{U}_{UN}\} &= \hat{U}_{\text{cell}} N_{\text{cell}_u} \\ \text{Im}\{\hat{U}_{UN}\} &= 0 \end{aligned} \right\} (4.4)$$

By solving the system of six variables and six equations given by (4.3) and (4.4), the phase angles are finally determined as follows:

$$\left. \begin{aligned} \alpha' &= \text{atan}(\text{Im}(\hat{U}_{VN})/\text{Re}(\hat{U}_{VN})) \\ \gamma' &= \text{atan}(\text{Im}(\hat{U}_{WN})/\text{Re}(\hat{U}_{WN})) \\ \beta' &= 360^\circ - \alpha' - \gamma' \end{aligned} \right\} (4.5)$$

In order to determine the performance of this method, it may be appropriate to calculate the maximum modulation index for the inverter configuration considered here. This will be expressed as the quotient between the maximum balanced line-to-line fundamental voltage obtained with the new configuration and the maximum line-to-line fundamental voltage with a healthy inverter:

$$\hat{a}_{fault} = \frac{|\hat{U}_{UV}|_{fault}}{|\hat{U}_{UV}|_{healthy}} \quad (4.6)$$

Table 4.1 summarizes the phase angles for the most representative bypass configurations, indicating the maximum modulation index that can be achieved in each case as well. For the considered case of one bypassed cell in phase U, balanced line-to-line voltages can be obtained by using reference angles equal to $\alpha'=135.52^\circ$, $\beta'=88.95^\circ$, $\gamma'=135.52^\circ$, as it is depicted in the phasor diagram of Fig. 4.3. The maximum modulation index achieved in this case is $\hat{a}=0.7$, which is higher than the modulation index obtained with the simple solution of three bypassed cells previously explained ($\hat{a}=0.5$, configuration IV in table 4.1).

The eq. (4.3) and (4.4) do not have a solution for some inverter configurations, as is the case of the configuration V in table 4.1. In this situation bypassing of additional cells in order to obtain a valid configuration is recommended.

It should be noted that this method is valid only for references without third harmonic injection, as the asymmetrical topology which results after the bypass of cells can not eliminate third harmonic components in the load voltages. For this reason, the method does not achieve the maximum possible modulation index and the capabilities of the inverter are not fully utilized. The improvement with this method is only moderate. For the configuration of two bypassed cells in the same row of cells, it may be convenient to bypass a third cell to obtain a balanced system which allows the use of the third harmonic injection.

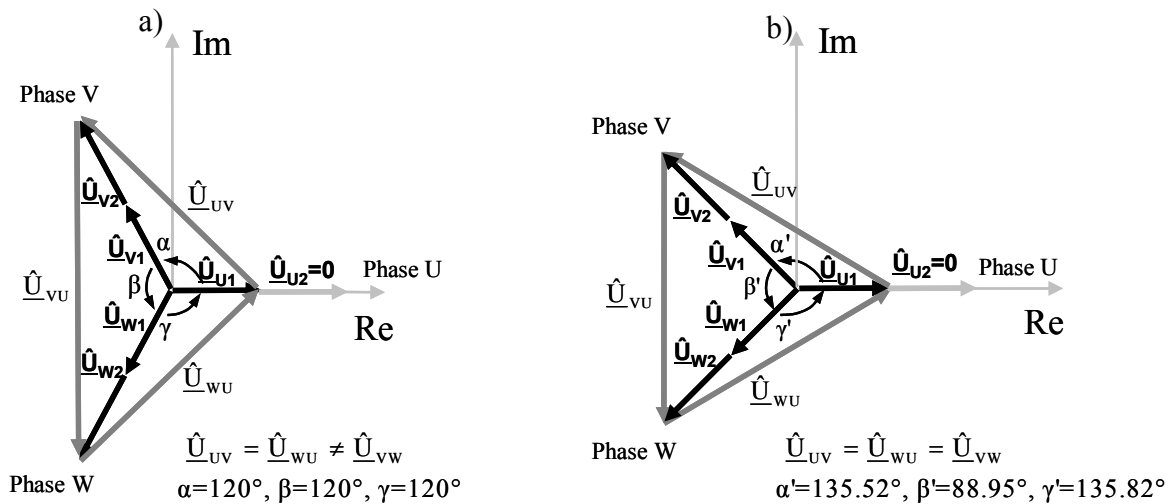


Fig 4.3. Phase voltage phasors for one bypassed cell: a) unbalanced operation of a SCHB inverter, b) balanced operation with phase shift in the references.

Table 4.1 Reference phase shift for different inverter configuration with PS-PWM

Case	Status of the Cells				Phase angle shift			Maximum modulation depth	
	Row	Phase U	Phase V	Phase W	Phase U	Phase V	Phase W	With 3 th Harmonic Injection	Without 3 th Harmonic Injection
0	1	ok	ok	ok	$\alpha= 120^\circ$	$\beta= 120^\circ$	$\gamma= 120^\circ$	$\hat{a}=1$	$\hat{a}=0.86$
	2	ok	ok	ok					
I	1	ok	ok	ok	$\alpha= 135.52^\circ$	$\beta= 88.95^\circ$	$\gamma= 135.52^\circ$	-	$\hat{a}=0.7006$
	2	bypass	ok	ok					
II	1	bypass	ok	ok	$\alpha= 60^\circ$	$\beta= 150^\circ$	$\gamma= 60^\circ$	-	$\hat{a}=0.5$
	2	bypass	ok	ok					
III	1	ok	ok	ok	$\alpha= 120.02^\circ$	$\beta= 60.01^\circ$	$\gamma= 179.97^\circ$	-	$\hat{a}=0.433$
	2	bypass	bypass	ok					
IV	1	ok	ok	ok	$\alpha= 120^\circ$	$\beta= 120^\circ$	$\gamma= 120^\circ$	$\hat{a}=0.5$	$\hat{a}=0.433$
	2	bypass	bypass	bypass					
V	1	bypass	ok	ok	-	-	-	-	-
	2	bypass	bypass	ok					
VI	1	bypass	ok	ok	$\alpha= 60^\circ$	$\beta= 150^\circ$	$\gamma= 60^\circ$	-	$\hat{a}=0.25$
	2	bypass	bypass	bypass					

4.3.2 Modified Fault Tolerant PS-PWM.

The standard PS-PWM method uses third harmonic injection in each voltage reference to increase the maximum reachable modulation index. In an inverter with bypassed cells this concept may be still applied to groups of cells which can work as a balanced three-phase system.

In order to understand this idea, the H-bridge multilevel inverter with the bypassed configuration depicted in Fig. 4.4.a will be considered. For the sake of simplicity, the cells in each phase can be regrouped in the equivalent topology depicted in Fig. 4.4.b, where each group can be classified as follows:

-Group A is constituted by three healthy cells, each one in a different phase. If only this group of cells is considered for the operation of the inverter and the other cells are bypassed, references with normal phase shift and third harmonic injection can be used. For this reason this group will be called a balanced group of cells.

-Group B consists of two healthy cells in different phases. Considering only this group of cells for the operation of the inverter, balanced load voltages can be obtained by a phase shift of the phase potential references according to the method previously explained. This configuration is equivalent to the case VI in the table 4.1.

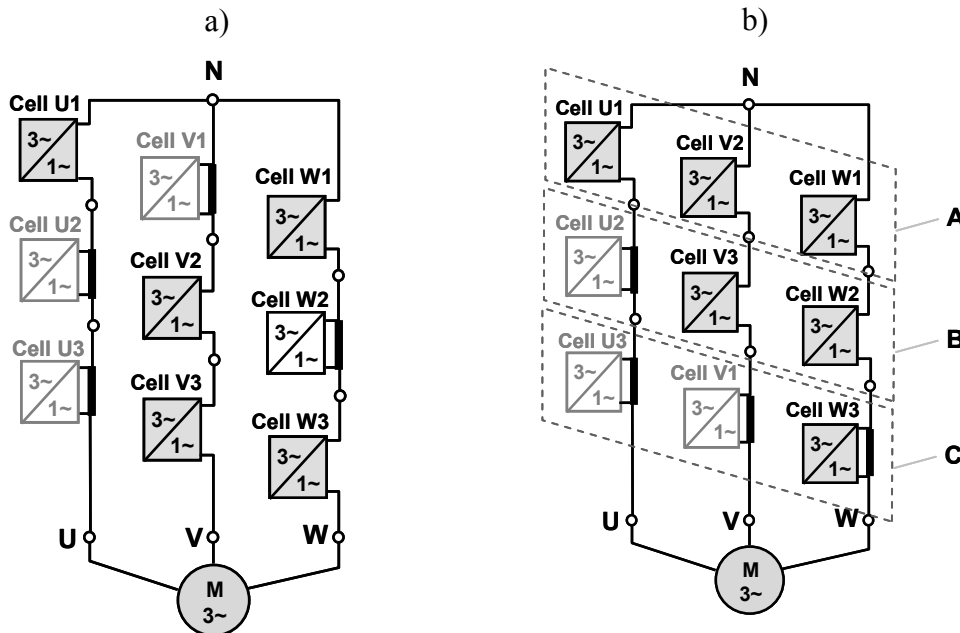


Fig 4.4. 7-level SCHB inverter: a) inverter with three bypassed cells; b) Same inverter with cells reorganized according to the operation mode in groups A,B, and C.

-Group C consists of one healthy cell in one phase. These cells will not be taken into consideration in this approach and they will be bypassed.

The proposed method works in the following manner. According to the type of the fault, a new topology of the inverter is defined after the bypass of the cells. The inverter is divided in different groups of cells, according to the presented classification, and the reference for the modulator of each cell is correspondingly modified to operate with or without phase shift and third harmonic injection. The group of cells which can work as a balanced system is fed with voltage references with standard phase shift and third harmonic injection. The so called group B of cells is fed with phase-shifted references and without third harmonic injection. The rest of the cells are bypassed. Because each group of cells delivers balanced output voltages, the resulting output voltages are also balanced.

The maximum modulation index in this case can be calculated by adding the voltage contribution of the groups A and B of cells. In the following, the maximum modulation index for the case of a bypass in the cell U2 in a 5-level inverter will be determined, keeping in mind that the same procedure can be extended to the other cases.

The maximum voltage contribution of the groups A and B of cells is proportional to the maximum amplitude of their respective references. As the references of those groups include third harmonic injection, a maximum normalized amplitude of $\hat{A}_1=2/\sqrt{3}$ is possible, as it is well known from the standard PWM theory. In this way, the fundamental voltages delivered by the group A of cells can be expressed as a function of the dc-link voltage U_d and the amplitude \hat{A}_1 by:

$$\left. \begin{aligned} u_{U1g}(t) &= \hat{A}_1 2U_d \cos(\omega t) \\ u_{V1g}(t) &= \hat{A}_1 2U_d \cos\left(\omega t + \frac{2\pi}{3}\right) \\ u_{W1g}(t) &= \hat{A}_1 2U_d \cos\left(\omega t - \frac{2\pi}{3}\right) \end{aligned} \right\} \quad (4.7)$$

On the other hand, the second group of cells V2, W2 corresponds to an unbalanced system which can be modified to regain balanced line-to-line voltages. This can be achieved by shifting the reference phase to $\alpha'=150^\circ$, $\beta'=60^\circ$, $\gamma'=150^\circ$. In this case, the fundamental voltages are given by:

$$\left. \begin{aligned} u_{U2g}(t) &= 0 \\ u_{V2g}(t) &= \hat{A}_2 2U_d \cos(\omega t + \frac{5\pi}{6}) \\ u_{W2g}(t) &= \hat{A}_2 2U_d \cos(\omega t - \frac{5\pi}{6}) \end{aligned} \right\}, \quad (4.8)$$

where \hat{A}_2 exhibits a maximum normalized amplitude of 1, as no third harmonic injection is possible. The resulting line-to-line voltages considering the two groups of cells are given by:

$$\left. \begin{aligned} u_{VUg}(t) &= u_{VNg} - u_{UNg} = (\sqrt{3}\hat{A}_1 + \hat{A}_2) 2U_d \cos(\omega t + \frac{5\pi}{6}) \\ u_{WVg}(t) &= u_{WNg} - u_{VNg} = (\sqrt{3}\hat{A}_1 + \hat{A}_2) 2U_d \cos(\omega t + \frac{3\pi}{2}) \\ u_{UWg}(t) &= u_{WNg} - u_{UNg} = (\sqrt{3}\hat{A}_1 + \hat{A}_2) 2U_d \cos(\omega t - \frac{\pi}{6}) \end{aligned} \right\}, \quad (4.9)$$

which are clearly balanced. Assuming that the maximum line-to-line voltage of a healthy inverter is given by $2\sqrt{3}\hat{A}_1 U_d$, the maximum modulation index is finally determined as:

$$\hat{a} = \frac{\sqrt{3}\hat{A}_1 + \hat{A}_2}{2\sqrt{3}\hat{A}_1} = 0.75. \quad (4.10)$$

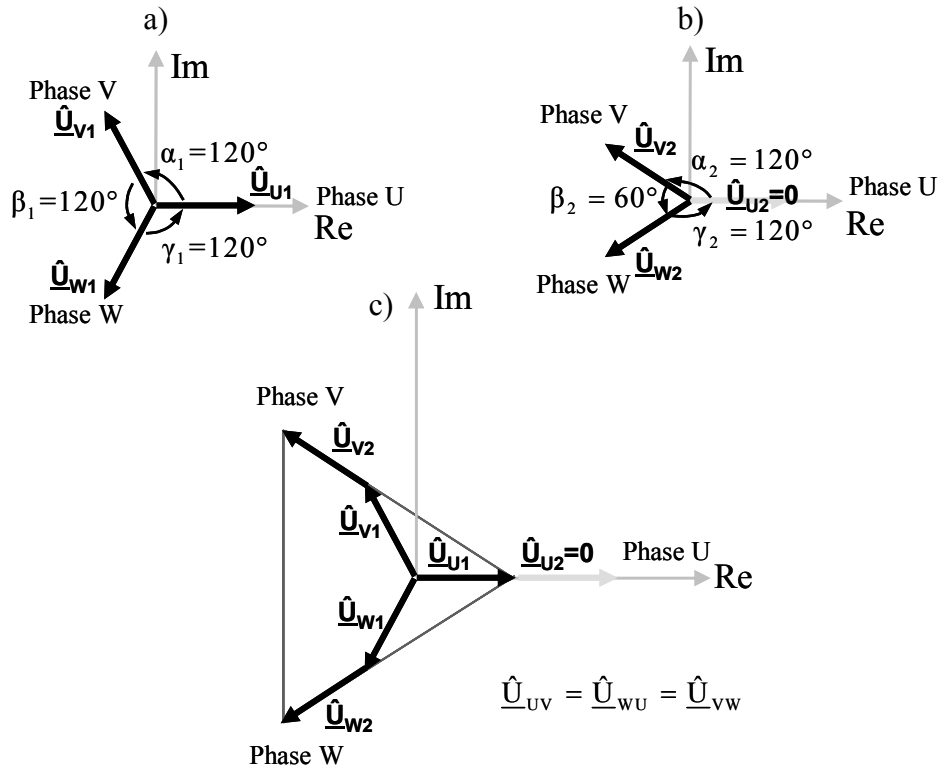


Fig 4.5. 7-level SCHB inverter: a) Phasors of the group A of cells; b) Phasors of the group B of cells; c) Phasors of the complete system.

The resulting value is higher than the maximum modulation index obtained with the first approach which does not consider third harmonic injection. The balance in the line-to-line voltages can also be confirmed by the equivalent phasor diagrams shown in Fig. 4.5 for each group of cells. From the analysis of the figure, it becomes clear that this approach also shifts the level of the neutral point of the inverter to obtain balanced line-to-line voltages. In this case however, the reference angles of cells in one phase show different values, which depend on the new inverter configuration.

Table 4.2 summarizes the phase shift of the references and the maximum modulation index obtained under different fault conditions with this optimization criterion. It should be noted that the configuration in case III corresponds to a system with a group A and a group C of cells. As this approach does not consider the use of the cell in group C, this cell is bypassed and the configuration in case IV is used. The same principle applies for the configuration in case V.

Table 4.2 Faulty cells and reference phase shift for a PS-PWM

Case	Status of the Cells				Phase angle shift				Maximum modulation depth
	Row	Phase U	Phase V	Phase W	Row	Phase U	Phase V	Phase W	
0	1	ok	ok	ok	1	$\alpha_1 = 120^\circ$	$\beta_1 = 120^\circ$	$\gamma_1 = 120^\circ$	$\hat{a}=1$
	2	ok	ok	ok	2	$\alpha_2 = 120^\circ$	$\beta_2 = 120^\circ$	$\gamma_2 = 120^\circ$	
I	1	ok	ok	ok	1	$\alpha_1 = 120^\circ$	$\beta_1 = 120^\circ$	$\gamma_1 = 120^\circ$	$\hat{a}=0.75$
	2	bypass	ok	ok	2	$\alpha_2 = 150^\circ$	$\beta_2 = 60^\circ$	$\gamma_2 = 150^\circ$	
II	1	bypass	ok	ok	1	$\alpha_1 = 150^\circ$	$\beta_1 = 60^\circ$	$\gamma_1 = 150^\circ$	$\hat{a}=0.5$
	2	bypass	ok	ok	2	$\alpha_2 = 150^\circ$	$\beta_2 = 60^\circ$	$\gamma_2 = 150^\circ$	
III	1	ok	ok	ok	1	-	-	-	Use config. IV
	2	bypass	bypass	ok	2	-	-	-	
IV	1	ok	ok	ok	1	$\alpha_1 = 120^\circ$	$\beta_1 = 120^\circ$	$\gamma_1 = 120^\circ$	$\hat{a}=0.5$
	2	bypass	bypass	bypass	2	-	-	-	
V	1	bypass	ok	ok	1	-	-	-	Use config. VI
	2	bypass	bypass	ok	2	-	-	-	
VI	1	bypass	ok	ok	1	$\alpha_1 = 150^\circ$	$\beta_1 = 60^\circ$	$\gamma_1 = 150^\circ$	$\hat{a}=0.25$
	2	bypass	bypass	bypass	2	-	-	-	

4.3.3 Fault tolerant Space Phasor Modulator

A third alternative to solve the problem of voltage balancing with bypassed cells considers the use of the space phasor modulation. In this approach the voltage references are replaced by a reference space phasor, which has to be synthesized by using the three nearest available voltage space phasors. In an inverter with bypassed cells the number of voltage states is reduced depending on the number of damaged cells. Because the number of available voltage space phasors also depends on the number of voltage states, a reduced number of space phasors can be expected. The first step to analyze the operation of the space phasor modulator with faulty cells is to determine the resulting space phasor diagram after the bypass of the faulty cells. From this diagram, aspects such as the maximum modulation index can be derived directly. The second important point is to determine which kind of sequence can be used for each configuration, and how the voltage states corresponding to each space phasor are determined. The firing pulse generation is an important aspect as well which also has to be discussed in order to keep the switching frequency at tolerable levels.

4.3.3.1 Maximum modulation index and reduction of freedom of degrees

Similar to the other two approaches, the modulation index will be used as an indicator of the performance of the proposed method. In SPM, the maximum modulation index will be given as the quotient between the maximum amplitude of the reference space phasor $\hat{u}_{1_faulty}^*$ corresponding to the inverter with bypassed cells and the maximum amplitude of the reference space phasor $\hat{u}_{1_healthy}^*$ with a healthy inverter:

$$\hat{a} = \frac{|\hat{u}_{1_faulty}^*|}{|\hat{u}_{1_healthy}^*|}, \quad a \leq 1 \quad (4.11)$$

The index obtained with eq. (4.11) is equivalent to the definitions given for PWM strategies. For this definition, linear operation of the inverter is assumed, i.e. the operation in the over modulation region will not be considered. In the following, each representative inverter bypass configuration will be analyzed.

Case I, One cell bypassed: the bypass of the cell U2 results in the equivalent space phasor diagram depicted in Fig. 4.6. The maximum modulation index \hat{a} is achieved when the reference phasor reaches the limiting circle depicted in the same figure, that means $\hat{a}=0.75$. The outer regions enclosed by dashed lines are available to obtain a higher voltage in transients, but they will not be considered in this first approach. The same space phasor

diagram is obtained if the cell U1 is bypassed in place of U2. The bypass of a cell in other phases produces a rotation of the space phasor diagram, but the maximum modulation index defined with this method remains unchanged. In this configuration each sector includes a voltage space phasor with redundancy greater than one, therefore sequences of four voltage states, i.e. *continuous-PWM*, or three voltages states, i.e. *discontinuous-PWM* are possible in this operating mode.

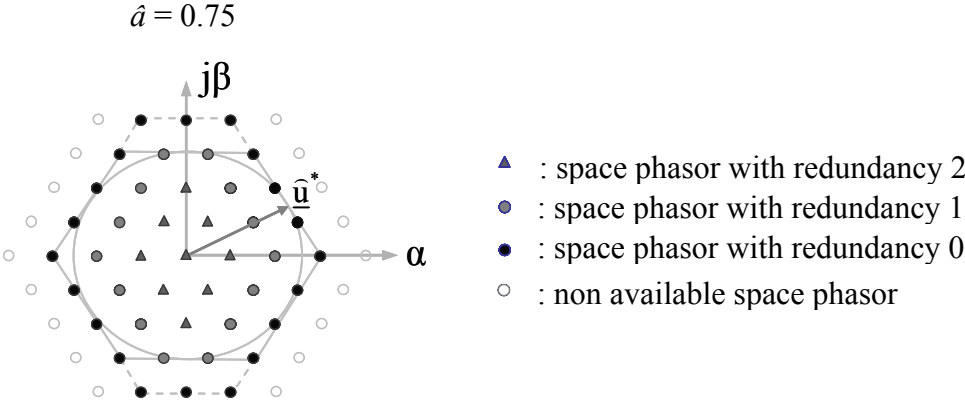


Fig. 4.6. Space phasor diagram and redundancy degrees for one bypassed cell in phase U.

Case II: Two cells bypassed in the same phase: the bypass of the cells U1 and U2 results in the space phasor diagram depicted in Fig. 4.7-a, indicating that a maximum modulation index of $\hat{a}=0.5$ can be achieved in this operation mode. Although the inverter generates voltages

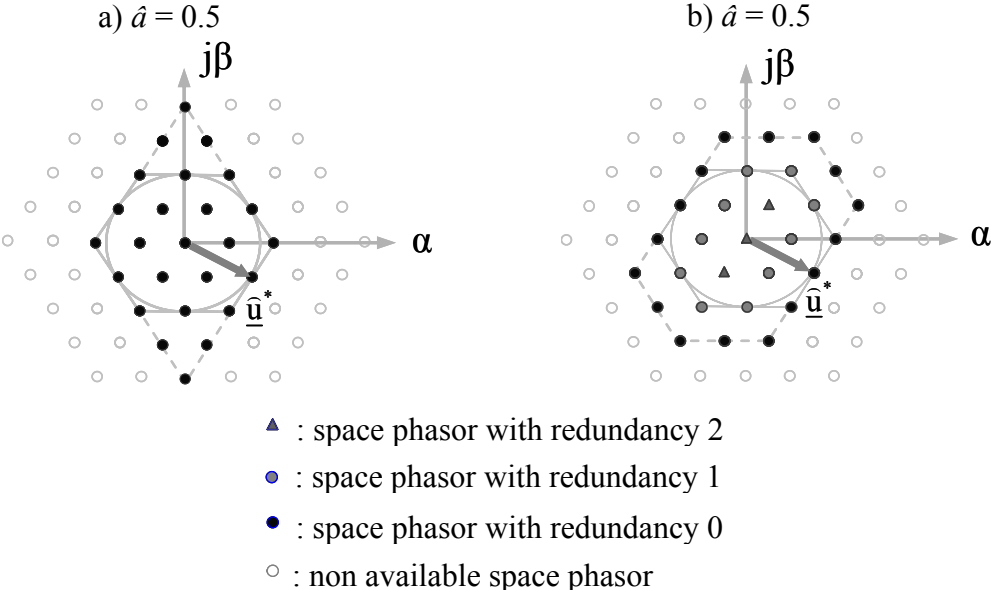


Fig. 4.7. Space phasor diagram and redundancy degrees; a) two bypassed cells in phase U, b) two bypassed cells in different phases.

with two phases, there are still three phases connected to the motor, which differentiates this operation mode from a single-phase inverter. Each space phasor is represented only by one voltage state, i.e. the redundancy for each space phasor is equal to zero. For this reason, *discontinuous-PWM* should be applied in this operating mode.

Case III: Two cells bypassed in different phases: the available space phasors depicted in Fig. 4.7-b for a bypass in cells U2 and V2 permit the operation at a maximum modulation index $\hat{a}=0.5$, the same modulation index that can be obtained with all cells bypassed in one row. Since the remaining healthy cell W2 only contributes with a single unbalanced voltage, the bypass of all three cells in the same row is recommended. It should be noted that the same action was carried out with the PS-PWM approach. In this case, however, it can be seen that the space phasors in the region enclosed by the dashed lines, which are the ones generated by W2, can not be utilized in steady state without causing a voltage unbalance.

Case IV: Three bypassed cells in different phases: the resulting inverter configuration corresponds to a three-level inverter which can deliver 50% of the maximum voltage. Continuous modulation is possible with this configuration.

Case V: Three cells are bypassed, two of them in one phase. As with the PS-PWM approach, the configuration in case VI delivers the same results.

Case VI: Four cells bypassed, two of them in the phase U, one in phase V and one in phase W: the available space phasors in this case allows the operation with a maximum modulation index of $\hat{a}=0.25$, as is depicted in Fig. 4.8. Only *discontinuous-PWM* is possible in this configuration.

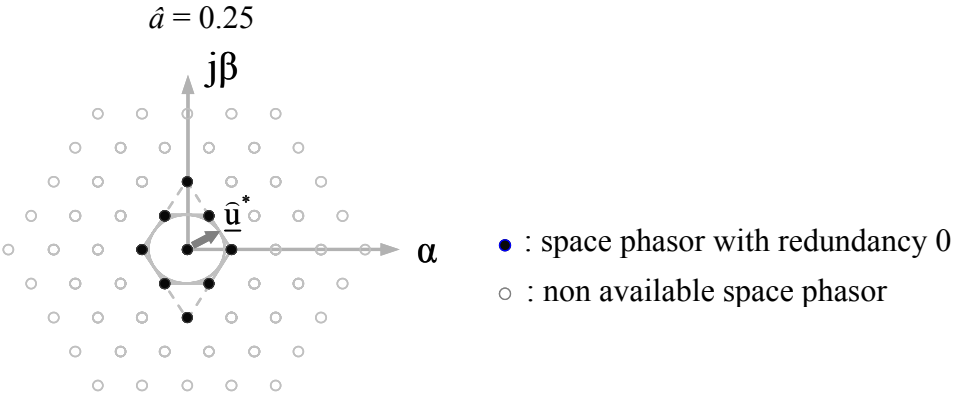


Fig. 4.8. Space phasor diagram Case VI

4.3.3.2 Calculation of optimum voltage states and sequence selection.

The SPM selects the optimal sequence out of a sequence matrix \mathbf{S} that contains all voltage states of one sector. In an inverter with bypassed cells, each valid voltage state must fulfil a more restrictive constraint which depends on the number of cells available in each phase N_{cell_U} , N_{cell_V} , N_{cell_W} :

$$\mathbf{s}_k = \begin{bmatrix} |u_{UN}| \\ |u_{VN}| \\ |u_{WN}| \end{bmatrix} \leq \begin{bmatrix} N_{cell_U} \\ N_{cell_V} \\ N_{cell_W} \end{bmatrix} \quad (4.12)$$

As a consequence, the number of available voltage states in each sector is reduced. E.g., for the sector depicted in Fig. 4.9, only the voltage states $\mathbf{S} = [s_{-3} \ s_{-2} \ s_{-1} \ s_0]^T$ are valid. These states generate a higher common mode voltage than the sequence that would be used in case of a healthy inverter configuration: $\mathbf{S} = [s_{-2} \ s_{-1} \ s_0 \ s_1]^T$ or $\mathbf{S} = [s_{-2} \ s_{-1} \ s_0 \ s_1]^T$; therefore the same principle used in PSPWM is applied, i.e. the neutral point of the inverter is shifted in order to achieve the desired voltage.

In the following, some aspects of the sequence generation for each bypass configuration will be discussed. It will be assumed that the state machine in Fig. 3.11 is modified to operate with fewer cells; that means, the firing pulses will be distributed only among the healthy cells in each phase.

Case I: One bypassed cell. Under this configuration each sector has at least one redundant space phasor available, therefore the application of sequences of four states or *continuous PWM* is possible. Because this approach generates one switching action each modulation period, the remaining cell in the phase with the bypass will assume this transition every modulation period, whereas the cells in the other phases exhibit one switching action every two periods. As a consequence, the cell in the phase with the bypass will work at twice the rated switching frequency, leading to twice the amount of switching losses, as is depicted in Fig. 4.10-a. Care needs to be taken to keep all semiconductors within tolerable temperature limits.

There are different ways to solve this problem. The easiest alternative is the increase of the modulation period T_s to twice the original value. In this manner, the switching frequency of a switch S_x of the cell in phase with the fault will be reduced to the nominal value, as it is shown in diagram of Fig. 4.10-b. The disadvantage of this approach is that the switches of the cells in the other phases are not fully utilized.

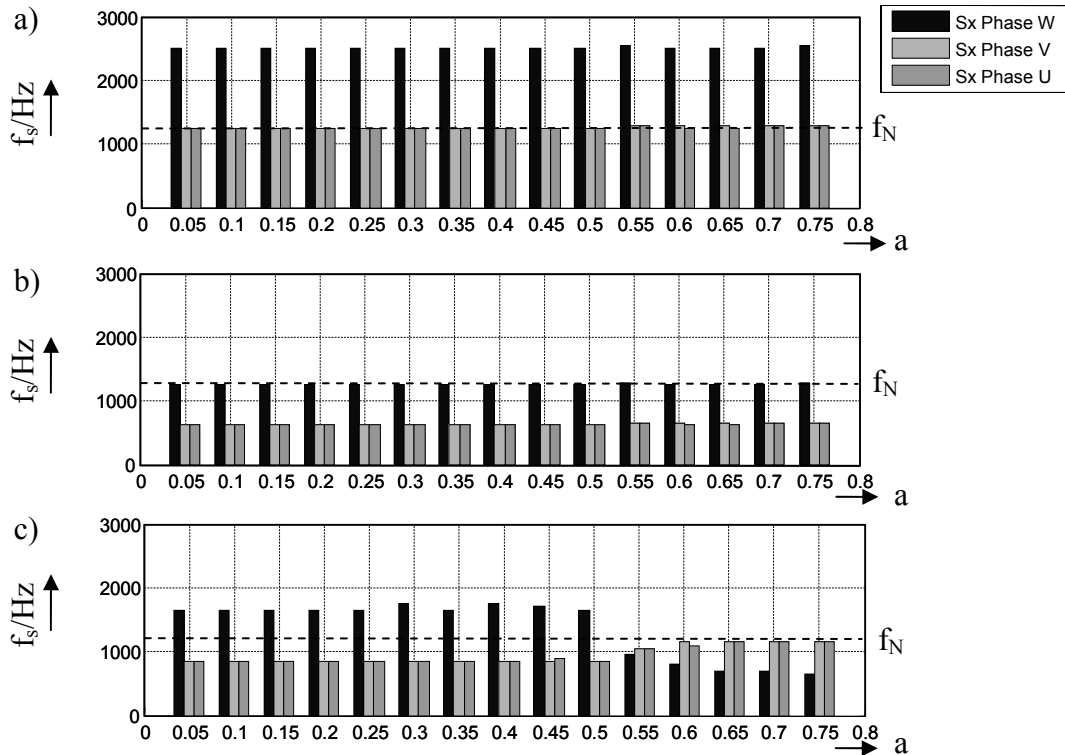


Fig. 4.10. Switching frequency of a switch S_x of phases U,V,W for different modulation indexes with one faulty cell in phase U. The nominal switching frequency is $f_N=1250$ Hz:

- a) *Continuous PWM* with $T_s=200$ μ s; b) *Continuous PWM* with $T_s= 400$ μ s; c)
discontinuous PWM with $T_s= 200$.

Other alternative considers the use of a different sequence approach. For example, with the *discontinuous PWM* only three voltage states are used each modulation period, and as a consequence only two phases exhibit a switching transition. As a result, the switching frequency in each phase is reduced to $2/3$ of the rated value. By using this method, the switching frequency of the cell in the phase with the bypass is increased only to a $4/3$ of the rated value. For higher modulation indexes, $a>0.5$, all switches work under nominal conditions, as it is depicted in Fig.4.10-c.

An additional optimization can be achieved by using the different sequences of voltage states available for $a<0.5$. As it is shown in Fig. 4.11, each sector in this region has a space phasor with redundancy degree of at least two. This results in three possible sequences for each sector which can be used to optimize the distribution of the firing pulses, provided that each sequence keeps a phase with constant voltage and without switching actions.

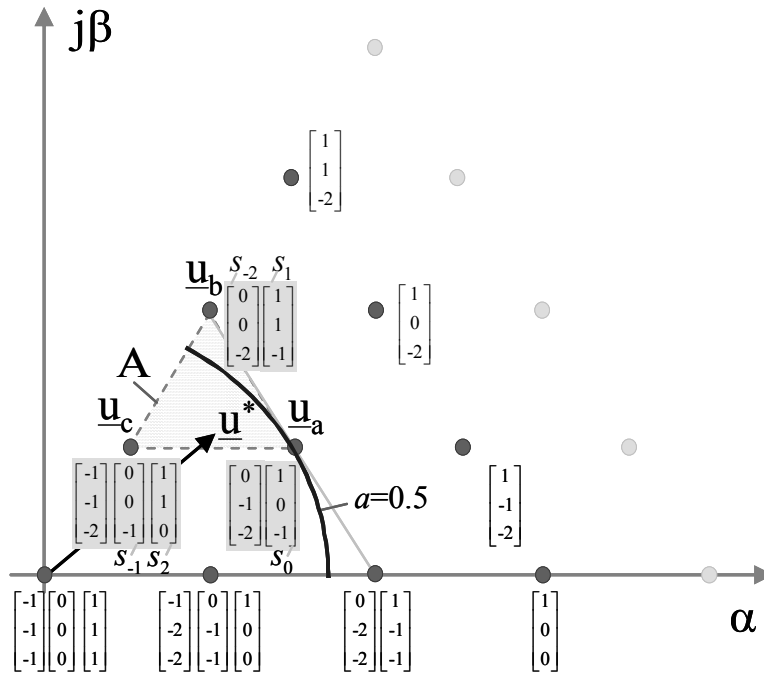


Fig. 4.11. A sextant of the space phasor diagram for one cell bypassed in phase U including all possible voltage states for each space phasor.

For the sector A depicted in Fig. 4.11, the following sequences are valid: $\mathbf{S}=[s_{-1} \ s_0 \ s_1]$, $\mathbf{S}=[s_0 \ s_{-1} \ s_2]$, $\mathbf{S}=[s_0 \ s_1 \ s_2]$. Ideally, the modulator should select a sequence that keeps the voltage constant in the phase with the bypassed cell, i.e. no switching transitions, and at the same time provides a low common mode voltage generation. In order to achieve this goal, the modulator first checks if the sequence with minimum common mode voltage fulfils this condition, in this case $\mathbf{S}=[s_{-1} \ s_0 \ s_1]$. If this sequence fails, then one of the other two sequences with higher common mode voltage must accomplish with this requirement: $\mathbf{S}=[s_0 \ s_{-1} \ s_2]$ or $\mathbf{S}=[s_0 \ s_1 \ s_2]$. They are alternated to obtain one switching action in the faulty phase each two modulation periods.

By the application of this algorithm in the region $a < 0.5$, the number of switching actions can be kept below the nominal values for the complete operation range, as it is shown in Fig. 4.12.

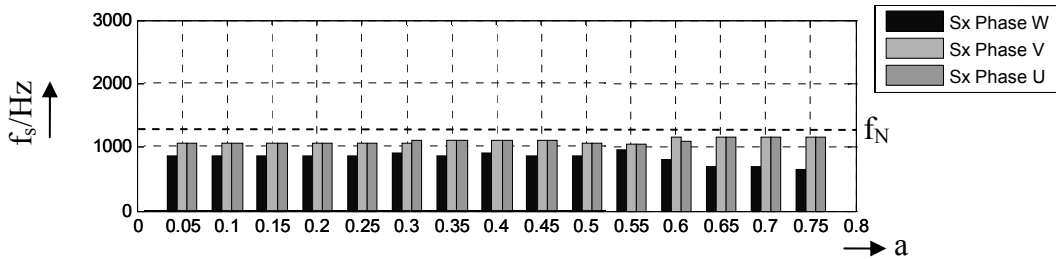


Fig. 4.12. Switching frequency of a switch Sx of phases U, V, W for different modulation indexes with one faulty cell in phase and *Discontinuous PWM* with optimized sequences, $T_s = 200 \mu s$. The nominal switching frequency is $f_N = 1250$ Hz.

Case II) Two cells bypassed in the same phase: In this operating mode each space phasor is represented by a single voltage state, therefore only *discontinuous PWM* is possible. No special considerations about the switching frequency are necessary, because there are two remaining cells in each phase available to distribute the firing pulses.

Case III) Two cells bypassed in different phases: In this case the procedure described in case IV is used.

Case IV) Three cells bypassed in different phases: this operating mode is equivalent to a three level inverter. The standard modulation method, i.e. *continuous PWM*, can be used if the modulation period T_s is adjusted to twice the original value.

Case V) Three cells bypassed two of them in one phase. The inverter configuration of case VI is considered.

Case VI) Four cells bypassed, two of them in the phase U, one in phase V and one in phase W: The available voltage space phasors have no redundancy degree, therefore only *discontinuous PWM* is possible and the modulation period T_s has to be adjusted to twice the original value to reduce the switching frequency.

The discussed operation modes for the main bypass configurations are summarized in table 4.3. The maximum output voltage obtained with this approach is the same as with the PS-PWM.

Table 4.2 Modulator operation modes for different bypass configurations.

Case	Status of the Cells				Maximum modulation depth	Modulation period	Modulation type
	row	Phase U	Phase V	Phase W			
0	1	ok	ok	ok	$\hat{a}=1$	T_s	Continuous Modulation
	2	ok	ok	ok			
I	1	ok	ok	ok	$\hat{a}=0.75$	T_s	Discontinuous Modulation
	2	bypass	ok	ok			
III	1	bypass	ok	ok	$\hat{a}=0.5$	T_s	Discontinuous Modulation
	2	bypass	ok	ok			
IV	1	ok	ok	ok	$\hat{a}=0.5$	$2T_s$	Continuous Modulation
	2	bypass	bypass	bypass			
VI	1	bypass	ok	ok	$\hat{a}=0.25$	$2T_s$	Discontinuous Modulation
	2	bypass	bypass	bypass			

4.3.4 Control strategy with faulty cells

An important aspect about the fault tolerant operation deals with the restrictions on the control variables caused by the new voltage limitation. Depending on the operating point, a sudden change of the voltage limit may also produce a fast variation of the frequency of the stator flux which results in an undesired torque transient. Therefore, it is relevant to develop a strategy that can drive the machine to the new operating point as smooth as possible. Depending on the number of faults, the new voltage limit can be applied immediately or after the machine has reached a convenient operating point. For example, in a non-critical fault such as insufficient DC-Link voltage smoothing, the bypass of the faulty cell is not required immediately, therefore the controller may first change the operating point of the machine and then carry on the bypass the faulty cell. On the contrary, a critical fault such a DC-link short circuit requires immediate attention. In this case the controller should first bypass the cell, changing the operating point afterwards. Both alternatives will be analyzed in the following sections.

4.3.4.1 Limiting values of the control variables for the field weakening operation

The reduction of the voltage available to the inverter directly affects mechanical power that can be delivered by the machine. As a result, a change in the starting point for the constant power operation, or field weakening, is needed. In large inductions machines, the following equation defines the boundary for field weakening operation with good approximation. It is given in terms of the stator flux frequency:

$$\hat{\omega}_1 = \frac{\hat{a} \cdot u_{1N}}{\Psi_{1N}} = \hat{a} \cdot \omega_{1N}, \quad (4.13)$$

where \hat{a} is the maximum modulation index given by the new inverter configuration. The stator flux magnitude in the field weakening region can also be defined as a function of the maximum modulation index:

$$\Psi_{\text{steady}}^* = \frac{\hat{\omega}_1}{\hat{\chi}_{1\text{steady}}} \Psi_{1N} = \frac{\hat{a} \cdot \hat{\omega}_{1N}}{\hat{\chi}_{1\text{steady}}} \Psi_{1N} \quad (4.14)$$

In order to comply with the requirement of constant power, the torque is also restricted within this operating region:

$$\hat{M}_{\text{fw}} = \frac{\hat{a} \cdot \hat{\omega}_{\text{mech}_N}}{\hat{\omega}_{\text{mech}}} \cdot M_N \quad (4.15)$$

Or alternatively, since the strategy is based on the rotor frequency ω_2 , the torque limiting value can be expressed in terms of this variable:

$$\hat{\omega}_{2fw} = \hat{M}_{fw} \cdot \frac{R'_2}{|\underline{\Psi}'_2(t)|^2} \frac{2}{3p} \quad (4.16)$$

The boundaries previously defined can be implemented by including the factor \hat{a} in the torque and flux limits, as it is shown in Fig. 4.14.

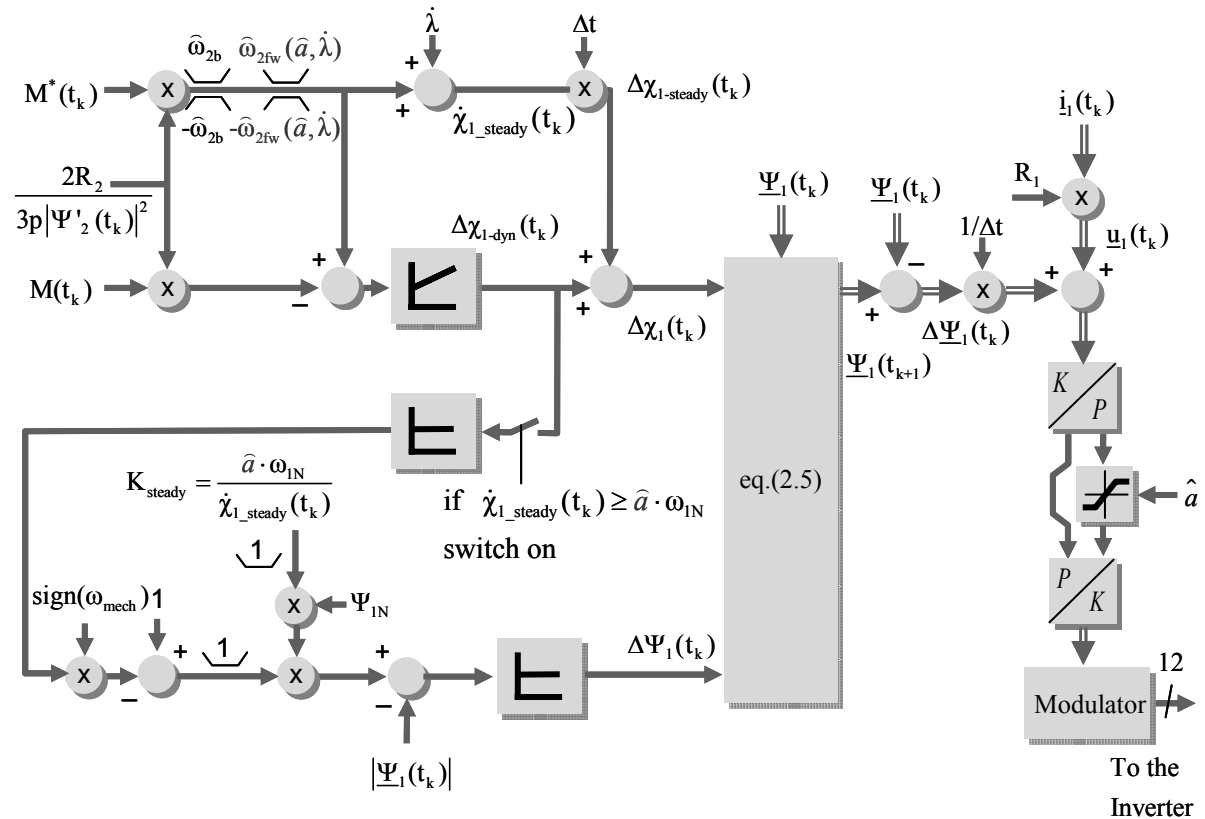


Fig 4.14. Torque and flux controller and their boundaries changed for a fault tolerant

The limiting values for the starting point of field weakening can be adjusted immediately if the machine operates under these limits, otherwise a sequence to adjust these limits is needed. The most noticeable effect of an abrupt limitation in the voltage consists in an undesired torque transient. As the stator voltage directly affects the rotational speed of the stator flux, the angle related to torque generation between stator flux and rotor flux space phasors:

$$\vartheta = \int \dot{\chi}_1 - \dot{\chi}_2 dt \quad (4.17)$$

may be reduced or even reach negative values due to the slow dynamics of the rotor flux. This effect can be avoided if the stator voltage is gradually reduced until the new limit has been reached; a non critical fault is required for this operation, though.

4.3.4.2 Change of the limiting values in a non critical fault

Different strategies can be used to drive the machine to an operating point which fulfils the new limits. The easiest approach consists of reducing the speed of the machine according to the new maximum value of the modulation index; e.g. for a maximum modulation index of $\alpha=0.5$, the speed should be reduced to 50% of the nominal value. Afterwards, the torque and flux limits can be changed without risk of problems associated to a non linear operation, as the control variables do not reach the limits. The user can now operate the machine to higher speeds by using the field weakening. The disadvantage of this approach is that the speed of the machine first needs to be reduced to the new operating point and then it can be increased by means of field weakening until the constrained electrical torque equals the load. A much better performance is obtained if the machine reaches the steady state speed in one step. In order to drive the machine to this new operating point, the limits of the torque and flux can be modified following a sequence, or they may be modified simultaneously. The first alternative yields a more predictable behaviour of the machine. The following procedure allows the change of torque and flux limits in four steps:

- Step 1 - Transitions A-B-C in Fig. 4.15: For a given operating point A, the electrical torque limit is adjusted according to the maximum modulation index after the bypass. If the machine operates with a load torque higher than this new restriction, as is the case in Fig. 4.15, the control drives the machine with the new torque limit until the speed reaches the stable point C, as it is depicted in the characteristic curve of the torque in Fig. 4.15.a
- Step 2 (transition C-D): When the machine reaches the new equilibrium point, the stator flux magnitude may be adjusted with the new limit according to the maximum modulation index (Fig. 4.15.b). The stator voltage decreases with the change of flux to the new maximum value.
- Step 3 (transition D-E): The stator voltage reaches the new restricted value in the operating point E. The modulator can now change to an operation mode with fewer cells and the output of the faulty cell is set to zero voltage.
- Step 4: The cell is bypassed and it is ready for its removal and repair.

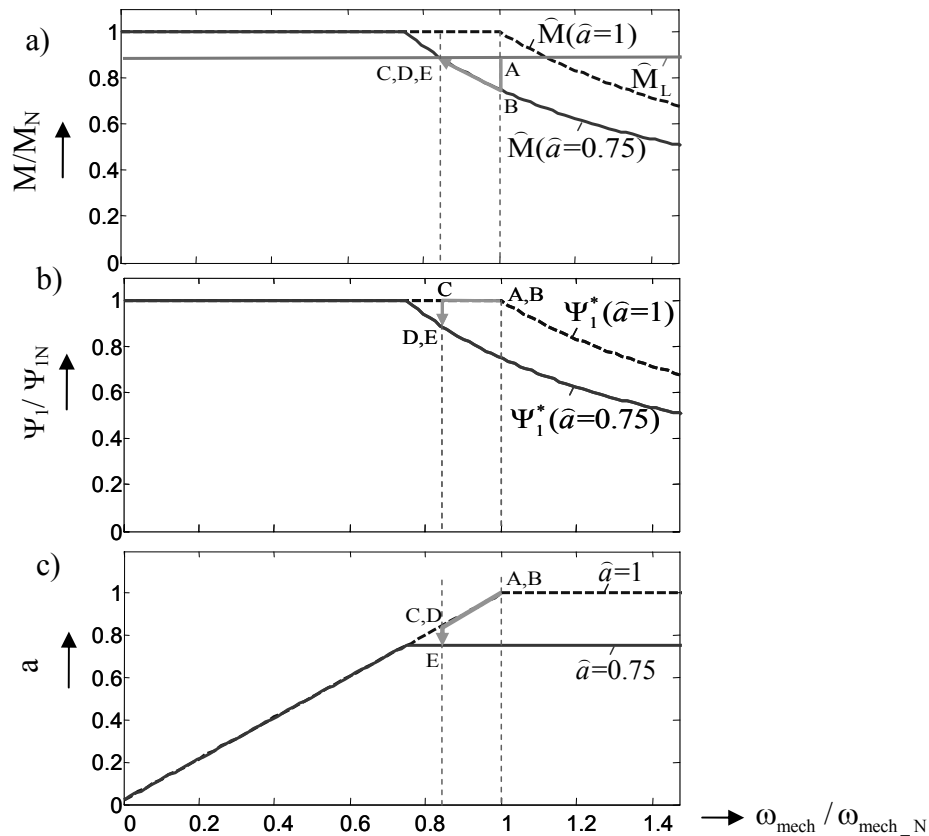


Fig 4.15. Change of the operating point for the bypass of one cell. The load torque is higher than the new limit of torque after the bypass. a) torque characteristic curve; b) flux characteristic curve; c) voltage characteristic curve.

If the torque limit has a higher value than the load torque, then a reduction of the speed is not necessary. In this case the torque delivered by the machine will not be affected and the control can proceed with the step two immediately, as it is shown in Fig. 4.16-b. The reduction of the voltage is in this case a consequence of the flux change, with a dynamics depending on the flux controller. This is also a gradual process, i.e. the voltage does not reach the steady state immediately.

It should be noted that the flux transition is not decoupled from the torque, however if the steady state part of the flux controller has a dynamic lower than the torque controller, the latter can compensate the influence of the flux in the torque. This opens the possibility to set limits of torque and flux at the same time, achieving in this way a shorter time for the voltage reduction and for the bypass of the cell.

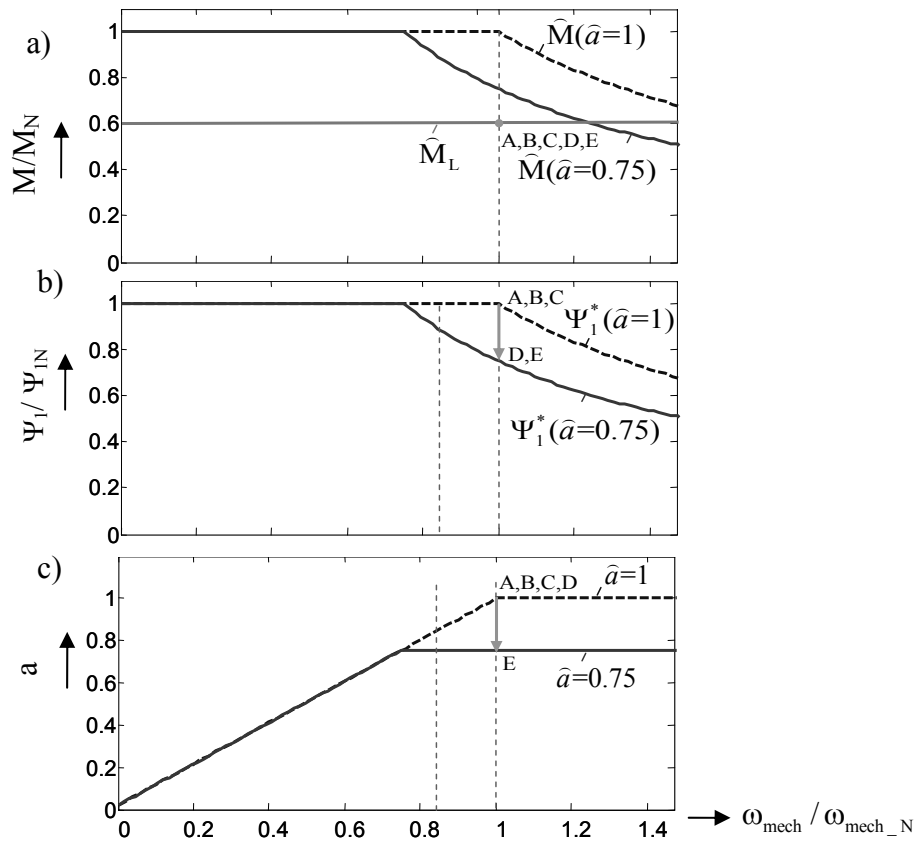


Fig 4.16. Change of the operating point for the bypass of one cell. The load torque is lower than the new limit of torque after the bypass. a) torque characteristic curve; b) flux characteristic curve; c) voltage characteristic curve.

4.3.4.3 Change of the limiting values in a critical fault

Critical failures such as short/open circuits demand an immediate attention of the controller. In two level inverters for example, short-circuits in IGBTs are managed directly by the drivers, turning off all the power switches of the inverter. Such failures are also detected by the cells of a H-bridge multilevel inverter. As a consequence, the faulty cell can not be used to reach a new operating point and the bypass of the cell is compulsory as soon as the fault is detected. For the following analysis, it will be assumed that the bypass of the cell can be made immediately, that means, the output of the cell will be zero after the fault detection without delay. This is not a very realistic consideration if mechanical bypass is used, although other alternatives based in semiconductors may accomplish this requirement at a higher cost [4].

Provided that the machine operates at rated speed, the controller must set the new limit for the stator voltage immediately, generating an unwanted and also unavoidable negative torque

transient. The new operating point must be reached quickly, therefore torque and flux limits are also set at the same time.

During the torque transient, the integral part of the torque controller could accumulate the generated error affecting the settling time. Strictly speaking, the torque controller enters in saturation, being unable to increase the torque due to the insufficient voltage and the restricted capability of the dynamic field weakening controller. Since no benefit is obtained by increasing the output of the torque controller in this operating point, the integrator of the torque controller is disabled. This behaviour is similar to the well known anti-windup of the PI controller in conventional control-loops and can be described as follows:

- If $|\underline{u}_1(t_k)|$ is in-bounds, the integrator operate as usual.
- If $|\underline{u}_1(t_k)| - \hat{u}_1 > \Delta_1$ and $M^* - M > 0$, the integrator operate as usual.
- If $|\underline{u}_1(t_k)| - \hat{u}_1 > \Delta_1$ and $M^* - M < 0$, the integrator is disabled.

The constant Δ_1 defines a small hysteresis band added to avoid oscillations. The integral part of the controller is enabled as soon as the output voltage is out of the saturation condition.

4.4 Summary of chapter 4

In this chapter, the operation of the H-bridge multilevel inverter under different fault conditions was analyzed. The industrial available version of this inverter includes the possibility of fault-tolerant operation by means of a bypass of the faulty cells. In case of fault detection in one phase, the simplest solution considers the bypass of all cells in the same row, in order to allow the operation with balanced voltages. This solution presents the disadvantage that healthy cells are bypassed and the inverter is not fully utilized. Three different alternatives were presented, based on the assumption that the neutral point N of the inverter is floating and is not connected to the neutral point of the machine.

The standard method uses a phase shift of the voltage references to generate balanced line-to-line voltages; this phase shift depends on the bypass configuration of the inverter. By using this method, a higher output voltage than with the simple solution is obtained, however it does not consider the use of third harmonic injection, therefore the inverter capability is not fully utilized.

A new method based on a modified PS-PWM approach was also presented. The main idea of this approach is that the inverter can be considered as the series connection of two systems: a symmetrical three-phase system of cells which operates with third harmonic injection and normal phase shift in the references and an unsymmetrical system which can be balanced by means of the phase shift reference approach. It was demonstrated that the output voltage obtained with this method is higher than the one achieved with the solution only considering the phase shift in the references.

A third new alternative is based on the space phasor modulation. It makes use of the inverter redundancies, i.e. the different voltages states which are available to generate each voltage space phasor. In case of the bypass of some cells, several voltage states of the inverter are invalid and can not be applied with the new inverter topology. This affects the number of available space phasors and the number of redundant states which can be used by the inverter. A relationship between the resulting inverter topology after the bypass and the maximum modulation index was found. With this relationship, the operation of the modulator can be restricted to a region where there are always valid voltage space phasors available. The SPM algorithm then calculates an optimal sequence, out of the selected space phasors. The difference with a healthy inverter is that some voltage states are lost after the bypassing of cells. Optimal sequences with minimum common mode voltage are not possible anymore,

therefore an alternative sequence with higher common mode voltage is used. In this way, the same concept of a phase shift of the neutral point is applied in this case.

Finally, a description of the new limits for the control variables was given. For an inverter operating with faulty cells, the maximum voltage is restricted to a new maximum value affecting the amount of mechanical power that can be delivered by the machine. As a result, a change in the starting point for the field weakening is needed. Flux and torque have to be constrained according to this maximum modulation index and a sequence of actions was defined in order to drive the machine smoothly to the new steady state point of operation.

5. EXPERIMENTAL RESULTS

The theoretical principles investigated in this work were validated by means of a hardware set-up whose main component is a 5-level H-bridge multilevel inverter prototype specially built for this purpose. The inverter is used to supply an induction machine which was coupled to a permanent magnet machine actuating as a variable load. In this chapter a description of this set-up will be given as well as some measurement results.

5.1 Multilevel Inverter

The multilevel inverter prototype is based on several H-bridge inverters units connected in series. Each inverter unit was built in a single board containing four discrete IGBTs of type IRGPH40UD, as it is shown in Fig. 5.1. A 2A gate driver HCPL-316J, with integrated desaturation detection and fault status feedback functions, was utilized for the switching of IGBTs. To supply the drivers of each IGBT, isolated DC-DC converters which operate with a single DC voltage supply of 5V were used. Each board also contains a dead time generation

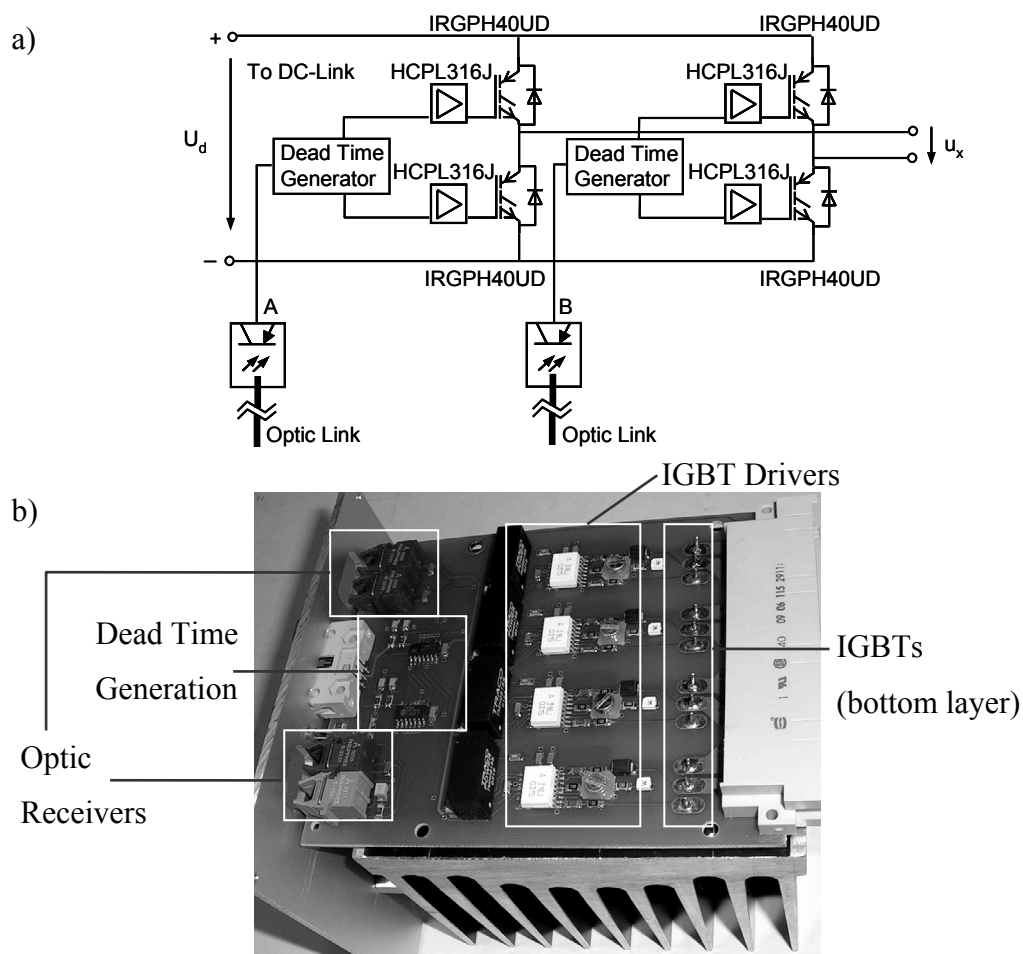


Fig. 5.1. H-bridge cell of the multilevel inverter: a) Circuit diagram; b) Hardware implementation.

circuit in order to avoid DC-link short circuits. At the same time, this circuit permits to define the state of the output voltage by simply using two binary signals. The connections with the main controller via optical fibers avoid the influence of noise in the firing pulses.

The cells were mounted in racks including boards with the DC links and braking-choppers. Each chopper consists of a power switch connected in series with a resistance of 180 ohms and the corresponding control circuit as it is shown in Fig. 5.2. The chopper control circuit uses basically the measurement of the corresponding DC link voltage and compares it with an adjustable voltage reference in order to generate the firing pulses. Finally, a transformer is needed to supply the rectifier of each DC-link board.

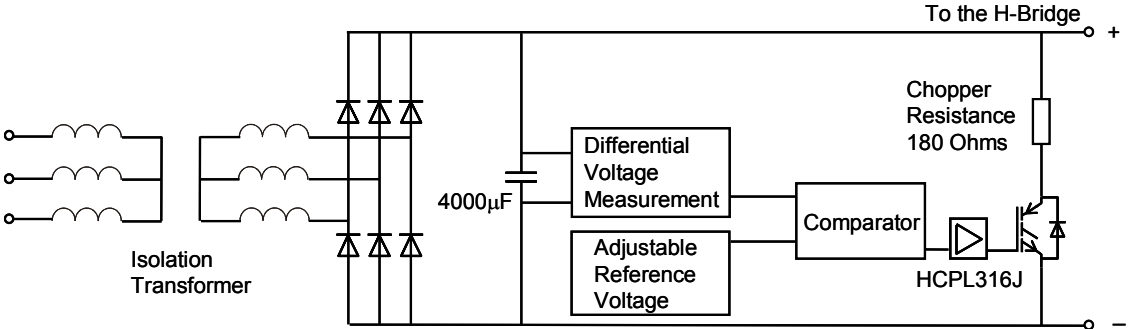


Fig. 5.2 Circuit diagram of the DC-link voltage for each cell.

The control scheme was implemented in a floating point DSP board based on the ADSP-21062 processor from Analog Devices, as it is shown in the schematic block diagram of Fig. 5.3. This board is specially devised for control tasks and includes sixteen independent A/D converters with a conversion time of 600 ns , four 10-bits D/A channels which can be used for the visualization of the variables in the oscilloscope.

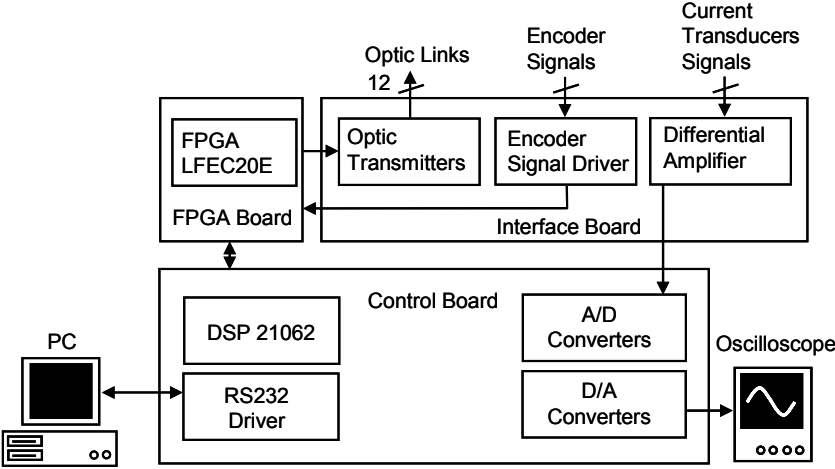


Fig. 5.3 Simplified scheme of the inverter controller.

In addition, a daughter board based on the LFEC20E FPGA from Lattice was utilized to help the DSP with the SPM algorithm. The firing pulses generated by the FPGA are transmitted to each cell by using an optic link.

Multiple alternatives are available for the programming of the DSP in the software environment. In this application a C language compiler is used. The communication between the DSP and the computer was carried out using the standard serial interface included in both equipments. The program can be stored in a flash EEPROM memory in order to preserve its contents after the turn-off of the power supply.

5.2 Laboratory set-up

The multilevel inverter prototype supplies a 5,5 kW asynchronous machine coupled to a synchronous permanent magnet machine working as a load, as it is depicted in Fig. 5.4. In order to obtain a variable load torque, the synchronous machine was connected to a three-phase adjustable resistance. The parameters of the asynchronous machine used in this set-up can be found in the appendix.

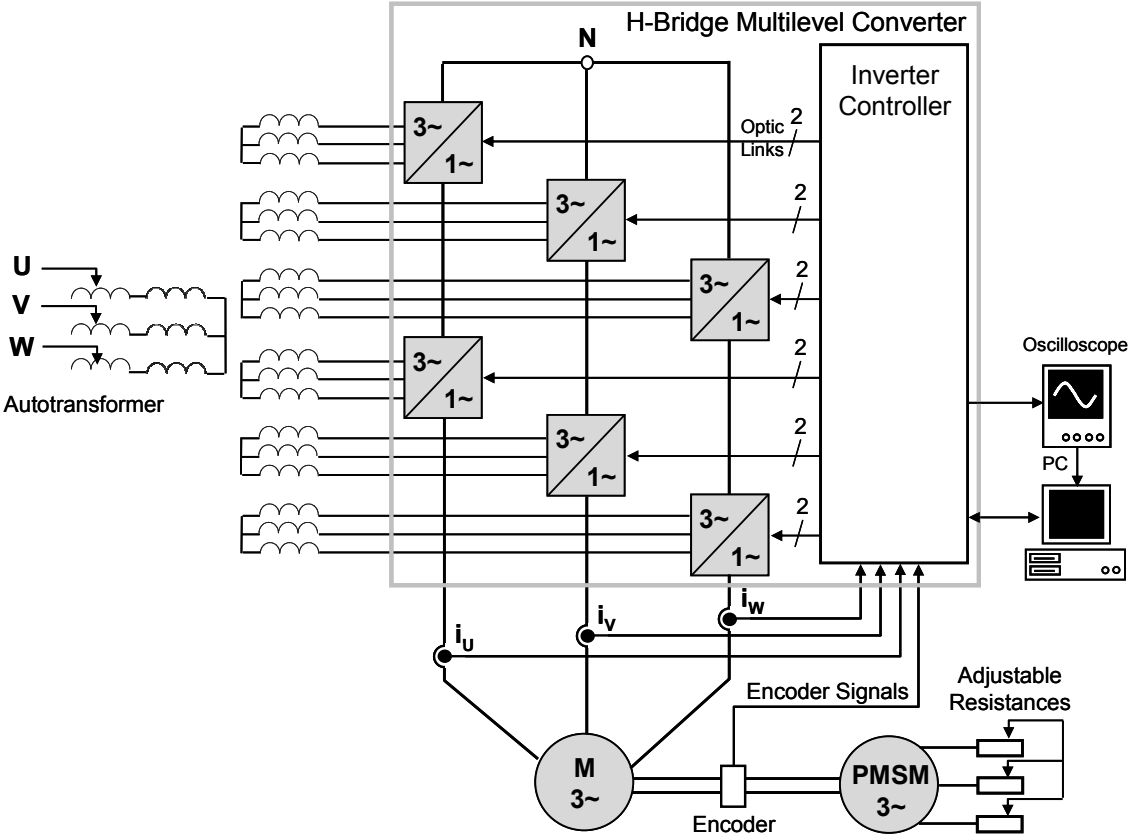


Fig. 5.4 Simplified scheme of the laboratory set-up.

5.3 Measurements of the steady state operation with bypassed cells

As it was discussed in chapter 4, the bypass of cells produces different inverter topologies, which can be classified according to the number and the position of the faulty cells. From all those configurations, some of them result in a balanced topology. In this case, the only action necessary to continue the operation of the inverter is the change of the maximum modulation index, as it occurs in case IV described in chapter 4. On the other hand, there are three inverter configurations corresponding to cases I, II and VI of table 4.2, which are unbalanced and in this case a modified modulation strategy can be applied to obtain balanced machine voltages. In the following, the inverter configurations of cases I and II will be carried out to verify the proposed method. It is to be remarked that Case VI is equivalent to case II, in the sense that one phase generates zero voltage. For this reason this case will not be considered.

For this test the autotransformer is adjusted to obtain a DC link voltage of $U_d=80V$ in each of the six cells of the 5-level inverter. Given this voltage, the stator flux reference is adjusted to $\Psi_{1N} \cdot k_u = 0.56 V/s$, in order to obtain rated speed at maximum modulation index. Fig. 5.5 shows the inverter voltages referred to its neutral point N and the phase currents for one bypassed cell in phase U.

The bypass of the cell is generated by the controller, which sets the firing signals to produce an output voltage equal to zero. The remaining cells operate according to the fault tolerant approach. As expected, the voltage in phase U exhibits only two levels, i.e. the inverter voltages are unbalanced, whereas the inverter current waveforms are sinusoidal. The small drop in the phase potentials is produced by the saturation voltage of the transistors. This effect is not significant with an inverter working at higher voltages.

Fig. 5.6 shows a test with two bypassed cells in a same phase. In this case the maximum available voltage is only 50% of the nominal value. As predicted, the resulting currents are still sinusoidal. A small current unbalance is caused by the DC-link voltage variation, which results in the higher load unbalance in the remaining healthy cells. Again, this effect can be avoided with higher DC-link voltage, since then the voltage variations caused by the choppers are less significant.

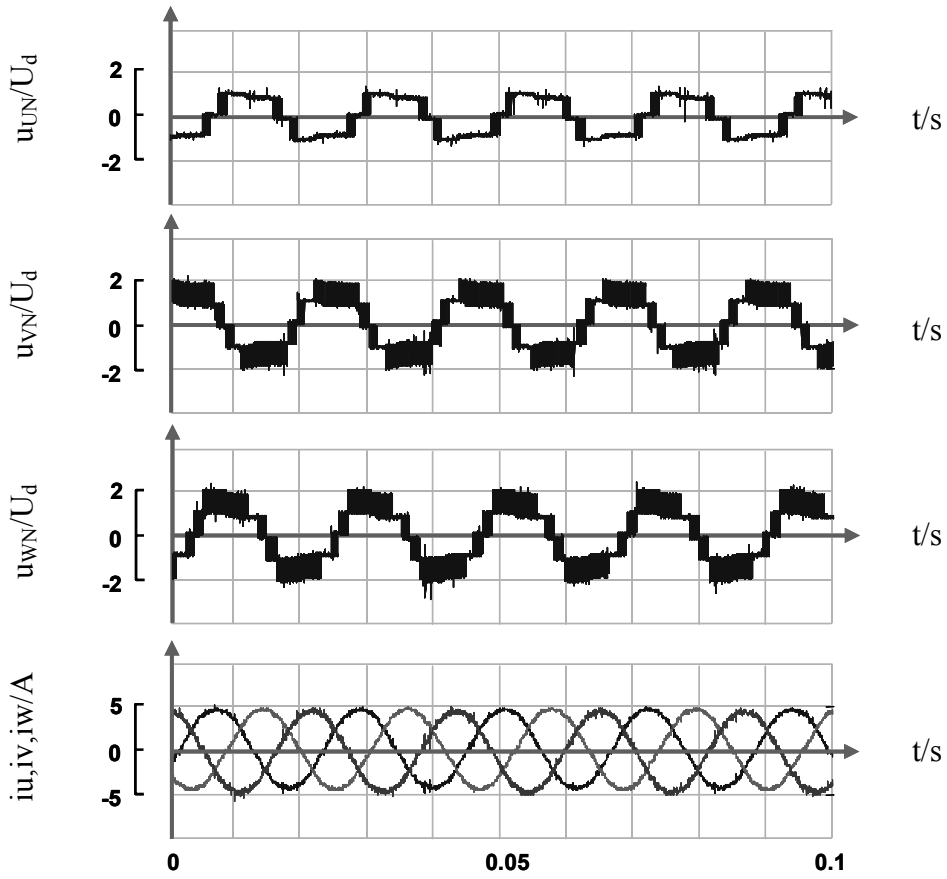


Fig. 5.5. Phase voltages and currents for one bypassed cell.

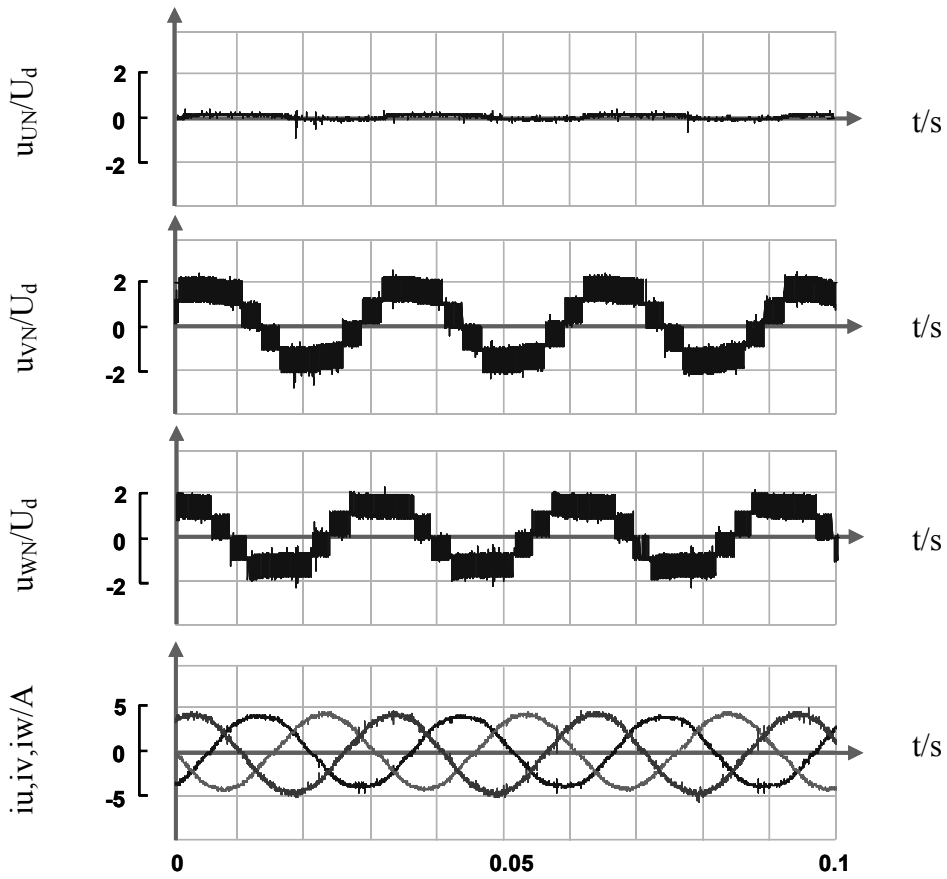


Fig. 5.6. Phase voltages and currents for two bypassed cells in the same phase.

5.4 Switching frequency with bypassed cells

One of the requirements of the multilevel SPM described in chapters 3 and 4 was to keep the switching frequency at nominal levels. In addition to the simple solution that considers a reduction of the modulation frequency, an optimization method was presented for the case of one bypassed cell at modulation indexes $a < 0.5$.

As it can be seen in Fig. 5.7-a for a healthy inverter configuration and $a=0.38$, the firing pulses of three IGBTs in different phases exhibit approximately the same switching frequency. In the case of one bypassed cell, the resulting firing pulses waveforms show a different switching frequency in each phase. In particular, the firing pulses in the remaining cell of phase U depicted in Fig. 5.7-b clearly exhibit a higher switching frequency than the firing pulses of nominal operation presented in Fig 5.7-a. Since this operation mode increases

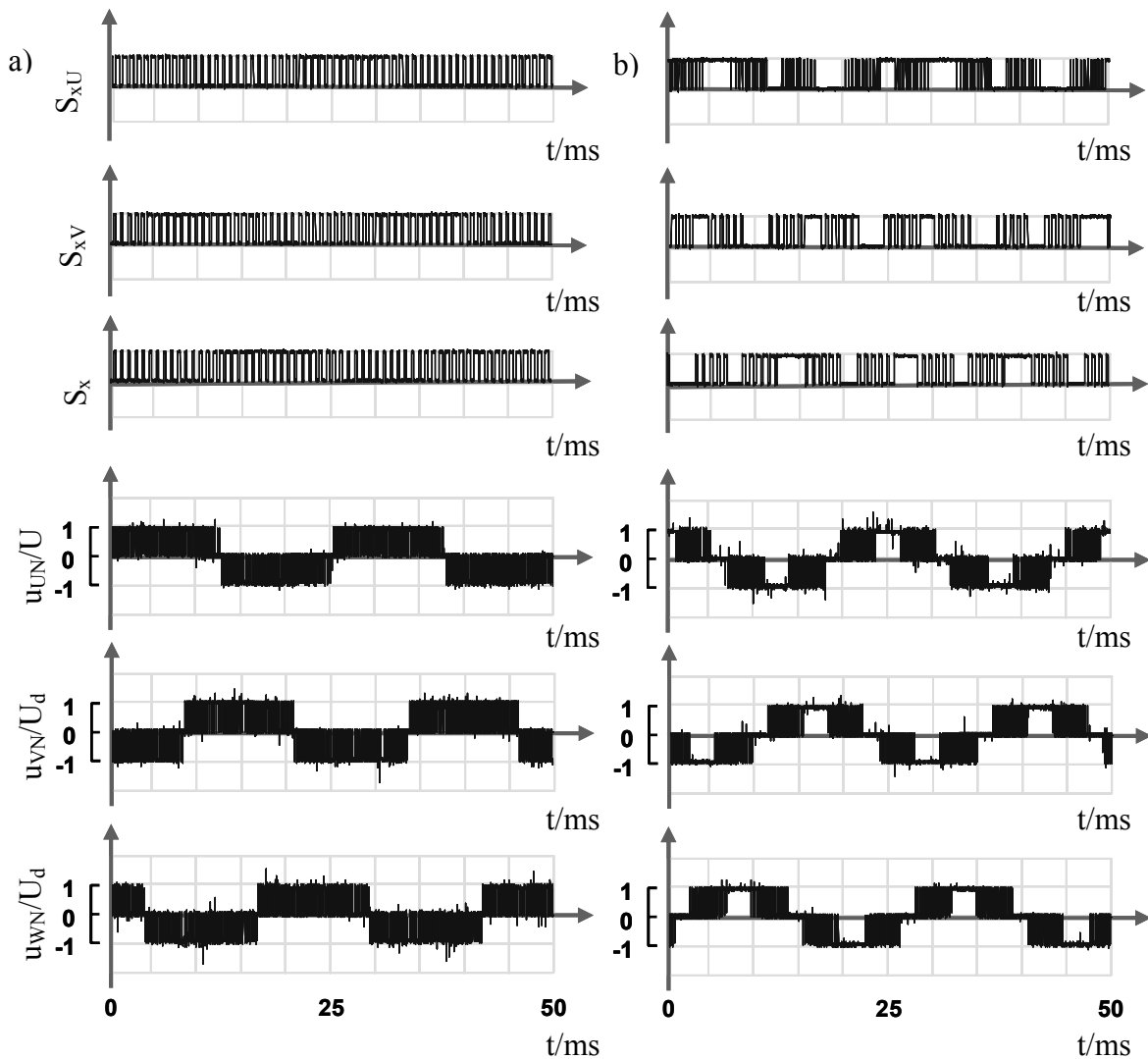


Fig. 5.7. Phase voltage and firing pulses waveforms; a) healthy inverter, b) one cell bypassed without sequence optimization.

the switching losses, the optimization by means of the change in the sequences described in chapter 4 will be applied.

Fig. 5.8 shows the resulting firing pulses after the optimization. The firing pulses are in this case distributed among the other two healthy cells, allowing a reduction of the switching frequency in the remaining cell as planned. It should be noted that the change introduced in the sequences does not affect the fundamental component of the phase potentials, only the common mode voltage. Since always the three nearest space phasors are selected, the line-to-line voltages are not affected by this optimization.

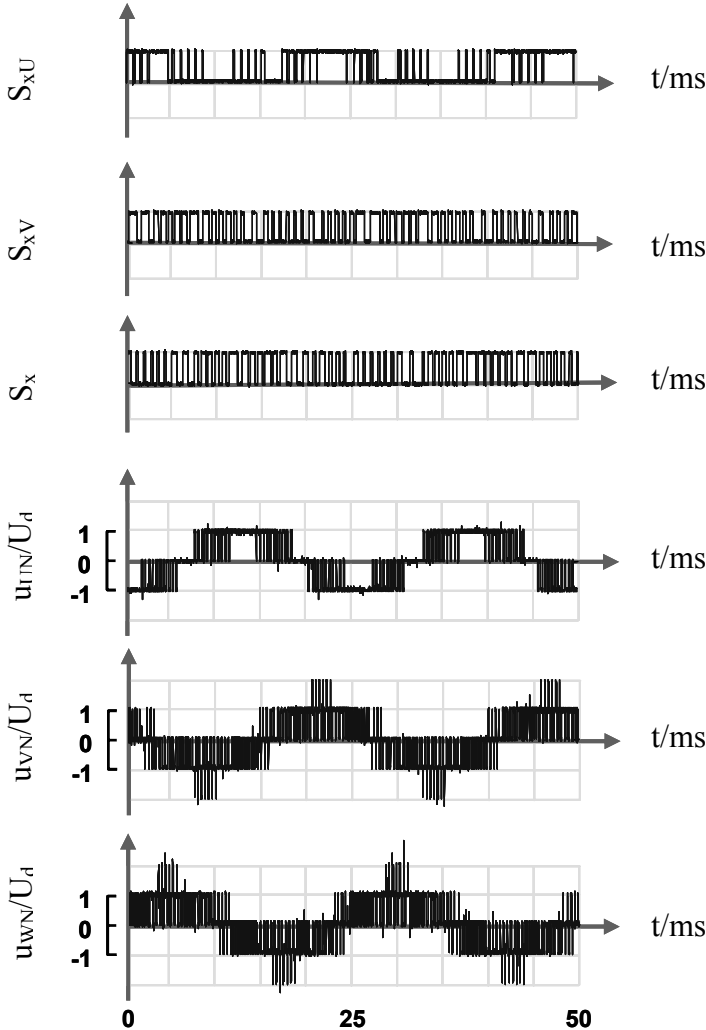


Fig. 5.8. Phase voltage and firing pulses waveforms one cell bypassed with sequence

5.5 Dynamic response of the torque controller with bypassed cells

The operation of the inverter with bypassed cells reduces the maximum available output voltage. The effects derived from this operation mode were analyzed in detail in chapter 4. In this section experimental results are given to show the torque response in the field weakening

region. For a healthy inverter operating at 75% of the nominal speed, a torque dynamics as it is depicted in Fig. 5.9 can be achieved. The reference torque is reached very fast, depending on the quality of the machine model, the tuning of the torque controller and the mechanical speed.

By operating the inverter with one bypassed cell, the maximum output voltage is only a 75% of the nominal value; therefore, almost all the inverter voltage is needed to maintain the machine running at the same speed. Nevertheless, the control can still change the stator flux trajectory in order to obtain an additional improvement in the torque response.

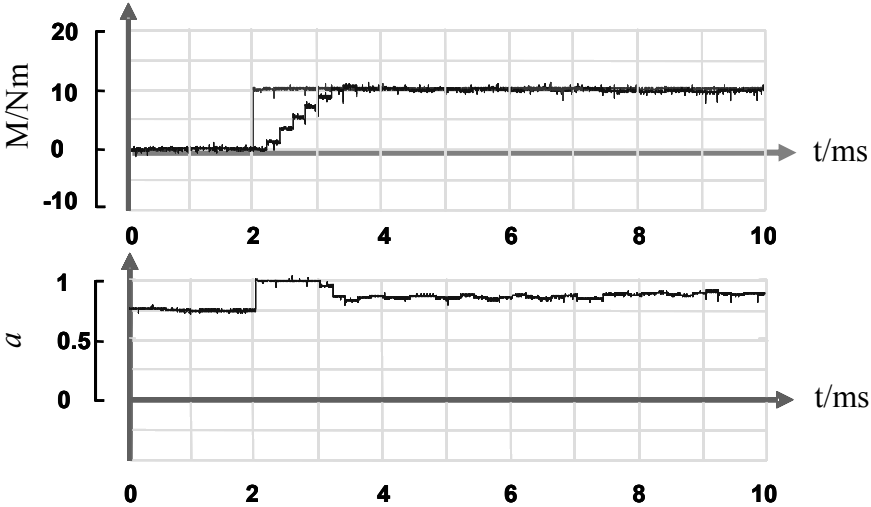


Fig. 5.9. Torque dynamic response for an healthy inverter at 75% of the nominal speed.

In comparison to the conventional field oriented control, a stator flux field oriented control scheme can generate a fast change in the flux trajectory, leading the stator flux space phasor faster to a steady state track. This short-cut effect is obtained in an approximated way by means of dynamic field weakening controller; as it is depicted in Fig. 5.10.

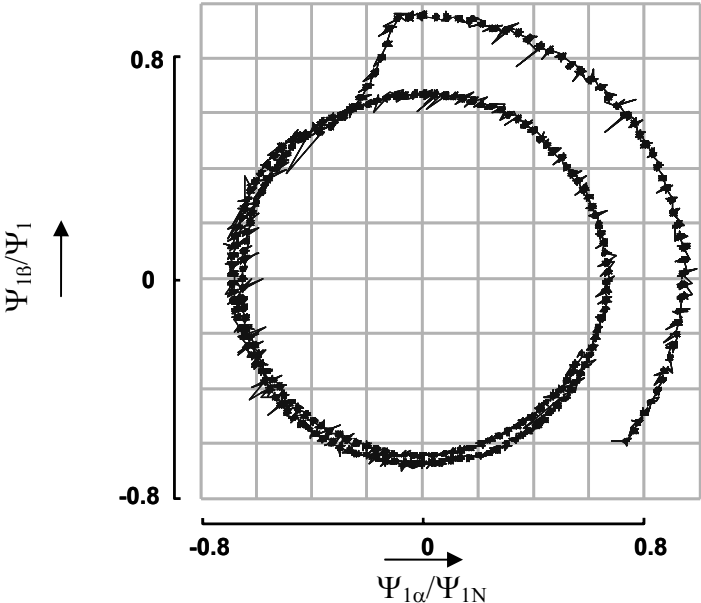


Fig. 5.10. Short-cut effect in the stator flux trajectory in the field weakening region.

The torque dynamic response can be obtained now only with a small voltage margin, as it is shown in Fig. 5.11 for the same operating conditions.

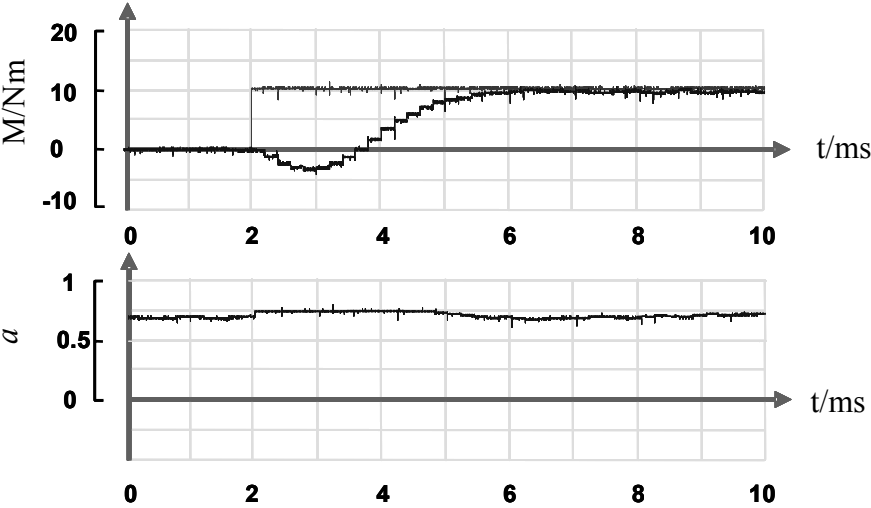


Fig. 5.11. Torque dynamic response for a healthy inverter at 75% of the nominal speed.

It should be noted that the advantages of the dynamic field weakening are not significant for a controller configured with a high voltage margin. In this case the torque dynamic response is mainly achieved by the voltage margin and the dynamic flux weakening produces only a small effect. Despite of the fact that a low voltage margin enables a better use of the inverter, it is always necessary for the stability of the control strategy. In the case of the operation with a too small voltage margin, the control scheme can easily operate in non-linear mode that can drive the machine to an unstable operation. As it is shown in Fig. 5.12, the torque starts to oscillate when the machine enters in the field weakening region with an insufficient voltage margin.

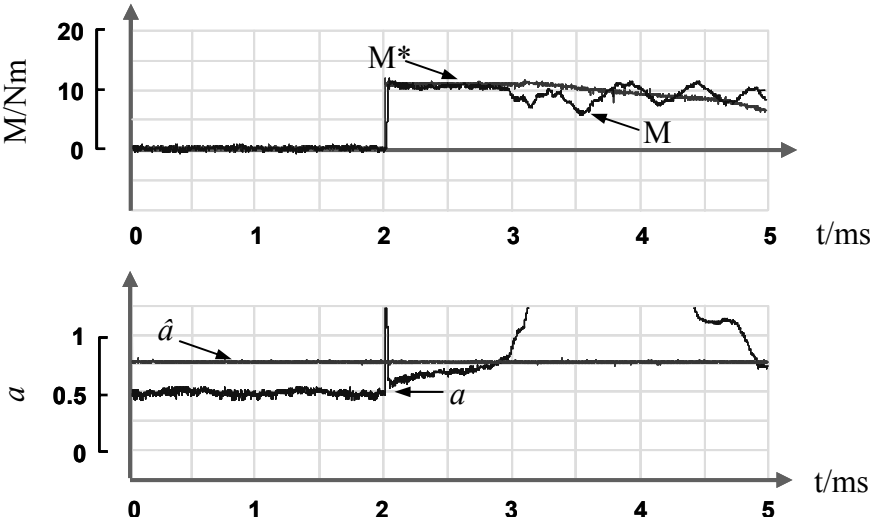


Fig. 5.12 Control instabilities due to insufficient voltage margin.

For the same case, a stable operation of the machines is obtained with a voltage margin between 5% and 10% of the maximum output voltage, as it is shown in Fig. 5.13.

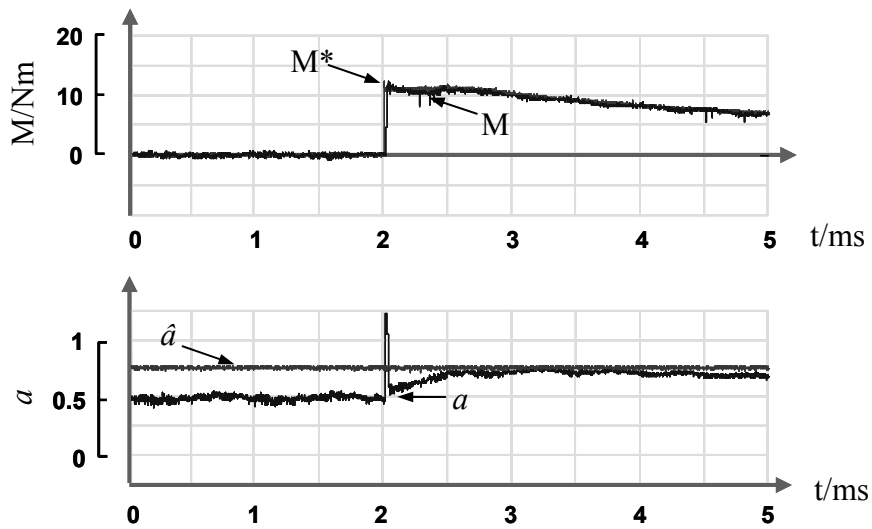


Fig. 5.13. Torque response with enough voltage margin.

5.6 Transition between two inverter configurations

Several approaches have been presented to adjust the control limits depending on the new topology after the bypass of the faulty cells. As it was described in chapter 4, a simple method to change the torque and flux limits with a non critical fault consists of the reduction of the machine speed according to the new maximum available voltage. Once the inverter output voltage reaches a value under the new maximum voltage limit, the faulty cells can be bypassed without affecting the torque and flux control. A second alternative considers the modification of the torque and flux limits in a sequence, that means, first the torque limit is applied, and after the machine has reached a new steady state operating point, the flux limit is adjusted. The advantage of this method is that the speed of the machine is reduced directly to the maximum value that can be achieved with the new inverter configuration. A third approach consists in changing all limits simultaneously, in this way the bypass of the cell can be carried out immediately. As it is advantageous to bypass a cell in a critical fault quickly, this case has been experimentally examined.

For the following test, the operating point of the machine is set at nominal speed value, and the load machine is adjusted to generate a load torque equal to $M_L=7$ Nm. The torque controller limit was adjusted to deliver a maximum torque of 10Nm. Additionally, it will be assumed that the bypass is executed synchronously with the control strategy, that means that

the bypass of the cell and the changes of the torque, flux, and modulation index limits occur at the same time.

Fig. 5.14 shows the calculated values of torque, flux and the measurement of the speed for the transition between a healthy inverter and a topology with one bypassed cell. The torque shows a small negative transient product of the fast change in the stator flux magnitude. The steady state value of torque experiments almost no variations, because the torque limitation at this speed has a value similar to the load torque. As a consequence, the speed of the machine does not show a significant variation.

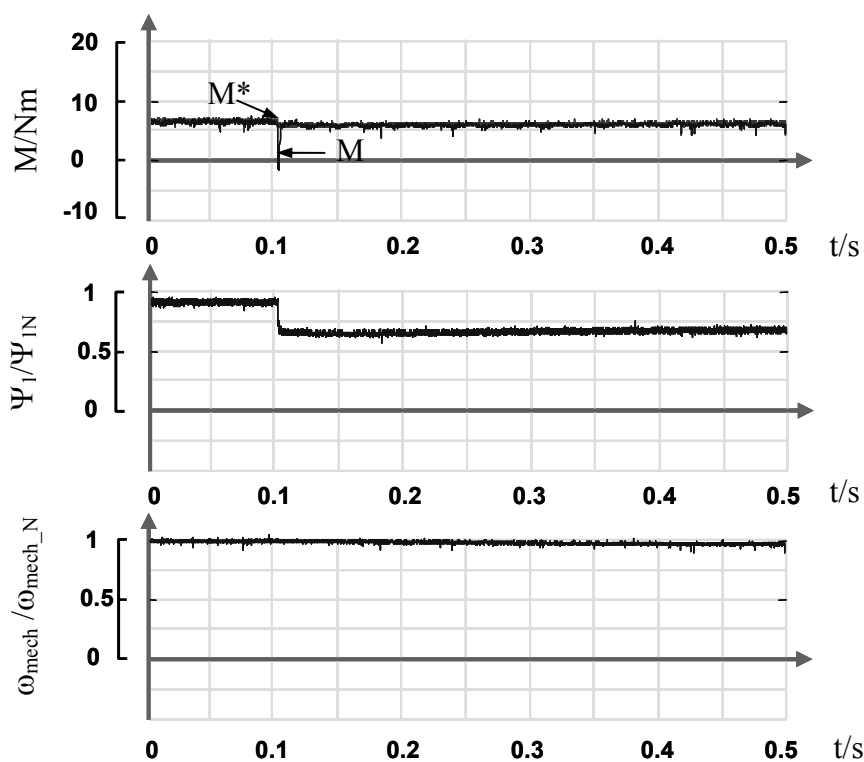


Fig. 5.14. Torque, flux and speed for a transition between a healthy inverter and an inverter with one bypassed cell.

For the same initial operating conditions, a transition between a healthy inverter and a topology with two bypassed cells in the same phase is presented in Fig. 5.15. In this case the voltage is limited to a 50% of the maximum value; therefore a higher negative torque during the transient is obtained. The maximum torque is reduced immediately by the new limitation imposed by the field weakening, for this reason the machine reduces its speed until the limitation in the torque controller equals the load torque. The torque transient has no significant effects in the velocity of the drive if the inertia is high enough.

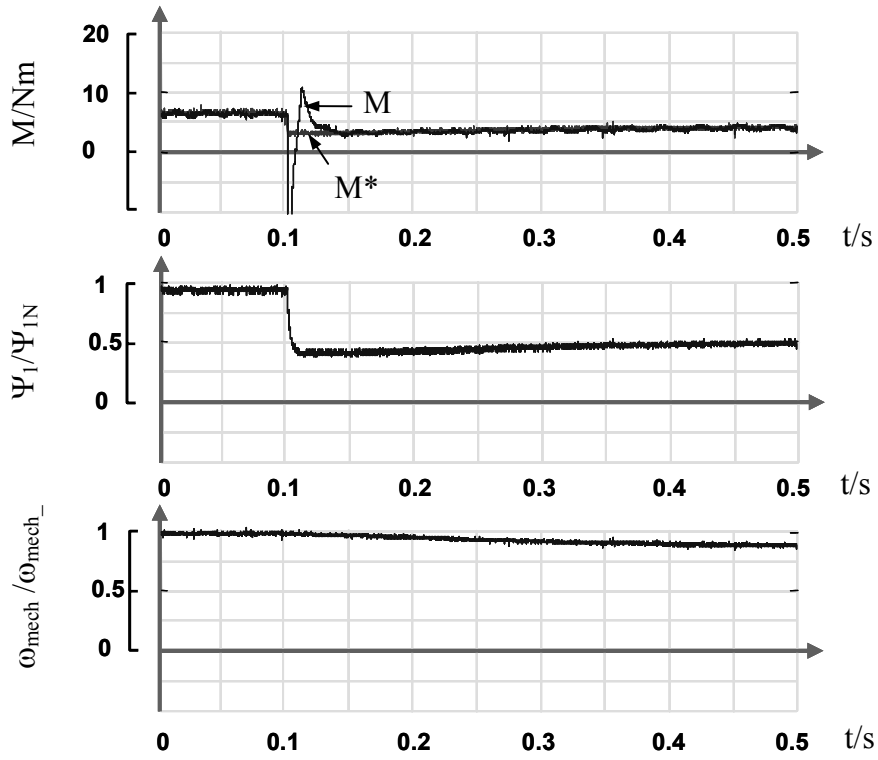


Fig. 5.15. Torque, flux and speed for a transition between a healthy inverter and the inverter two bypassed cells.

5.7 Summary of chapter 5

The theoretical approaches developed for the fault tolerant operation in H-bridge multilevel inverters were validated by means of an experimental set-up consisting of a 5-level inverter, an induction machine and a load machine. The stator flux field oriented control scheme was programmed in a floating point DSP platform, whereas a FPGA was used to support the processor in the modulation task.

The obtained results show that the balanced operation of the induction machine for different unbalanced topologies of the multilevel inverter is possible. Additionally, the optimization of the sequences of the voltage states enables a better distribution of the firing pulses in the cells of the inverter with bypassed cells. It is also shown that the stator flux oriented control is specially suited for the operation of the inverter with bypassed cells at reduced voltage ratings, since an improvement in the torque dynamics can be achieved with a very low voltage margin. This effect is obtained by means of an additional reduction in the stator flux which causes a short-cut effect in the stator flux trajectory.

Finally, the transition between a healthy inverter and an inverter topology with bypassed cells was also examined. It was shown that the torque, flux and voltage limits can be adjusted simultaneously in order to enable a fast bypass of the faulty cells.

6. CONCLUSIONS

In this work, a new approach for the fault tolerant operation of the H-bridge multilevel inverter is developed. The proposed method is based on the space phasor modulation and it uses the redundant voltage states generated by the multilevel inverter to compensate the asymmetrical inverter topology resulting of the bypass of one or more faulty cells. The proposed strategy, as other established approaches, utilizes the fact that the middle point of the machine is not connected to the neutral point of the inverter, so that the voltage difference between these two points can be conveniently adjusted to regain the load balance.

A throughout analysis of the resulting configurations after the occurrence of different fault types, demonstrates that the number of available voltage space phasors and, thus, the number of redundant voltage states decrease with the number of bypassed cells. Despite of this fact, the inverter can still supply the load with balanced voltages by means of the remaining voltage space phasors providing that the maximum modulation index is properly reduced and the selected sequences correspond to valid voltage states. In order to achieve this goal, a multilevel space phasor modulation algorithm is proposed, which fulfils different optimization criteria dealing with minimum common mode voltage generation, selection of sequences according to a minimum number of switching actions and the distribution of the firing pulses among the healthy cells. The complexity of the modulator was overcome by using a FPGA, which relieves the processor of these optimization tasks. In this way, the processor delivers only the three voltage states corresponding to the three nearest selected space phasors respect to a reference, whereas the algorithm programmed in the FPGA selects the valid set of voltage states, according to the resulting topology after the fault. Then, it is shown that suitable modification of the sequences and reduction of the modulation period allows, despite of the new topology, a switching frequency close to the nominal levels. The results obtained in a laboratory set-up of a SCHB multilevel prototype demonstrate that balanced currents can be obtained for different asymmetrical inverter topologies.

As a consequence of the reduction in the available inverter output voltage, the machine can not operate with nominal values of torque and flux. For this reason, the new limits for torque and flux are analyzed and different criteria to change those limits are defined. The new limits preserve the nominal torque, to the detriment of the maximal reachable speed. The defined field weakening operating point allows higher speeds provided that the load torque does not surpass the new limits.

The transition that occurs when a cell is bypassed in a healthy inverter is also studied. The experimental results show that a fast transition is possible, if the torque, flux and voltage limits of the inverter are simultaneously adjusted. In this manner, the inverter can react very fast in case of a severe fault such a short circuit of the cell, too. The torque overshoot generated during the transition will be damped for the case of loads with a high inertia. Since the operation of the inverter with bypassed cells may require of the maximal achievable output voltage to maintain the speed of the process within acceptable levels, a high performance of the control strategy in the field weakening region is required. The stator flux oriented control permits to guide the stator flux trajectory through a short-cut in order to quickly reach the steady state and thus a higher torque dynamic response is obtained.

7. ABSTRACT

The operation of the H-bridge multilevel inverter under fault conditions is examined in this work. In the event of a fault, the cell with problems can be bypassed in order to continue the operation of the inverter. The voltage unbalance that results from the asymmetrical topology in some inverter configurations was compensated by modifying the modulation scheme. Two different approaches were considered: the Phase Shift-PWM (PS-PWM) strategy and the multilevel Space Phasor Modulation (SPM). Aspects such as the generation of firing pulses generation and the use of optimal sequences were also discussed. The proposed modulation schemes were confirmed by simulation and experimental results in a 5-level H-bridge multilevel inverter.

8. ZUSAMENFASSUNG

Die vorliegende Arbeit befasst sich mit dem theoretischen und experimentellen Erforschung des Fehlertolerantbetriebs von einem H-Brücke Mehrpunkt-Wechselrichter. Dieser Art von Wechselrichter besteht aus mehrere hintereinander geschaltete H-Brücken, die so genannten Zellen, die eine Phasenspannung mit mehreren Stufen erzeugen können.

Im Fehlerfall, können die Zellen überbrückt werden um den Fehlertolerantbetrieb des Wechselrichters zu ermöglichen. Diese Lösung verursacht eine Unsymmetrie in der Topologie die durch die Anpassung des Pulsbreitmodulators und die Regelverfahren kompensiert werden kann. Zwei verschiedene Modulationverfahren für Mehrpunktwechselrichter wurden untersucht, die Standard Phase Shift-PWM (PS-PWM) und Raumzeigermodulation. Andere Aspekte wie die Erzeugung der Schaltpulsen und die Optimierung des Sequenzen wurden auch im Betracht gekommen. Die vorgeschlagenen Steuerverfahren wurden schließlich in einem Laborprototyp untersucht.

9. BIBLIOGRAPHY

- [1] Bernet, S.; "State of the Art and Developments of Medium Voltage Converters – An Overview," in Proceedings of the International Conference PELINCEC, Warsaw, Poland, Oct. 16-19, 2005.
- [2] Maischak, D.; "Schnelle Drehmomentregelung im gesamten Drehzahlbereich," VDI Verlag, Reihe 8, No 479.
- [3] Hammond, P.; "A New Approach to Enhance Power Quality for medium Voltage AC Drives," IEEE Trans. on Ind. Appl., Vol. 33, Jan./Feb. 1997, pp. 202 – 207.
- [4] Hammond, P; "Multiphase power supply with series connected power cells with failed cell bypasss," U.S.patent 6.222.284, Apr. 2001.
- [5] Rodriguez, J.; Hammond, P.W.; Pontt, J.; Musalem, R.; Lezana, P.; Escobar, M.J.; "Operation of a Medium-Voltage Drive Under Faulty Conditions," IEEE Transactions on Industrial Electronics, Vol. 52, Issue 4, Aug. 2005, pp.1080 – 1085.
- [6] McGrath,B.P.; Holmes,D.G. Lipo, T.A; "Optimised Space Vector Switching Sequences for Multilevel Inverters," IEEE Applied Power Electronics Conference (APEC) 2001, Anaheim, CA, Mar. 4-8, 2001, vol. 2, pp 1123-9.
- [7] Sanmin Wei et al, "Comparison of Control Schemes for Multilevel inverters with faulty Cells", in Proceedings of the International Conference IECON 2004.
- [8] Kovacs, K.P., Racs, I. "Transiente Vorgänge in Wechselstrommaschinen," Verlag der Ungarischen Akademie der Wissenschaft, Bd. I, BdII, Budapest, 1959.
- [9] Meyer, M.; "Selbstgeführte thyristor-Stromrichter," Siemens Aktiengesellschaft Berlin und München, dritte Auflage, 1974, ISBN 3-8009-1168-X.
- [10] Rendusara, D.A.; Cengeli, E.; Enjeti, P.N., Stefanovic, V.R.; Gray, J.W.; "Analysis of common mode voltage-"neutral shift" in medium voltage PWM adjustable speed drive (MV-ASD) systems," IEEE-Transactions on Power Electronics, Vol. 15, Issue 6, Nov. 2000, pp. 1124-1133.
- [11] Brückner, T.; Bernet, S.; Güldner H.;"The Active NPC Converter and its Loss-balancing Control", IEEE-Transactions on Industrial Electronics, Vol. 52, No 3, Jun. 2005.
- [12] Lavieville J.P.; Cariere, P.; and Meynard, T.; "Electronic circuit for converting electrical energy and power supply installation making use thereof," US patent 5668711, sep. 1997.
- [13] Baker, R.H.; Bannister, L.H.; "Electric Power Converter," U.S. Patent 3 867 643, Feb.1975.

- [14] Hammond, P.; "Medium voltage PWM drive and method," U.S. patent 6 166 513, Dec 2000.
- [15] Springmeier, F.; "Direkte Ständergrößen-Regelung von Induktionsmaschinen am wechsellrichter," VDI Verlag, Reihe 21, No 133.
- [16] Tolbert, L.; Peng, F.-Z., Habetler, T.; "Multilevel Converters for Large Electric Drives," IEEE Trans. on Ind. Appl., Vol. 35, Jan./Feb. 1999, pp. 36 – 44.
- [17] Celanovic, N., Boroyevich, D.; "A fast space-vector Modulation Algorithm for Multilevel Three-Phase Converters", IEEE Transaction on Industry Applications, Vol. 37, Issue 2, Mar-Apr 2001, pp. 637-641.
- [18] Haoran, Z.; Von Jouanne, A.; Shaoan, D.; Wallace, A.K.; Fei W.; "Multilevel inverter modulation schemes to eliminate common-mode voltages," IEEE Transactions on Industry Applications, Vol. 36, Issue 6, Nov.-Dec. 2000 pp. 1645 – 1653.
- [19] McGrath, B.P.; Meynard, T.A.; Gateau, G.; "Optimal Modulation of Flying Capacitor and Stacked Multicell Converters Using a State Machine Decoder" in proceedings of the IEEE 36th Annual Power Specialist Conference PESC 2005, Jun. 12-16, 2005.
- [20] Welchko, B.A.; Lipo, T.A.; Jahns, T.M.; Schulz, S.E. "Fault tolerant three-phase AC motor drive topologies; a comparison of features, cost and limitations," IEEE Transactions on Power Electronics, Vol.19, Issue 4, Jun.2004, pp.1108–1116.
- [21] Kastha, D.; Bose, B.K.; "Investigation of fault modes of voltage-fed inverter system for induction motor drive," IEEE Transactions on Industry Applications, Vol. 30, Issue 4, July-Aug. 1994 ,pp. 1028 – 1038
- [22] Fuchs, F.W.; "Some diagnosis methods for voltage source inverters in variable speed drives with induction machines - a survey," The 29th Annual Conference of the IEEE Industrial Electronics Society, 2003. IECON '03. Vol. 2, 2-6 Nov. 2003, pp. 1378 – 1385.
- [23] Richardeau, F.; Baudesson, P.; Meynard, T.A.; "Failures-tolerance and remedial strategies of a PWM multicell inverter," IEEE Transactions on Power Electronics, Vol. 17, Issue 6, Nov.2002 ,pp. 905–912.
- [24] Xiaomin, K.; Corzine, K.A.; Familant, Y.L.; "A unique fault-tolerant design for flying capacitor multilevel inverter," IEEE Transactions on Power Electronics Vol. 19, Issue 4, Jul. 2004, pp.979 – 987.
- [25] Rothenhagen, K.; Fuchs, F.W.; "Performance of diagnosis methods for IGBT open circuit faults in voltage source active rectifiers," IEEE 35th Annual Power Electronics Specialists Conference, 2004. PESC 04. Vol. 6, 20-25 Jun. 2004 pp.4348 – 4354.

10. APPENDIX : PARAMETERS OF THE MACHINE

Manufacturer:	System Antriebstechnik, Dresden GmbH.
Nominal power:	5.5 kW
Nominal voltage U_{LL} :	360 V, line-to-line
Nominal current:	12.7 A, star-connection
Nominal Frequency ω_{IN} :	52 Hz
Nominal Speed ω_{mech_N} :	1500 rpm
Nominal Torque M_N :	35 Nm
$\cos(\varphi)$:	0.81
Pole pairs p:	2

The nominal stator flux will be expressed as a function of the maximum values of the nominal voltage and the nominal frequency of the machine:

$$\Psi_{IN} = \frac{\sqrt{2} \cdot U_{LL}}{\sqrt{3} \cdot \omega_{IN}}. \quad (10.1)$$

